Characteristics of Selected Major Sudden Stratospheric Warming Events and their Links to European Cold Waves in Extended Range Ensemble Forecasts

Masterarbeit im Fach Meteorologie
von

Selina Kiefer

Juli 2020

INSTITUT FÜR METEOROLOGIE UND KLIMAFORSCHUNG
KARLSRUHER INSTITUT FÜR TECHNOLOGIE (KIT)

Referent:	Prof. Dr. Joaquim Pinto
Korreferent:	Prof. Dr. Peter Braesicke

Abstract

Sudden stratospheric warming (SSW) events which lead to a reversal of the stratospheric polar night jet in winter are discussed in literature as a potential source of increased predictability of European cold waves on the subseasonal to seasonal time-scale. One displacement-type (D-type) and three split-type (S-type) SSW events of the past 20 years are therefore investigated using the ERA-Interim reanalysis data set. The focus of this analysis lies on the characteristics of the SSW events and their potential links to European cold waves. The S-type events with their onset dates on 3 February 2001, 24 January 2009 and 25 January 2010 show a similar evolution in the middle stratosphere. Maximum westerly winds and minimum polar-cap averaged temperatures precede the rapid deceleration of the stratospheric polar night jet and temperature increase. These events feature generally stronger and longer-lasting easterly winds in the middle stratosphere compared to the D-type event. All three S-type events are followed by an equatorward displacement of the tropospheric mid-latitude jet stream over the North Atlantic ocean and a shift of the North Atlantic Oscillation (NAO) to its negative phase. Both indicate a downward influence of the SSW events on surface weather. Nevertheless, these events cannot be linked to European cold waves directly, at least not with the methods used in this thesis. Only the D-type SSW event with its onset date on 23 November 2000 is suggested to be linked directly to the European cold wave occurring between 21 and 25 December 2000. Therefore, this event is analyzed with the European Centre for Medium-Range Weather Forecasts (ECMWF) S2S reforecasts in addition to the ERA-Interim reanalysis. An improvement in the European 2 metre temperature anomaly distribution is found when the geopotential height anomalies in the lower stratosphere, caused by the SSW event, are represented correctly in the S2S reforecast initialized on 25 November 2000. Since the anomalies show non-negligible differences in the exact location and magnitude in comparison to the ERA-Interim reanalysis, the prediction of the European and Scandinavian mean temperature is not improved. The same applies to the NAO index. Hereby it is important to note that the investigated reforecast is the only reforecast comprising both, the European cold wave associated with the SSW event and an initialization with easterly winds in the middle stratosphere. To make a quantitative statement about a possible increase in the predictability of European cold waves after SSW events, further case studies need to be investigated. The large multi-model ensemble forecasts of the S2S data base are a good basis herefore. This thesis clearly demonstrates the high case-to-case variability of the characteristics and downward impacts of SSW events. Therefore, exploratory case studies are necessary to understand the phenomena of the coupling between SSW events and European cold waves.

Zusammenfassung

Plötzliche Stratosphärenerwärmungen (SSWs), die zu einem Richtungswechsel des stratosphärischen Strahlstroms in der winterlichen Polarnacht führen, werden in der Literatur als mögliche Quellen einer erhöhten Vorhersagbarkeit von europäischen Kältewellen auf subsaisonalen bis saisonalen Zeitskalen gehandelt. Eine SSW, die zu einer Verschiebung des polaren Wirbels Richtung Äquator führt (D-Typ), und drei SSW, die eine Teilung des polaren Wirbels zur Folge haben (S-Typ), werden daher mit dem ERA-Interim Reanalysedatensatz untersucht. Der Fokus der Analyse liegt auf den Eigenschaften der SSW-Ereignisse und möglichen Verbindungen zu europäischen Kältewellen. Die S-Typ-Ereignisse, deren Anfänge am 3. Februar 2001, 24. Januar 2009 und 25. Januar 2010 liegen, zeigen eine ähnliche Entwicklung in der mittleren Stratosphäre. Die stärksten Westwinde und geringsten Temperaturen über der Polkappe sind vor dem schnellen Abbremsen des stratosphärischen Strahlstroms in der Polarnacht und dem Anstieg der Temperaturen zu finden. Diese SSW-Ereignisse zeigen extremere und länger anhaltende Ostwinde in der mittleren Stratosphäre als das D-Typ-Ereignis. Auf alle drei S-Typ-Ereignisse folgt eine äquatorwärtigen Verschiebung des troposphärischen nordatlantischen Strahlstroms in den mittleren Breiten und eine negativen Phase der Nordatlantischen Oszillation (NAO). Beides legt einen Einfluss der SSW-Ereignisse auf das Bodenwetter nahe. Trotzdem können diese Ereignisse nicht direkt mit europäischen Kältewellen verknüpft werden, zumindest nicht mit den in dieser Arbeit angewendeten Methoden. Nur die D-Typ-SSW mit Beginn am 23. November 2000 wird mit einer europäischen Kältewelle zwischen dem 21. und 25. Dezember 2000 in Verbindung gebracht. Daher wird dieses Ereignis zusätzlich zur Untersuchung mit dem ERA-Interim Reanalysedatensatz auch mit dem S2S Re-Vorhersagedatensatz des Europäischen Zentrums für mittelfristige Wettervorhersage (EZMW) analysiert. Eine verbesserte Vorhersage der Verteilung der europäischen 2-Meter-Temperaturanomalien wird beobachtet, wenn die von der SSW verursachten Anomalien der geopotentiellen Höhe in der unteren Stratosphäre korrekt in der S2S Re-Vorhersage mit Initialisierung am 25. November 2000 dargestellt werden. Da die Anomalien im Vergleich zur ERA-Interim Reanalyse nicht vernachlässigbare Unterschiede in der exakten Position und Stärke zeigen, ist eine Verbesserung der Vorhersage der mittleren europäischen und skandinavischen Temperatur nicht zu finden. Dasselbe gilt für die Vorhersage des NAO-Index. Die untersuchte Re-Vorhersage ist die einzige, die mit Ostwinden in der mittleren Stratosphäre initialisiert wird und gleichzeitig die mit der SSW in Verbindung gebrachte europäische Kältewelle enthält. Um eine quantitative Aussage über eine mögliche Erhöhung der Vorhersagbarkeit von europäischen Kältewellen nach dem Auftreten von SSW-Ereignissen zu treffen, müssen weitere Vorhersagen analysiert werden. Die großen Multi-Modell Ensemble-Vorhersagen des S2S Datensatzes sind hierfür eine gute Basis. Diese Arbeit zeigt die hohe Variabilität der Eigenschaften und bodengerichteten Einflüsse der SSW-Ereignisse. Daher sind detaillierte Fallstudien nötig, um die Kopplung zwischen diesen Ereignissen und europäischen Kältewellen zu verstehen.

Contents

1 Introduction

In winter, the polar stratosphere is characterized by strong westerly winds encircling the pole (Butler et al., 2015). These westerly winds are called „stratospheric polar night jet“ or „stratospheric polar vortex“. Variabilities in this stratospheric polar vortex are known to be able to affect tropospheric weather in mid- and high-latitudes (Tripathi et al., 2015).
In spring, the stratospheric polar night jet reverses from westerly to easterly wind speeds (Butler et al., 2015) due to increased radiative heating by the rising sun. But also in winter, temporal reversals of the stratospheric polar night jet are possible. These so-called major „sudden stratospheric warming“ (SSW) events have first been observed 1952 by Scherhag (Butler et al., 2015).
In 1971, Matsuno developed a simple model to demonstrate the development of SSW events from upward propagating planetary-scale waves which penetrate into the stratosphere. Wave breaking in the upper stratosphere-lower mesosphere region, which is characterized by prevailing easterly winds, leads to an increase of temperatures and the formation of a new layer with easterly winds where the following waves break. This so-called „critical layer interaction“ is typical for the top-down development of an SSW event.
In the middle stratosphere, a temperature increase between 30 K and 40 K in the time-range of a few days is usually observed in combination with SSW events (Butler et al., 2015). The deposition of easterly momentum due to the breaking of tropospheric easterly waves leads to a deceleration of the westerly stratospheric polar night jet (Kidston et al., 2015; Matsuno, 1971). The weakened polar vortex is then either displaced off the pole or split into two parts (Charlton and Polvani, 2007).
In some cases, the large temperature and wind anomalies caused by an SSW event have an influence on surface weather (Charlton-Perez et al., 2018). Hereby, especially the region over the North Atlantic ocean is sensitive to changes in the stratospheric circulation but also the North Pacific ocean can be affected according to Charlton-Perez et al. (2018) and Afargan-Gerstman and Domeisen (2020). Concerning the region of the North Atlantic ocean, changes in the stratospheric circulation induced by SSW events result in the negative phase of the North Atlantic Oscillation (NAO) at the surface. Although different studies find different fractions of SSW events which have an influence on the NAO, they agree that the likelihood of an NAO- phase is increased after SSW events in comparison to climatological or strong stratospheric polar vortex conditions.
The negative phase of the NAO is one of the primary drivers of European cold waves in winter (Butler et al., 2015). According to King et al. (2019) especially Scandinavia experiences more cold extremes in the 2 months after an SSW event than under climatological conditions.
A correct prediction of European cold waves on the subseasonal to seasonal time-scale is an important factor for both, society and economy (Cattiaux et al., 2010). According to Cattiaux et al. (2010) cold waves in the currently warming climate strongly affect social protection, sectors of energy supply and public as well as industrial transport. Since SSW events affect European

surface weather up to 2 months after their occurrence, they are discussed as a potential source of increased predictability of European cold waves on subseasonal to seasonal time-scales (Baldwin et al., 2003; Garfinkel et al., 2017; Vitart et al., 2017).
Therefore, the following thesis investigates four major SSW events of the past 20 years concerning their characteristics and potential links to European cold waves. The theoretical concepts needed to characterize and associate SSW events with European cold waves are describes in chapter 2. Chapter 3 comprises the data and methods used in this thesis. The chapters 4 to 6 contain the detailed analysis of the chosen SSW events, sorted by the strength and duration of easterly winds in the middle stratosphere. The event which features the strongest and longest-lasting easterly winds is thereby described first. In chapter 7, the investigated SSW events are compared to each other and discussed with literature. Chapter 8 sums up the most important results of this thesis and gives an outlook.

2 Theoretical Concepts

2.1 Atmospheric Circulation

2.1.1 The Navier-Stokes Equation for Atmospheric Motions

The Navier-Stokes equation describes essentially Newton's second law and comprises all relevant forces in an air parcel, a symbolic volume of air. The visualization of air as parcels is used for the easier formulation of pressure balances (Holton, 2010). The Navier-Stokes equation can be written as:

$$F = F_{\mathrm{c}} + F_{\mathrm{p}} + F_{\mathrm{f}} + F_{\mathrm{g}}, \tag{2.1}$$

where F_{c} is the Coriolis force, F_{p} the pressure gradient force, F_{f} the friction and F_{g} gravitiy.
The Coriolis force F_{c} describes the influence of the Earth's rotation on the air parcel (Holton, 2010). It is latitude and height depended:

$$F_{\mathrm{c}} = -\mathrm{f} \cdot \left(\vec{k} \times \vec{v}\right), \mathrm{f} = 2\Omega \cdot \sin\left(\Phi\right). \tag{2.2}$$

The Coriolis parameter f comprises the Earth's rotation rate $\Omega = 7.3 \cdot 10^{-5}\mathrm{s}^{-1}$ and the sine of the latitude Φ. The height dependency is calculated inside the cross-product, where the unit vector $\vec{k} = (0,0,1)^{\mathrm{T}}$ is multiplied with the 3-dimensional velocity $\vec{v}$ of the air parcel.
The pressure gradient force F_{p} describes the influence of different pressure levels in the same height. Since the circulation in the troposphere is always seeking an equilibrium, air is transported from higher pressure levels to lower pressure levels along the pressure gradient $\vec{\bigtriangledown} p$:

$$F_{\mathrm{p}} = -\frac{1}{\rho}\vec{\bigtriangledown} p. \tag{2.3}$$

The friction force F_{f} is usually neglected whenever suitable or parametrized in models when needed.
The gravitational force F_{g} is only relevant for vertical movements:

$$F_{\mathrm{g}} = \vec{k} \cdot \mathrm{g}. \tag{2.4}$$

The gravitational constant g is latitude and height depended but its dependency on latitude is usually neglected (https://apps.ecmwf.int/codes/grib/param-db/?id=129, last viewed 2 September 2019).
The resulting force F can then be decomposed in its Eulerian form, featuring the local time derivate and an advection term :

$$F = \frac{\partial \vec{v}}{\partial t} + \left(\vec{v} \cdot \vec{\bigtriangledown}\right)\vec{v}. \tag{2.5}$$

The Navier-Stokes equation can now be written in the following form:

$$\frac{\partial \vec{v}}{\partial t} + \left(\vec{v} \cdot \vec{\bigtriangledown}\right) \vec{v} = -\mathrm{f} \cdot \left(\vec{k} \times \vec{v}\right) - \frac{1}{\rho} \vec{\bigtriangledown} p + \vec{k} \cdot \mathrm{g} + F_{\mathrm{f}}. \tag{2.6}$$

In the undisturbed atmosphere, all forces balance each other.

2.1.2 The Transformed Eulerian Mean Equation for the Zonal-Mean of Atmospheric Circulations

The stratospheric circulation is little turbulent due to the lack of surface contact and the lesser density of air (Baldwin et al., 2003). Therefore, only the zonal component of the Navier-Stokes equation is relevant:

$$\frac{\partial u}{\partial t} + u\frac{\partial u}{\partial x} + v\frac{\partial u}{\partial y} + w\frac{\partial u}{\partial z} = \mathrm{f} \cdot v - \frac{1}{\rho}\frac{\partial}{\partial x} p + F_{\mathrm{fx}}. \tag{2.7}$$

The three dimensions of the air parcel's velocity are described as $(u,v,w)^{\mathrm{T}}$, the three cartesian dimensions as $(x,y,z)^{\mathrm{T}}$. Since the zonal-mean zonal flow is the variable of interest when looking at the stratospheric polar night jet, a Reynold's averaging is applied:

$$\begin{aligned} &\left(\frac{\partial(\bar{u}+u')}{\partial t}\right) + \left((\bar{u}+u')\frac{\partial(\bar{u}+u')}{\partial x}\right) + \left((\bar{v}+v')\frac{\partial(\bar{u}+u')}{\partial y}\right) + \left((\bar{w}+w')\frac{\partial(\bar{u}+u')}{\partial z}\right) \\ &= \left(\mathrm{f} \cdot (\bar{v}+v')\right) - \frac{1}{\rho}\left(\frac{\partial(\bar{p}+p')}{\partial x}\right) + \left(\bar{F_{\mathrm{fx}}} + F'_{\mathrm{fx}}\right), \end{aligned} \tag{2.8}$$

where $\bar{x}$ indicates the zonal-mean and x' the deviation from the zonal-mean. Derivates from the zonal-mean are small and are therefore neglected:

$$\frac{\partial \bar{u}}{\partial t} + \bar{u}\frac{\partial \bar{u}}{\partial x} + \bar{v}\frac{\partial \bar{u}}{\partial y} + \bar{w}\frac{\partial \bar{u}}{\partial z} = \mathrm{f} \cdot \bar{v} - \frac{1}{\rho}\frac{\partial}{\partial x}\bar{p} + \bar{F_{\mathrm{fx}}}. \tag{2.9}$$

The zonal derivate of the zonal-mean flow is zero by definition:

$$\frac{\partial \bar{u}}{\partial t} + \bar{v}\frac{\partial \bar{u}}{\partial y} + \bar{w}\frac{\partial \bar{u}}{\partial z} = \mathrm{f} \cdot \bar{v} - \frac{1}{\rho}\frac{\partial}{\partial x}\bar{p} + \bar{F_{\mathrm{fx}}}. \tag{2.10}$$

Since the Earth is a sphere, it is easier to look at spherical coordinates instead of cartesian coordinates. The transformation of the formular in spherical coordinates leads to:

$$\frac{\partial \bar{u}}{\partial t} = \bar{v}\left(\mathrm{f} - \frac{1}{\cos(\Phi)\mathrm{a}} \cdot \cos(\Phi)\frac{\partial \bar{u}}{\partial \Phi}\right) - \bar{w}\frac{\partial \bar{u}}{\partial z} - \frac{1}{\rho\cos(\Phi)\mathrm{a}}\frac{\partial \bar{p}}{\partial \theta} + \bar{F_{\mathrm{fx}}}. \tag{2.11}$$

It is now depending on the latitude Φ, the longitude θ and the height z. The Earth's radius a is latitude depended as well. The friction term is still named $\bar{F_{\mathrm{fx}}}$ as it will not be considered explicitly.

To describe the behaviour of the stratospheric polar vortex, different terms of the equation are substituted appropriately. The pressure gradient force is substituted by the Eliassen-Palm flux

since the stratospheric zonal-mean zonal flow disturbances are typically forced by waves (Baldwin et al., 2003). The divergence of the Eliassen-Palm flux $\vec{\bigtriangledown} \cdot \vec{F}$ describes such a wave-forcing:

$$\frac{\partial \bar{p}}{\partial \theta} \equiv \vec{\bigtriangledown} \cdot \vec{F}.$$

$$\vec{\bigtriangledown} \cdot \vec{F} = \vec{\bigtriangledown} \cdot$$

$$\left(0, \rho \cdot \mathrm{a} \cdot \cos(\theta) \left(\frac{\frac{\partial \bar{u}}{\partial z} \bar{v'\Theta'}}{\frac{\partial \Theta}{\partial z} - \bar{v'u'}} \right), \rho \cdot \mathrm{a} \cdot \cos(\theta) \left[\mathrm{f} - \frac{1}{\mathrm{a} \cdot \cos(\theta)} \left(\frac{\partial \bar{u}}{\partial \Theta} \cos(\theta) \right) \cdot \frac{\bar{v'\Theta'}}{\frac{\partial \bar{\Theta}}{\partial z}} - \bar{w'u'} \right] \right)^{\mathrm{T}}.$$

Using the Eliassen-Palm flux instead of the pressure gradient force leads to the dependency of the formular on the potential temperature Θ instead of the pressure p. The potential temperature is calculated as a function of temperature and pressure:

$$\Theta = T \left(\frac{p_{\mathrm{sfc}}}{p} \right)^{\frac{\mathrm{R_l}}{\mathrm{c_p}}}. \tag{2.12}$$

$\mathrm{R_l}$ is the gas constant of dry air and $\mathrm{c_p}$ the specific heat capacity of it. Substituting the pressure gradient force with the Eliassen-Palm flux leads to:

$$\frac{\partial \bar{u}}{\partial t} = \bar{v} \left(\mathrm{f} - \frac{1}{\cos(\Phi)\mathrm{a}} \cdot \cos(\Phi) \frac{\partial \bar{u}}{\partial \Phi} \right) - \bar{w} \frac{\partial \bar{u}}{\partial z} - \frac{1}{\rho \cos(\Phi)\mathrm{a}} \vec{\bigtriangledown} \cdot \vec{F} + \bar{F_{\mathrm{fx}}}. \tag{2.13}$$

In the next step, the mean meridional circulation is expressed differently, adding the originally neglected height dependence again:

$$\bar{v} \equiv \bar{v}^{\star} \tag{2.14}$$

$$\bar{v}^{\star} = \bar{v} - \frac{1}{\rho} \frac{\mathrm{R}}{\mathrm{H}} \frac{\partial}{\partial z} \left(\rho_0 \frac{\bar{v'T'}}{N^2} \right), N^2 = \sqrt{\frac{g}{\Theta} \frac{\mathrm{d}\Theta}{\mathrm{d}z}}.$$

The equation is now depending on the Brunt-Väisälä frequency N^2 which itself is depending on potential temperature, the gravitational constant and height. It is a measure of stability of the air mass (Holton, 2010). Other dependencies of the formular are the universal gas constant R, the scale height H, the density of the air at the surface ρ_0 and the temperature T. Using the alternative expression of the mean meridional circulation, the original formular modifies to:

$$\frac{\partial \bar{u}}{\partial t} = \bar{v}^{\star} \left(\mathrm{f} - \frac{1}{\cos(\Phi)\mathrm{a}} \cdot \cos(\Phi) \frac{\partial \bar{u}}{\partial \Phi} \right) - \bar{w} \frac{\partial \bar{u}}{\partial z} - \frac{1}{\rho \cos(\Phi)\mathrm{a}} \vec{\bigtriangledown} \cdot \vec{F} + \bar{F_{\mathrm{fx}}}. \tag{2.15}$$

The equation is now called a transformed Eulerian Mean (TEM). Analogously, the mean vertical circulation is also expressed differently with the inclusion of the originally neglected vertical component:

$$\bar{w} \equiv \bar{w}^{\star} \tag{2.16}$$

$$\bar{w}^{\star} = \bar{w} + \frac{\mathrm{R}}{\mathrm{H}} \frac{\partial}{\partial y} \left(\frac{\bar{v'T'}}{N^2} \right).$$

This leads to:

$$\frac{\partial \bar{u}}{\partial t} = \bar{v}^{\star} \left(\mathrm{f} - \frac{1}{\cos(\Phi)\mathrm{a}} \cdot \cos(\Phi) \frac{\partial \bar{u}}{\partial \Phi} \right) - \bar{w}^{\star} \frac{\partial \bar{u}}{\partial z} - \frac{1}{\rho \cos(\Phi)\mathrm{a}} \vec{\bigtriangledown} \cdot \vec{F} + \bar{F_{\mathrm{fx}}}. \tag{2.17}$$

The last change to the equation is only a different notation for the small scale processes, which are usually not resolved by models:

$$\vec{F_{\mathrm{fx}}} \equiv \bar{X}. \tag{2.18}$$

The TEM equation can now finally be written as:

$$\frac{\partial \bar{u}}{\partial t} = \bar{v}^{\star}\left(\mathrm{f} - \frac{1}{\mathrm{a}\cdot\cos(\Phi)}\cos(\Phi)\frac{\partial \bar{u}}{\partial \Phi}\right) - \bar{w}^{\star}\frac{\partial \bar{u}}{\partial z} + \frac{1}{\rho_0 \cdot \mathrm{a}\cdot\cos(\Phi)}\vec{\bigtriangledown}\cdot\vec{F} + \bar{X}. \tag{2.19}$$

This is the formulation used by Kidston et al. (2015). They divide the TEM equation in seven parts to show the different influences on the zonal-mean stratospheric circulation:

$$\underbrace{\frac{\partial \bar{u}}{\partial t}}_{1} = \underbrace{\bar{v}^{\star}}_{2}\left(\underbrace{\mathrm{f}}_{3} - \underbrace{\frac{1}{\mathrm{a}\cdot\cos(\Phi)}\cos(\Phi)\frac{\partial \bar{u}}{\partial \Phi}}_{4}\right) - \underbrace{\bar{w}^{\star}\frac{\partial \bar{u}}{\partial z}}_{5} + \underbrace{\frac{1}{\rho_0 \cdot \mathrm{a}\cdot\cos(\Phi)}\vec{\bigtriangledown}\cdot\vec{F}}_{6} + \underbrace{\bar{X}}_{7}. \tag{2.20}$$

The term number 1 describes the change of the zonal-mean zonal flow. When looking at the polar cap, this is equivalent to changes of the polar vortex. The term number 2 describes the mean meridional circulation which is dependent on the heat flux and stability. The influence of the coriolis force on the zonal-mean zonal flow is described in term 3. Derivatives of the mean meridional circulation can be transported across latitudes, described by term 4. Derivates of the zonal-mean zonal-flow can also be transported vertically, described by term 5. This transport is dependent on the heat flux and stability. Disturbances of the zonal-mean zonal flow leading to derivations of it are usually forced by anomalously strong upward propagating waves. This is described by term 6, the Eliassen-Palm flux. It is dependent on densitiy, turbulence and stability. Processes which are typically not resolved by models, such as friction and small-scale gravity waves, are described by term 7.

2.2 Dynamics of Sudden Stratospheric Warming Events

2.2.1 Theoretical Description by the Model of Matsuno (1971)

Matsuno (1971) proposes a simple numerical model to show the development of SSW events originating from tropospheric wave forcing. It is based on the adiabatic, geostrophic potential vorticity equation which can be derived from the Navier-Stokes equation, equation (2.6). In a first step the so-called vorticity equation is obtained by taking the curl of it. For the interaction between the troposphere and stratosphere, only the vertical component is relevant:

$$\left(\frac{\partial}{\partial t} + u\frac{\partial}{\partial x} + v\frac{\partial}{\partial y} + w\frac{\partial}{\partial z}\right)\vec{\zeta}_z = \mathrm{f}\left(\frac{\partial u}{\partial x} - \frac{\partial v}{\partial y}\right) + \frac{1}{\rho}\left(\frac{\partial}{\partial x}\frac{\partial p}{\partial y} - \frac{\partial}{\partial y}\frac{\partial p}{\partial x}\right) + F_{\mathrm{fz}}. \tag{2.21}$$

The vorticity $\vec{\zeta}$ with its vertical compenent ζ_{z}, is also called the relative vorticity of an air parcel and measures the local rotation. It is defined as:

$$\vec{\zeta} = \vec{\bigtriangledown} \times \vec{u},\ \zeta_{\mathrm{z}} = \left(\frac{\partial v}{\partial x} - \frac{\partial u}{\partial y}\right). \tag{2.22}$$

In a next step, adiabatic conditions are assumed, meaning that neither heat nor mass is exchanged by the air parcel with its environment (Holton, 2010). This leads to the neglection of friction, since friction leads to exchange of mass and heat between the air parcel and its surroundings.
Besides the relative vorticity, also the potential vorticity can be used to express the rotation of an air parcel. It is a combination of the Earth's planetary vorticity and the local vorticity of the air parcel, relative to the potential temperature. The potential temperature can thereby be used as a measure of height and the potential vorticity expressed in isentropic coordinates:

$$P = \frac{1}{\rho}\left(2\Omega + \vec{\nabla} \times \vec{u}\right)\vec{\nabla} \cdot \Theta. \tag{2.23}$$

In spherical, isentropic coordinates, the potential vorticity is written as:

$$P \equiv q = \frac{1}{\rho}\left[-\frac{\partial v}{\partial z}\frac{\partial \Theta}{\mathrm{a}\cos(\theta)\partial\lambda} + \frac{\partial u}{\partial z}\frac{\partial \Theta}{\mathrm{a}\partial\theta} + \left(2\Omega\sin(\theta) + \frac{\partial v}{\mathrm{a}\cos(\theta)\partial\lambda} - \frac{\partial[u\cos(\theta)]}{\mathrm{a}\cos(\theta)\partial\theta}\right)\frac{\partial\Theta}{\partial z}\right], \tag{2.24}$$

with terms containing the vertical velocity and the Coriolis force. Terms proportional to the cosine of latitude are neglected and the distance to the Earth is set constant to the Earth's radius a.
The vorticity equation, equation (2.21), is then expressed in spherical coordinates with the potential vorticity used instead of the relative vorticity. This results finally in the adiabatic, geostrophic potential vorticity equation. Matsuno (1971) uses this equation in a simple, comprehensive form in his model:

$$\left(\frac{\partial}{\partial t} + \bar{\omega}\frac{\partial}{\partial\lambda}\right)\mathscr{L}_p(\phi) + \frac{\partial\bar{q}}{a\,\partial\theta}\,v = 0,\ \bar{\omega} = \frac{\bar{u}}{\mathrm{a}\cos(\theta)}. \tag{2.25}$$

The zonal mean angular velocity of the air parcel is expressed with $\bar{\omega}$. It is important to note, that v is the disturbance velocity in latitudinal direction in Matsuno's notation, and not, as before, the velocity in y-direction. To describe the generation of potential vorticity from the disturbance heights of isobaric surfaces ϕ, Matsuno uses an operator $\mathscr{L}$. This operator is dependent on the latitude θ, the longitude λ, the height z, the pressure p, the Earth's angular speed of rotation Ω and radius a as well as the Brunt-Väisäla frequency N. The potential vorticity in isentropic coordinates is given as $\bar{q}$.

Using an alternative expression for v leads to:

$$\left(\frac{\partial}{\partial t} + \bar{\omega}\frac{\partial}{\partial\lambda}\right)\mathscr{L}(\phi) + \frac{\partial\bar{q}}{\partial\theta}\frac{1}{\sin(\theta)^2\cos(\theta)}\frac{\partial\phi}{\partial\lambda} = 0. \tag{2.26}$$

This differential equation is now solved numerically in Matsuno's model. The wave solution for equation (2.26) uses thereby the following ansatz, introducing a new variable ψ:

$$\phi(\lambda,\theta,z,t) = \mathrm{e}^{\mathrm{i}m\lambda}\mathrm{e}^{\frac{z}{2\mathrm{H}}}\psi(\theta,z,t), \tag{2.27}$$

$$\bar{\phi}(\lambda,\theta,z,t) = \mathrm{e}^{\frac{z}{2\mathrm{H}}}\bar{\psi}(\theta,z,t). \tag{2.28}$$

The advantage of this new variable is the reduced dependency on only three variables, latitude, height and time, instead of four. The longitudinal dependence is expressed with exponential functions containing the longitudinal wavenumber m. Without disturbances, $\psi(\theta,z,t) = 0$.

Matsuno (1971) investigates the development of SSW events from tropospheric wave disturbances that start on the surface. Therefore, the lower boundary conditions of his model are expressed as:

$$\psi(\theta, z = 0, t) = F(\theta, t), \frac{\partial \bar{\psi}}{\partial t} = 0. \tag{2.29}$$

A perturbation of ψ is thereby equivalent to a perturbation of $\bar{u}$ or $\bar{T}$. The forcing is described as a sine peaking at a specific latitude, here 60°N, in combination with a function $f(t)$ describing the suggested treatment of the disturbance by the model:

$$F(\theta, t) = \sin[\pi(\theta - 30^\circ)/60^\circ]\, \phi_{\max} f(t), 30^\circ \leq \theta \leq 90^\circ, \tag{2.30}$$

$$F(\theta, t) = 0, \text{otherwise}. \tag{2.31}$$

At the top of Matsuno's model in 110 km, the disturbance is 0:

$$\psi(\theta, z = 110\,\text{km}, t) = 0 \frac{\partial \bar{\psi}}{\partial t} = 0. \tag{2.32}$$

2.2.2 Development from Tropospheric Wave Forcing

In the following, the development of an SSW event in a typical wintertime stratospheric circulation from a wavenumber-2 tropospheric wave disturbance is shown according to Matsuno (1971). The typical wintertime circulation in the middle stratosphere is marked by the westerly polar night jet encircling the pole. In Matsuno's notation, this case is called „C2“ and comprises a sphere with a model wall at the equator, thus, modelling only the flow in the northern hemisphere. The typical wintertime wind distribution in the troposphere and stratosphere contains continuous westerly wind conditions between 20°N and the pole with maximum westerly winds in 10 km and 65 km height (Figure 2.1 left). This circulation can be disturbed by mechanically, thermally or turbulently excited waves propagating from the troposphere into the stratosphere (Schneidereit et al., 2017). The modelled wavenumber-2 disturbance fits roughly to the wavenumber-2 disturbance observed before the sudden stratospheric warming event in 1963 (Figure 2.1 right). Thus, the simple model by Matsuno (1971) serves the purpose of demonstrating the qualitative development of sudden stratospheric warming events.

Tropospheric planetary-scale waves, such as Rossby waves, can only propagate in westerly wind fields (Baldwin and Dunkerton, 1999). This is shown by the Charney-Drazin criterion for wave propagation (Holton, 2010):

$$0 < \bar{u} - c < u_c, u_c = \mathrm{f}\left(\frac{1}{m}\right)^2. \tag{2.33}$$

This criterion essentially states that the difference between the mean zonal background flow $\bar{u}$ and the wave's group velocity c has to be greater 0 but also smaller than a critical velocity u_c. This critical velocitiy itself is a function of the wavenumber m. For waves with wavenumber 1, the critical velocity is higher than for waves with wavenumber 2 and higher. Waves with wavenumber 1 can therefore propgate into stronger mean background zonal flows than waves with wavenumber 2 with the same group velocity. For stationary waves, the group velocity is 0 and the penetrating of upward propagating waves solenmly depends on the mean background zonal flow.

In the troposphere and stratosphere, the mean background zonal flow is westerly, making $\bar{u}$ positive (Figure 2.1 left). In the polar stratosphere, this flow resembles basically the polar vortex which is then perturbed by upward propagation planetary-scale waves. The easterly acceleration of these waves increases with height as the amplitude of the planetary-scale wave increases with decreasing air density (Matsuno, 1971; Kidston et al., 2015). According to Charlton and Polvani (2007) SSW events are preceded by strong polar vortex conditions, meaning that the mean background flow velocity is largely positive. Following Matsuno (1971) easterly propagating waves with a positive group velocity can propagate into this strong mean background zonal flow. Westward propagating waves with a negative group velocity cannot.

In regions with easterly mean background flow, for example in the region of the upper stratosphere and lower mesosphere, $\bar{u}$ turns negative. When easterly propagating waves enter these regions, it is impossible to meet the lower condition of the Charney-Drazin criterion. The amplitude of the easterly propagating waves dampens rapidly (Figure 2.2 left). The waves break and decelerate the westerly jet by depositing easterly angular momentum (Matsuno, 1971; Kidston et al., 2015). Kidston et al. (2015) explain the deceleration of the westerly jet as an effect of the conservation of angular momentum and mass. When breaking waves deposit angular momentum in the stratosphere, the circumpolar jet slows down and transports momentum to the pole to conserve angular momentum. The stratospheric circulation becomes less symmetric and the polar vortex can be displaced off the pole and in some cases eventually break up (Limpasuvan et al., 2004; Butler et al., 2015). This can be detected in the geopotential heights on a fixed pressure level, where the vortex core is located at the lowest geopotential height values (Figure 2.3). The geopotential height is defined as:

$$Z = \frac{\Phi}{g_{\mathrm{sfc}}}, \quad \Phi = \int_0^h g \, \mathrm{d}z, \tag{2.34}$$

with the geopotential Φ and the gravitational constant at the surface g_{sfc}. When substituting g according to the ideal gas law, the geopotential can be expressed as:

$$\Phi = \int_0^h \frac{p(z)}{\mathrm{R_l} T(z)} \mathrm{d}z. \tag{2.35}$$

This means, that the geopotential height on a given pressure level $p(z)$ increases when the temperature increases (Limpasuvan et al., 2004).

To regain the geostrophic balance in the stratosphere after the disturbance of the stratospheric polar vortex, a mean-residual circulation is induced which moves mass into the stratosphere over the polar cap (Coy and Pawson, 2015; Kidston et al., 2015). Due to continuity, the additional mass over the pole is transported downward, while in the lower latitudes mass is transported upward (Matsuno, 1971; Kidston et al., 2015; Limpasuvan et al., 2004). This leads to an adiabatic warming and a high pressure system at the surface on the pole and adiabatic cooling and a surface low pressure system in lower latitudes. Over the pole, the sinking of air masses leads to warm temperature anomalies in the regions below and low temperatures in the regions above the region of the sinking motion (Figure 2.2 right). When this process happens in the course of a few days, the warming over the pole is called a „sudden stratospheric warming“.

2.2.3 Downward Propagation of Stratospheric Anomalies

Matsuno (1971) calls the interaction between the breaking waves and easterly background flow „critical layer interaction“, where the critical layer is the region with easterly winds. The breaking of waves leads to the formation of a new critical layer in the region of breaking. Thus, leading to a downward shift of the positive temperature and easterly wind anomalies. Above the critical layer, the polar jet recovers slowly, driven by radiative cooling due to absence of wave activity (Baldwin and Dunkerton, 1999, Tripathi et al., 2015). The recovery of the polar vortex takes on average 10 days in the middle stratosphere and 40 days in the lower stratosphere due to different radiative dumping scales (Charlton and Polvani, 2007). It is only possible during polar night as the increased radiative heating in spring due to the rising sun prevents the reformation of the polar vortex.

The critical layer itself, respectively the stratospheric anomalies, can descend down into the troposphere and change surface weather pattern (Baldwin et al., 2003). A particularly sensitive area for the coupling between the troposphere and stratosphere is the lower stratosphere (Charlton and Polvani, 2007). Stratospheric anomalies persist there for several weeks up to 2 month, being prevented from frictional dissipation by the Coriolis force (Limpasuvan et al., 2004). In the lower stratosphere, the anomalies induce non-local dynamical effects that influence the tropospheric circulation and sometimes even propagate down to the surface (Karpechko et al., 2018; Baldwin et al., 2003; Hinssen et al., 2011). This results then in one of the strongest dynamical couplings between troposphere and stratosphere (Charlton and Polvani, 2007). Usually though, there is a hydrostatic balance, a geostrophic balance and a thermal-wind balance at the tropopause which hinder stratospheric anomalies from entering the troposphere. The hydrostatic balance can be expressed with the hydrostatic approximation which results from the balance between the pressure gradient force and buoyancy:

$$\frac{\mathrm{d}p}{\mathrm{d}z} = -\rho \cdot g. \tag{2.36}$$

The geostrophic balance describes the balance between the Coriolis force and the pressure gradient force and the thermal wind balance is given with the thermal wind equation:

$$-\frac{\partial \vec{v_g}}{\partial p} = \frac{\mathrm{R_l}}{\mathrm{f}p} \cdot \vec{k} \times \vec{\bigtriangledown}_{\mathrm{p}} T. \tag{2.37}$$

This equations describes the vertical change of the geostrophic wind $\vec{v_g}$ in hydrostatic approximation.

These balances can be disturbed when the momentum forcing in the stratosphere is strong and persistent enough to penetrate through the tropopause to the surface (Limpasuvan et al., 2004). This so-called „downward control“ principle is controversially discussed in literature. According to Limpasuvan et al. (2004) the main reason for discussion is the small mass of the stratosphere in comparison to the troposphere. In winter, the stratosphere contains less than 25% of the atmospheric mass of the extratropics which leads to a larger momentum forcing in the troposphere than in the stratosphere. The principle of downward control is therefore probably only working, when the stratospheric anomalies project onto the modes of tropospheric variability, such as the NAO pattern well. If this is the case, stratospheric anomalies can descend into the troposphere and influence surface weather.

The wind and temperature anomalies caused by an SSW event are related via the thermal wind equation. Integrating this equation between two pressure levels leads to thermal wind $\vec{v_T}$:

$$\vec{v_T} = \frac{R_l}{f} \ln\left(\frac{p_0}{p_1}\right) \vec{k} \times \vec{\bigtriangledown}_p \bar{T} \tag{2.38}$$

and is dependent on the mean temperature $\bar{T}$ of the atmospheric layer between the pressure levels p_0 and p_1. When looking at the lower pressure level, the warm temperature anomalies precede the easterly wind anomalies (Limpasuvan et al., 2004). According to Limpasuvan et al. (2004) this time-lag between warming temperatures and easterly winds is around 10 days in 10 hPa height.
When the stratospheric stratopsheric anomalies propagate down into the troposphere, the mass, and therefore the pressure, is slowly redistributed. The change in pressure is thereby proportional to a change in temperatures according to the ideal gas equation:

$$p = R_l T g. \tag{2.39}$$

This redistribution of mass leads to a decrease of the tropopause height through up- and downwelling processes, an increase of pressure over the polar cap and an reduction of it over the mid-latitudes. This is the manifestation of the negative phase of the Arctic Oscillation (Baldwin et al., 2003; Wang et al., 2010). A balancing movement of airmasses transports the cold polar surface air from the pole into the mid-latitudes and further equatorwards, which leads to cold waves in the northern hemisphere mid-latitudes. Temperature changes below the tropopause are though much less than above it due to the lower lapse rate of the troposphere (Kidston et al., 2015).
In literature, there are numerous time scales for the downward propagation of stratospheric anomalies discussed, reaching from days to 2 months (Baldwin et al., 2003; Tripathi et al., 2015; Manney et al., 2009). In general, the downward propgation is faster in the beginning of the winter than at its end (Baldwin and Dunkerton, 1999). According to Charlton-Perez et al. (2018) the response time from the troposphere to changes in the stratospheric circulation is on average 20 days.
An open research question according to Kidston et al. (2015) is the exact role of tropospheric eddy feedbacks which are an important factor in the troposphere-stratosphere coupling. They are initialized when the mass between the troposphere and stratosphere is redistributed. These eddy feedbacks are associated with the altering of tropospheric weather systems and the propagation of tropospheric waves which influence the strength and position of the tropospheric jets in the high- and mid-latitudes.

2.2.4 Precursors for Tropospheric Wave Forcing

Especially before the development of SSW events featuring a breakup of the polar vortex in the stratosphere, the polar vortex is reduced in size and strength by the breaking of upward propagating planetary-scale waves at the vortex edges (Baldwin and Dunkerton, 1999; Limpasuvan et al., 2004; Charlton and Polvani, 2007). This is called „preconditioning“ of the polar vortex. It leads to a smaller moment of inertia of the polar vortex due to its reduced size (Limpasuvan et al., 2004). Therefore, poleward and upward propagating planetary-scale waves can enter the stratosphere more easily and lead to SSW events (Manney et al., 2009; Limpasuvan et al., 2004). According to Charlton and Polvani (2007) a typical situation for preconditiong is a largely positive zonal

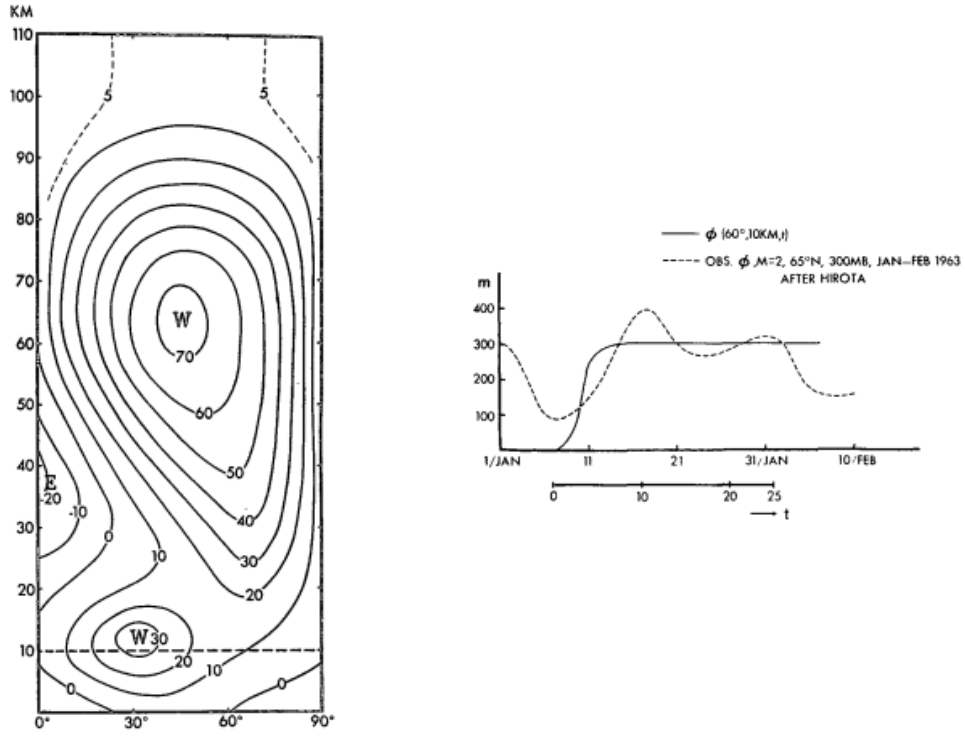

Figure 2.1: **Set-Up of Matsuno's Model for a Wavenumber-2 Disturbance in a Typical Northern Hemisphere Wintertime Wind Distribution.** Figure 9 of Matsuno (1971) (left): „Initial distribution of zonal winds, adopted as the initial condition for cases C1-C3". Figure 3 of Matsuno (1971) (right): „The amplitude of waves forced at the lower boundary (solid line). The dashed line shows the observed amplitude of the m=2 wave at 300 mb in January-February 1963 (data from Dr. Hirota)."

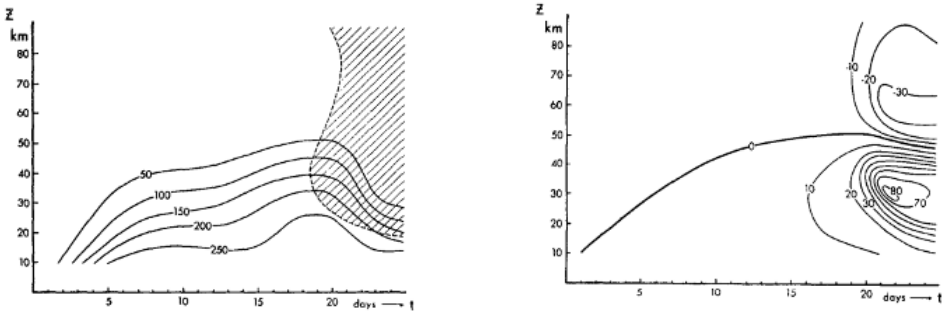

Figure 2.2: **Wave Amplitude and Temperature, Calculated with Matsuno's Model.** Figure 12 of Matsuno (1971) (left): „Time-height section of the wave amplitude at 60°N, case C2. Hatched area indicates easterly mean flow." Figure 14 of Matsuno (1971) (right): „Time-height section of temperature [deviation (°C) from the initial temperature] at the pole, case C2."

wind anomaly in the troposphere and stratosphere, centered at 70°N. This can be linked to positive mean sea level pressure anomalies over the North Atlantic ocean, Alaska and the Ural which are often observed before SSW events (Karpechko et al., 2018). According to Lee et al. (2019) the high pressure system over the Ural is amplified by Rossby wave-breaking and co-occurs with the

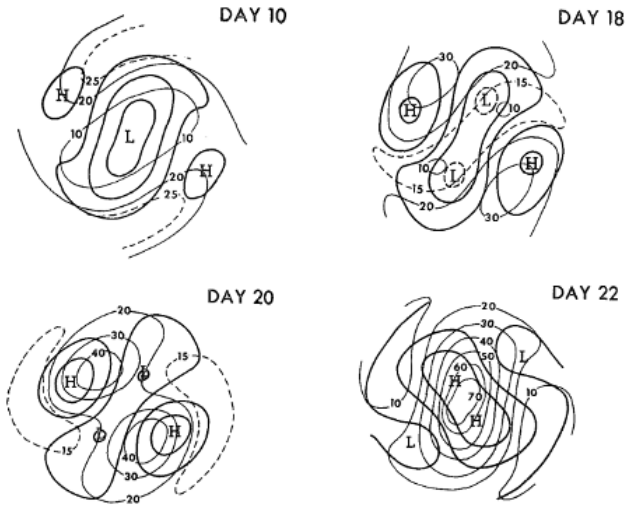

Figure 2.3: **Time Evolution of Isobaric Heights and Temperature, Calculated with Matsuno's Model.** Figure 15 of Matsuno (1971): „Time evolution of isobaric heights (500 m contours, thick lines), temperature (°C, thin lines), and the surface auf p= p_0 exp(-30 km/H) ≈13 mb for case C2. Temperature is shown as deviation from its initial value at the pole. The contours cover the area north of 30°N."

so-called „Scandinavia-Greenland dipole" which is characterized by an anomalously strong mean sea level pressure gradient between Scandinavia and Greenland. In 35% of the cases, this dipole is observed in the 15 days prior to the central date of the SSW event. The Scandinavia-Greenland dipole requires the poleward shift of the North Atlantic storm track which is associated with the positive phase of the NAO. This NAO+ phase itself is often associated with a strengthened polar vortex. This is a typical situation observed prior to an SSW event (Lee et al., 2019; Charlton and Polvani, 2007).

Another often observed situation before SSW events is blocking which is often mentioned in literature as a typical precursor for SSW events (Tripathi et al., 2015).

Blocking patterns over the Atlantic ocean often precede SSW events which lead to a displacement of the polar vortex off the pole (Yu et al., 2018; Martius et al., 2009). According to Martius et al. (2009) their frequency maxima are located east of Greenland and over Scandinavia. If these SSW events take place in early winter, usually a strong Aleutian high is observed prior to the event (Baldwin and Dunkerton, 1999). Both situations lead to a wavenumber-1 flow in the troposphere according to Martius et al. (2009). The corresponding, upward propagating Rossby wave is tilted westwards with height and shows a baroclinic structure. Blocking patterns over either the Pacific ocean or both, the Atlantic and Pacific ocean, with frequency maxima over the eastern Pacific, Alaska and west of Greenland, often precede SSW events which lead to a split of the polar vortex. A wavenumber-2 tropospheric circulation is developed. The upward propagating Rossby waves are also tilted westward with height but show a more barotropic structure. This modulation of upward propagating planetary-scale tropospheric waves, such as Rossby waves, is confirmed by Woollings et al. (2018). These waves can penetrate into the stratosphere more easily and interefere there with climatological planetary waves when the tropospheric block is located beneficially.

Especially in the case of SSW events leading to a split of the polar vortex, the location of the tropospheric blocks relative to each other matters. When the westward with height tilted upward propagating Rossby waves are located beneficially, the tropospheric wave with wavenumber 2 interferes constructively with the climatological stratospheric wave with wavenumber 1. In the upper stratosphere, this can lead eventually to the split of the polar vortex. It is also possible that first an anomalously strong upward propagation of Rossby waves with a wavenumber 1 is observed followed by an anomalous upward propagation of Rossby waves with wavenumber 2 (Tripathi et al., 2016). According to Martius et al. (2009) in the case of SSW events which lead to a displacement of the polar vortex off the pole, a beneficial location of the tropospheric wave with wavenumber 1 and the climatological stationary wave pattern is important. The climatological stationary wave pattern is enhanced which can lead to the development of an SSW event when the upward propagating Rossby wave, induced by the block, penetrates into the stratosphere. According to Tripathi et al. (2015) these upward propagating Rossby waves have to be anomalously strong for longer than a week in order to trigger an SSW event. Nevertheless, the blocking duration is not the dominant factor of the linkage between blocks and SSW events. Furhtermore, blocking might be necessary for the development of an SSW event but it is not found to be sufficient by Manney et al. (2009). This is confirmed by the fact that some models produce the observed blocking patterns but not the following SSW (Tripathi et al., 2016).

Controversially discussed as a precursor of SSW events is the snow cover extent in early winter which may enhances the upward propagation of planetary-scale waves (Tripathi et al., 2015). Another open research question is the linkage between SSWs and certain phases of the Madden Julian Oscillation (MJO) (Tripathi et al., 2015). When MJO and La Niña conditions are phased beneficially, they enhance a wavenumber-2 tropospheric wave-forcing (Schneidereit et al., 2017). According to Schneidereit et al. (2017) La Niña conditions also favor blocking anticyclones over the Pacific ocean and north of Scandinavia. The MJO, especially phase 7 and 8, form a low pressure anomaly, centered over the central North Pacific, and a high pressure anomaly centered over Canada. This leads to a quasi-stationary pattern of troughs and ridges, enhancing a wavenumber-2 flow pattern in the troposphere. When MJO phases 7 and 8 co-occur with La Niña conditions, this quasi-stationary pattern is strengthened, leading to an amplification of upward propagating Rossby waves.

The linkage between the different states of the El Niño-Southern Oscillation (ENSO) and SSW events is also discussed controversially in literature. According to Tripathi et al. (2015) some studies find that events occur twice more likely during El Niño than during La Niña but other studies do not find a difference between the two phases. One reason for this discrepancy might the difficulty to separate the influence of ENSO and the Quasi-Biennual Circulation (QBO) (Lehtonen and Karpechko, 2016). During the QBO east phase, weak vortex events including SSWs are twice as likely as during the QBO west phase (Baldwin and Dunkerton, 2001; Tripathi et al., 2015).

Changes in the Brewer-Dobson Circulation (BDC) are another discussed phenomena which possibly influences the occurrence of SSW events (Zhang and Tian, 2019). According to Zhang and Tian (2019) the BDC influences not only the state of the polar vortex but also the tropospheric jet streams and surface temperatures. When the BDC is enhanced, the meridional transport of air masses to the polar stratosphere is increased. The temperature over the polar cap rises, leading to a weaker polar vortex and possibly SSW events.

Other discussed influences on the state of the polar vortex are volcanic eruptions, anthropogenic changes, including increased greenhouse gas concentrations, and the solar cycle (Butler et al., 2015).

2.2.5 Resonant Excitation of the Polar Vortex

In some cases, SSW events are observed without the typical tropospheric precursors or vortex preconditioning (Tripathi et al., 2015). According to Tripathi et al. (2015) in these cases the stratospheric polar vortex is excited by small planetary-scale waves in such a way that resonance is created. Although an enhanced upward propagation of planetary-scale waves from the troposphere into the stratosphere does not take place, the polar vortex is deformed or even disrupted. This mechanism is called the „resonant excitation“ of the polar vortex. According to Tripathi et al. (2015) a resonant excitation of a polar vortex in a baroclinic structure leads to the displacement of the vortex off the pole, a resonant excitation of the polar vortex in a barotropic structure to a breakup of it. Especially in the latter case, very small changes in the tropospheric wave forcing or the stratospheric circulation can lead eventually to very large changes of the polar vortex state.

2.3 Characteristics of Sudden Stratospheric Warming Events

SSW events are characterized in the stratosphere, in heights of 30 to 50 km, by a temperature increase of 30 to 40 K in the time range of a few days (Butler et al., 2015). As the land-sea contrast in the southern hemisphere is not favorable for the formation of strong planetary-scale waves which are needed for the occurrence of SSW events, SSWs occur almost exclusively in the northern hemisphere (Butler et al., 2015). In extreme cases, also called major SSWs, the anomalously high upward-propagation of tropospheric planetary-scale waves leads to a reversal of the stratospheric polar night jet from westerlies to easterlies (Butler et al., 2015; Charlton and Polvani, 2007; Karpechko et al., 2018). The polar vortex is then either displaced off the pole or split into two parts of comparable size (Figure 2.4; Butler et al., 2015, Charlton and Polvani, 2007).
SSW events which lead to a displacement of the polar off the pole are called „displacement-type“ (D-type) events (Charlton and Polvani, 2007). During the displacement of the vortex filament, it is distorted into a „comma-shape“ (Figure 2.4 top). The circulation in the stratosphere is thereby still characterized by a wavenumber-1 structure (Charlton and Polvani, 2007). The occurrence of D-type SSW events is equally likely during the whole winter but due to the increased likelihood of SSW events which lead to a split of the polar vortex in mid-winter, SSW events in early winter are usually D-type events (Baldwin and Dunkerton, 1999; Charlton and Polvani, 2007). In literature, the D-type events occurring in early winter are sometimes referred to as „Canadian Warmings“ (Butler et al., 2015).
SSW events which lead to a breakup of the polar vortex into two parts of comparable size are called „split-type“ (S-type) events (Figure 2.4 bottom). Nearly half of all SSW events belong to this type (Charlton and Polvani, 2007). During these events, the circulation in the stratosphere resembles a wavenumber-2 structure (Charlton and Polvani, 2007). In general, S-type events are characterized by a more sudden and deeper extending wind-reversal than D-type events (Butler

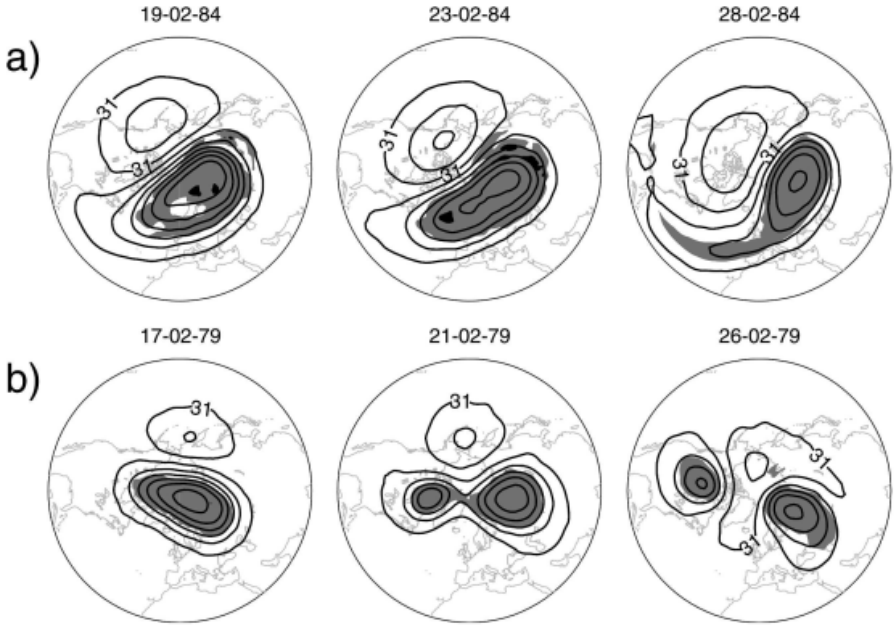

Figure 2.4: **Different Types of SSW events.** Figure 1 of Charlton and Polvani (2007): „Polar stereographic plot of geopotential height (contours) on the 10-hPa pressure surface. Contour interval is 0.4 km, and shading shows potential vorticity greater than 4.0×10^{-6} $\mathrm{Kkg^{-1}m^2s^{-1}}$. (a) A vortex displacement type warming that occurred in February 1984. (b) A vortex splitting type warming that occurred in February 1979. “

et al., 2015). Middle-stratospheric temperatures are increased slightly stronger and influenced up to 20 days longer (Charlton and Polvani, 2007). S-type SSW events show a clear seasonality with the highest probability of occurrence in January and February (Charlton and Polvani, 2007).

2.4 Downward Impact of Sudden Stratospheric Warming Events

2.4.1 Blocking in the Middle Troposphere

The term atmospheric „blocking“ is not defined in a unique way. In general, a large-scale meridional, horizontal tropospheric circulation which leads to changes in the prevailing zonal flow and storm tracks is referred to as blocking (Liu, 1994; Woollings et al., 2018). Other common characteristics found in literature are persistence and quasi-stationarity (Woollings et al., 2018). According to Liu et al. (1994) a persistence criterion is usually applied to exclude minor variability in the troposphere not related to the blocking pattern. Depending on the study, time scales from a single day to a week are given as the minimal duration of blocking (Tibaldi and Molteni, 1990; Tripathi et al., 2015). Although blocking patterns are often indicated as being especially persistent, it has to be kept in mind that they are generally not more persistent than the zonal flow regime (Liu, 1994).

Typical blocking situations are stationary ridges embedded in a large-amplitude Rossby wave pattern with a phase-speed near zero (Figure 2.5a); Woollings et al., 2018). The so-called „Ω“ block

is not a stationary ridge but also associated with a stationary Rossby wave pattern (Figure 2.5b); Woollings et al., 2018). According to Buehler et al. (2011) it is one of the two dominant blocking patterns over the North Atlantic region. In comparison with stationary ridges, its amplitude is generally larger and it features some closed contours of geopotential height isolines inside the high pressure area (Woollings et al., 2018). This high pressure area is usually called the „blocking anticyclone“ (Buehler et al., 2011). Upstream and downstram of it are low pressure systems located forming an Ω which is visible in the 500 hPa geopotential height isolines (Buehler et al., 2011; e.g. Figure 6.11 top).

The second dominant blocking pattern over the North Atlantic ocean is a „high over low“ pattern at the same longitude (Figure 2.5e); Buehler et al., 2011). This kind of blocking pattern develops when large-scale Rossby waves break anticyclonically (Figure 2.5d); Woollings et al., 2018). In literature, it is also called a „Dipole-“ or „Rex-“ block, referring to the first studies of atmospheric blocking done by Rex in 1950 (Woollings et al., 2018; Liu, 1994).

Blocking frequencies are generally higher in winter than in summer, with the blocking anticyclones being usually located over the oceans in winter and over the continents in summer (Woollings et al., 2018). In winter, blocking is often observed before SSW events and therefore seen as a typical tropospheric precursor of these events (Martius et al., 2009).

According to Domeisen et al. (2020) blocking furthermore plays an important role in determining the tropospheric response of SSW events. Especially the so-called European blocking is important for the formation of European cold waves after SSW events. When the European blocking, a ridge over the British Isles, is present at the time of the formation of the SSW, colder than usual 2 metre temperatures are found over central and northern Europe after the event. The lowest anomalies are observed 20 days and 40 days after the SSW when simultaneously a so-called Greenland blocking situation is present. This blocking situation is characterized by an enhanced ridge over Greenland, leading to lower temperature anomalies than usually over Europe. This link between blocking and the tropospheric response of SSW events is though not confirmed by Garfinkel et al. (2017) who state that the tropospheric response to an SSW event is independent of the tropospheric state.

Controversially discussed in literature is the question if SSW events have an influence on the occurrence of blocking. Charlton-Perez et al. (2018) state that blocking itself is not influenced by the state of the polar vortex, as it occurs usually during neutral polar vortex states. This is in contrast to Woollings et al. (2018) who mention a significant increase of blocking in the high-latitudes and a longer duration of this blocks after SSW events, especially in the region of the Atlantic ocean.

According to Woollings et al. (2018) independent of the possible coupling to SSW events, blocking situations can influence European surface weather by changing the prevailing zonal flow which transports relatively warm oceanic air into Europe. During a blocking situation, relatively cold polar air is transported downstream into Europe leading possibly to cold waves. Only a minor effect in winter is the unusual cooling of the region below the blocking anticyclone due to the reduced cloud cover.

Besides the influence on European temperatures, blocking patterns over the North Atlantic ocean influence precipitation (Woollings et al., 2018). The actual influence of the blocking system on temperatures and precipitation depends strongly on its geographical location and type (Woollings et al., 2018). Blocking patterns near the British Isles, for example, influence surface temperatures and precipitation over Europe (Buehler et al., 2011). According to Woollings et al. (2018) below

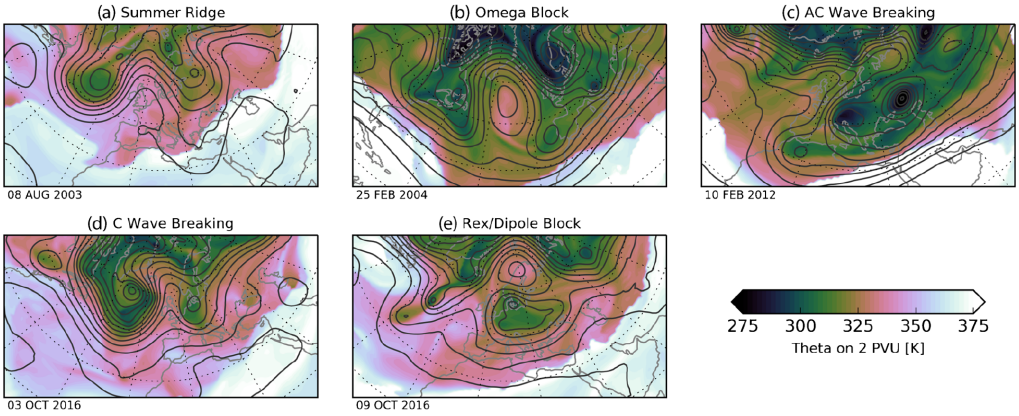

Figure 2.5: **Examples of North Atlantic blocks.** Figure 1 of Woollings et al. (2018): „Snapshots of (colour shading) potential temperature θ on the dynamical tropopause (PV = 2 PVU) and (contour lines) geopotential height at 500 hPa (contour spacing 60 m) for the dates indicated. Data is from ERA-Interim“.

the blocking anticyclone precipitation is drastically reduced to zero, while below the low pressure systems up- and downstream of it precipitation is increased strongly. This is due to the forced pathway of storms around the anticyclone. The stagnant air masses below the anticyclone lead furthermore to an accumulation of pollutants which affects air quality.
Unlike a possible influence of blocking events on the stratospheric circulation, the severity of changes in temperature and precipitation due to a blocking situation is largely depending on its persistence leading up to several weeks of anomalous surface weather. This is confirmed by Buehler et al. (2011) who found that the number of days with cold spells increase with the duration of the blocking situation.

2.4.2 The Mid-Latitude North Atlantic Jet Stream in the Lower Troposphere

Tropospheric zonal-mean winds are decreased by up to $5\,\mathrm{ms}^{-1}$, when stratospheric anomalies, caused by an SSW event, are present in the lower stratosphere (Lehtonen and Karpechko, 2016). When these anomalies influence the troposphere, usually the mid-latitude tropospheric jet stream over the North Atlantic ocean is displaced from its climatological position (Afargan-Gerstman and Domeisen, 2020). According to Afargan-Gerstman and Domeisen (2020) the shift of the jet stream starts on average 10 days after the occurrence of the SSW event and persists in its new position up to 1 month.
A fraction of 2/3 of the SSW events show a zonally symmetric tropospheric response, leading to an equatorward displacement of the mid-latitude jet stream over the North Atlantic ocean. This co-occurs with the negative phase of the NAO and a weaker than usual strom track over Europe. The remaining 1/3 of the SSW events are followed by a zonally asymmetric tropospheric response, leading to a poleward displacement of the mid-latitude jet stream over the North Atlantic ocean. The North Atlantic storm track is then stronger than usual.
Besides the stratospheric variability, also the internal tropospheric variability, such as blocking patterns, can influence the position of the mid-latitude jet stream. Woollings et al. (2018) describe the onset of a block by a poleward displacement of subtropical air in the time range of 1-3 days.

This creates an extended ridge, which penetrates into the midlatitude jet stream. The jet stream can then be displaced southward or split, with its remnants located up- and downstream of the blocking pattern (Manney et al., 2009; Martius et al., 2009).

2.4.3 The North Atlantic Oscillation at the Surface

One of the most important factors that determine wintertime surface temperatures in the northern hemisphere is the NAO (Wang and Chen, 2010). It describes the oscillation of atmospheric air masses in the northern Atlantic ocean (Hurrell et al., 2003). This oscillation of air masses leads to a varying strength of the climatological high, located in the area of the Azores, and the climatological low, located in the region of Iceland. For the development of the two phases of the NAO, called NAO+ and NAO-, Rossby wave breaking plays a substantial role (Benedict et al., 2004). According to Benedict et al. (2004) synoptic-scale wave disturbances travelling from west to east are transformed into north-south direction, forming the typical NAO pressure dipole between the areas around Iceland and the Azores. The positive phase of the NAO is preceded by two anticyclonic Rossby wave breaking events. One over the west coast of North America and the other one over the subtropical North Atlantic ocean. The NAO+ phase is therefore characterized by a stronger than usual low pressure system in the region of Iceland and a stronger than usual high pressure over the region of the Azores (Figure 2.6 left, top plot; Leckebusch et al., 2008). The pressure over the polar cap is lower than usual and an enhanced frequency of high pressure systems, associated with blocking, is observed over Europe (Baldwin et al., 2003; Blessing et al., 2005).
The negative phase of the NAO is preceded by a cyclonic Rossby wave breaking over the North Atlantic ocean (Benedict et al., 2004). This NAO phase is characterized by a weaker than usual low pressure system in the region of Iceland and a weaker than usual high pressure system over the region of the Azores (Figure 2.6 left, bottom plot; Leckebusch et al., 2008). The mid-latitude jet stream over the North Atlantic ocean is displaced southward with blocking patterns mostly located over the western North Atlantic ocean and south of Greenland (Butler et al., 2015; Blessing et al., 2005).
The NAO is part of the AO which spans across the northern part of the northern hemisphere and includes the polar vortex in the stratosphere (Baldwin and Dunkerton, 1999). Therefore the AO, and subsequently the NAO, are strongly influenced by the state of the polar vortex (Baldwin and Dunkerton, 1999; Baldwin et al., 2003; Blessing et al., 2005). In the stratosphere, a strong polar vortex resembles an AO+ signature, a weak and disorganized polar vortex an AO- signature (Baldwin and Dunkerton, 2001; Lehtonen and Karpechko, 2016). This AO signature propagates downward in approximately 10 days from 10 hPa to the tropopause with the possibility to reach the surface (Figure 2.6 right; Baldwin and Dunkerton, 2001). According to Charlton-Perez et al. (2018) and Afargan-Gerstman and Domeisen (2020) the troposphere over the northern Atlantic ocean is more sensitive to the stratospheric state than over the northern Pacific. According to Charlton-Perez et al. (2018) especially the negative phase of the NAO is sensitive to the stratospheric variability, occurring in 1/3 of all cases after a weak polar stratospheric vortex but only in 5% after a strong polar stratospheric vortex. This sensitivity of the NAO- phase to the occurrence of SSW events is confirmed by Domeisen (2019) as such. But she additionally states that 2/3 of

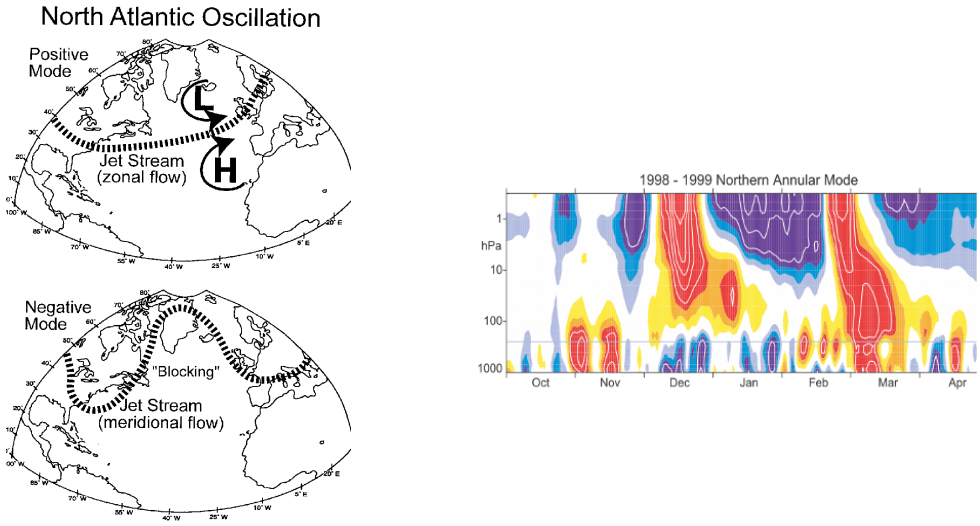

Figure 2.6: **Schematic of the NAO Phases and Downward Propagation of Stratospheric AO Signals.** Figure 1 of Bradbury et al. (2002) (left): „Schematic Illustration of North Atlantic Atmospheric Conditions During Positive (upper panel) and Negative (lower panel) Phases of the North Atlantic Oscillation (NAO). During positive NAO winters the atmospheric pressure gradient between Iceland and the Azores is at a maximum and the mid-latitude westerlies dominate air circulation throughout the region. During negative NAO winters the Icelandic low is weak and Atlantic blocking occurs more frequently.“ Figure 1 of Baldwin and Dunkerton (2001) (right): „Time-height development of the northern annular mode during the winter of 1998 –1999. The indices have daily resolution and are nondimensional. Blue corresponds to positive values (strong polar vortex), and red corresponds to negative values (weak polar vortex). The contour interval is 0.5, with values between $\geq$0.5 and -0.5 unshaded. The thin horizontal line indicates the approximate boundary between the troposphere and the stratosphere.“

the SSW events are either followed by a persistent NAO- phase or a change from NAO+ to NAO- and 1/4 of the SSW are followed by both. Although a non-negligible number of SSW events is followed by the negative phase of the NAO, it has to be kept in mind that less than 1/4 of the NAO- phases observed in winter are preceded by an SSW event (Domeisen, 2019).
Besides a possible influence of SSW events, the negative phase of the NAO is also prone to the influence of the MJO, showing a significantly higher chance of an NAO- phase 10 days after the MJO is in phase 6 (Vitart et al., 2017). Lee et al. (2019) explains this teleconnection with an enhanced vertical heat flux and upward propagation of Rossby waves over the region of the MJO which leads to a warmer stratosphere and a weaker stratospheric polar vortex in winter. This teleconnection from the MJO, in this study the MJO phase 7, to the NAO- phase via the stratosphere is especially likely during La Niña conditions. The NAO- regime can furthermore directly be influence by a teleconnection between ENSO and the North-Atlantic-European region, which is strongest for moderate El-Niño-conditions.

2.4.4 European 2 Metre Temperatures

Especially over Europe and the North Atlantic ocean, a significant influence of SSW events on surface weather is observed (Domeisen et al., 2020). European 2 metre temperatures depend on the phase of the NAO which can be influenced by SSWs (Wang and Chen, 2010; Charlton-Perez

et al., 2018; Afargan-Gerstman and Domeisen, 2020). During the negative phase of the NAO in winter, North America, northern Eurasia and Siberia experience colder than usual 2 metre temperatures (Butler et al., 2015). The midlatitude jet-stream is shifted southward leading to a movement of cold polar air into the mid-latitudes, a so-called „cold air outbreak“ (CAO) (Butler et al., 2015). Since the likelihood of occurrence of NAO- phases is increased after SSW events, an influence of SSW events on European surface temperatures, especially on wintertime cold waves, is suggested (Charlton-Perez et al., 2018).

According to King et al. (2019) especially the cold extremes over Scandinavia are stronger in the 2 months after an SSW while colder than usual mean 2 metre temperatures are found to be present also before the SSW event (Figure 2.7). They propose the hypothesis, that the mean changes in weather patterns are small in the time around an SSW event but the likelihood of cold snaps is increased in the 2 month after the SSW event. Garfinkel et al. (2017) confirm the latter part of this hypothesis. They state that more cold snaps are observed when the polar vortex is in a weak state, for example during an SSW event, than in a strong state. In addition to that, the cold snaps observed during weak vortex states last up to 6 weeks longer than the ones observed during strong vortex states.

The first part of the hypothesis by King et al. (2019) is confirmed by Lehtonen and Karpechko (2016). In their study they find that especially for D-type SSW events, the mean 2 metre temperature anomalies over northern Eurasia are lower before the SSW event than in the month after it. They link the lower 2 metre temperature anomalies in the time before an SSW event to atmospheric blocking situations which modulate the upward propagating Rossby waves, possibly leading to the SSW event.

Blocking itself can also lead to cold waves in winter without an SSW event when the pattern is persistent for longer than a week (Woollings et al., 2018). Then, temperature and moisture anomalies can develop, leading to an increased number of days with colder and drier than usual conditions in the region of the blocking anticyclone (Woollings et al., 2018). According to Lehtonen and Karpechko (2016) this influence of blocking on the 2 metre temperatures is by far stronger than the influence of SSW events. It has also to be kept in mind that the NAO and the eventual European surface temperatures are strongly influenced by the internal troposperic variability which can suppress the stratospheric influence (Tripathi et al., 2015; Domeisen et al., 2020).

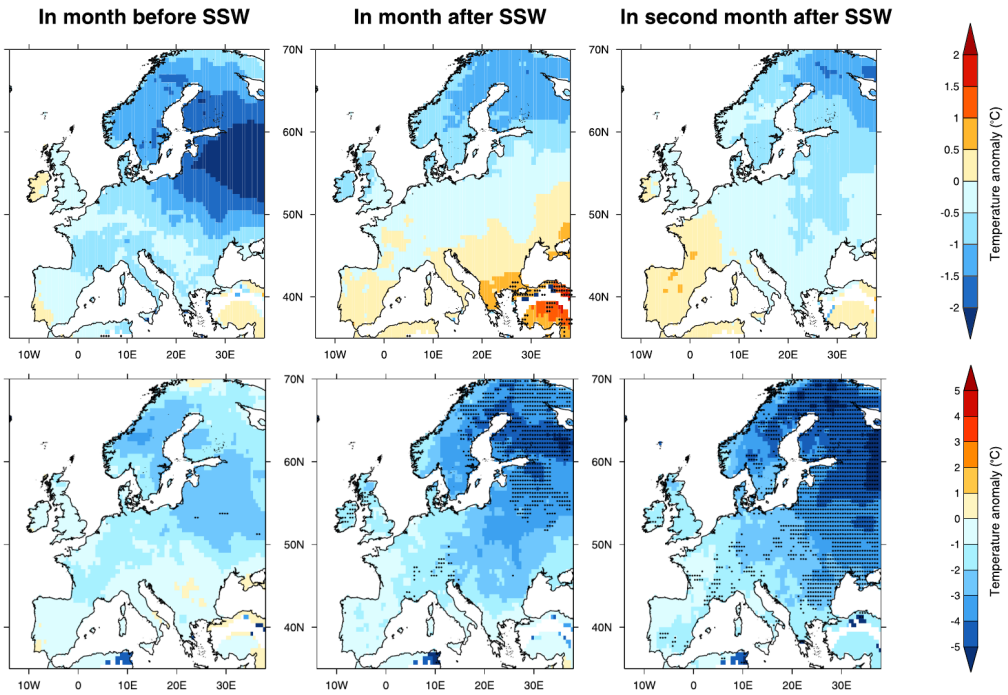

Figure 2.7: **Comparison of Mean and Extreme European Daily Minimum Temperatures around SSW Events.** Figure 3 of King et al. (2019) (top row): „Monthly average daily minimum temperature before and after central dates of SSW events. Stippling indicates at least 75% of grid box anomalies across individual SSW events are of the same sign. Anomalies are calculated from a daily climatological average for 1979–2016 to remove the influence of the seasonal cycle.“ Figure 5 of King et al. (2019) (bottom row): „Average anomalous intensity of the coldest minimum temperatures before and after central dates of SSW events. Stippling indicates at least 75% of grid box anomalies across individual SSW events are of the same sign. Anomalies are calculated from a daily climatological average for 1979–2016 to remove the influence of the seasonal cycle.“

3 Data and Methods

3.1 ERA-Interim Reanalysis Data Set

For the description of the atmospheric state, the reanalysis data set from the European Center for Medium Range Weather Forecast (ECMWF), ERA-Interim, is used in this thesis. According to King et al. (2019) this data set is suitable for the description of the mean surface response to SSW events. Numerous previous studies, e.g. by Afargan-Gerstman and Domeisen (2020), Charlton-Perez et al. (2018) or Karpechko et al. (2018) underline the suitability of the ERA-Interim reanalysis data set for the investigation of SSW events and their influence on tropospheric weather. Using the ERA-Interim reanalysis data set constraints the analysis to the period between 1 January 1979 and 31 August 2019. The winter 2019/2020 is therefore not investigated in this thesis. The used horizontal resolution of the data is 1.5°x1.5°. In the vertical, 37 pressure levels are available between 1 and 1000 hPa. Except the geopotential height, all needed variables are directly given in the ERA-Interim data set. The geopotential height is calculated from the geopotential by dividing it through the gravitational constant. For doing this, the ECMWF recommends to neglect the latitudinal dependency of the gravitational constant and to use a fixed value of $9.80665\,\mathrm{ms}^{-2}$ instead for all latitudes (https://apps.ecmwf.int/codes/grib/param-db/?id=129, last viewed 2 September 2019). This is done in this thesis. For every variable, the daily mean of all available times is used unless stated otherwise.

3.2 Subseasonal To Seasonal Reforecast Data Set

The Subseasonal To Seasonal (S2S) data set is the used extended range ensemble forecast data set in this thesis. According to Vitart et al. (2017) the S2S data set is suitable to investigate SSW events concerning their impact on the predictability of surface weather on the subseasonal to seasonal time-scale. Studies, e.g. by Kautz et al. (2020) or Karpechko et al. (2018) demonstrate this. The S2S data set consist of both, near-realtime forecasts and reforecasts with lead times up to 60 days from 11 operational forecast centers worldwide (Vitart et al., 2017; Vitart et al., 2012). In this thesis, only the data from the ECMWF is used. Since near-realtime forecasts are only available from 2015 onwards, reforecasts are used in this thesis to increase the number of winters for analysis. These reforecasts are initialized twice weekly with the ERA-Interim renalysis as initial conditions and computed for the same date of initialization for the last 20 years (https://confluence.ecmwf.int/display/S2S/ECMWF+Model+Description+CY46R1; last viewed 25 May 2020). ECMWF reforecasts are produced „on-the-fly“ using always the latest version of the Integrated Forecasting System (IFS) of the ECMWF for the computation (https://confluence.ecmwf.int/display/S2S/ECMWF+Model+Description+CY46R1; last viewed 25 May 2020). To take advantage of this, only model-versions of the years 2019 and 2020 are

used in this thesis. Therefore, the earliest winter which is investigated in this thesis is the winter 1999/2000.
The reforecast verification is done with the ERA-Interim reanalysis data set (Kautz et al., 2020; Karpechko et al., 2018). For a better comparison between the S2S reforecasts and the ERA-Interim reanalysis, the same horizontal resolution as the ERA-Interim reanalysis data is used for the S2S reforecasts, but in the vertical, only 10 pressure levels between 10 and 1000 hPa are available. All variables needed in this thesis, including the geopotential height, are directly available in the S2S data set but only with 1 value per day.
In contrast to the reanalysis data, the reforecast data on subseasonal to seasonal time scales can be affected by a significantly large and non-negligible model error (Vitart et al., 2012). This is especially important when looking at extremes.

3.3 Calculation of Climatologies and Standard Deviations

Climatologies are needed to calculate anomalies from the mean state of the atmosphere. However, in literature, a unique recommendation how to calculate a climatology best suited for the given application of this thesis cannot be found. Therefore, three different types of climatologies are computed and compared with each other. For every climatology, all available data from ERA-Interim, reaching from 1 January 1979 to 31 August 2019, are used for the calculation. The simplest approach to calculate a climatology is to use a multi-year daily mean, called „daily climatology“ hereafter. Another possibility is the use of a running mean over a certain number of days. This ensures that sporadic and small-scale events do not have a strong influence on the climatology, which is especially important for short time series. According to Baldwin and Dunkerton (1999) a 10-day running mean is suitable to exclude synoptic-scale variations from the data. Therefore, the length of the running mean is set to 10 days. To spare computing power, the daily climatology is computed first and then the running mean is applied. To preserve the length of the time series, the necessary number of days from the daily climatology are pasted to the end and the beginning of the time series before applying the running mean. In case of the S2S data, which has a maximum length of 46 days per reforecast, the missing values at the beginning and end of the time series are replaced manually by the nearest valid value. To minimize the missing values due to the running mean on the one hand, but still excluding small-scale variations on the other hand, a shorter window of 7 days for the running mean is tested as well. As a third possibility for calculating climatologies, blocks of 10 and 7 days are used. In this case the mean over a fixed number of days is taken. So every day in this fixed number of days has the same value. Sporadic events and synoptic-scale variations are completely removed in this approach. The missing values are substituted the same way as done for the running-mean climatologies.
For the calculation of standard deviations with ERA-Interim, only the time-step for 00 UTC is used to reduce the download load. The standard deviations are then calculated as a multi-year daily standard deviation over all available dates and averaged over the analyzed time-period unless stated otherwise. For the calculation of the standard deviations with the S2S data, all perturbed ensemble members from the available reforecasts with the same initialization date are used. The

daily standard deviation is calculated in a first step and then the multi-year daily mean of the daily standard deviations is computed. Unless stated otherwise, the resulting standard deviations are averaged over the investigated time period in a last step.

3.3.1 Comparison of Different ERA-Interim Climatologies

To compare the different climatologies with each other, the Pearson's correlation coefficient over the Euro-Atlantic sector, 30°N to 80°N and 80°W to 60°E, is computed exemplarily for the 2 metre temperature and the mean sea level pressure. The Euro-Atlantic sector is chosen as reference area, because it is an important region for the downward influence of SSW events on surface weather (Charlton-Perez et al., 2018). In all cases, the correlation between the climatologies is higher for the 2 metre temperature climatologies than for the mean sea level pressure climatologies. It is lowest for the comparison between the daily climatology and blocks of either 10 or 7 days (not shown). The differences between the daily climatology and running mean climatologies with either 10 or 7 days are marginal, smallest for climatologies with a running mean of 10 days (Figure 3.1). The correlation coefficient is exceeding 0.91 for both, the 2 metre temperature climatologies and the mean sea level pressure climatologies. Comparing the running mean climatologies of 10 and 7 days, the correlation coefficients show values over 0.99 (not shown). Keeping in mind that the 7-day running mean climatology has less missing values which is especially important for the S2S reforecasts, the 7-day running mean climatology is used in this thesis.
For the calculation of horizontal ERA-Interim climatologies, the daily mean of 4 times per day is used. Only for the climatology needed for the vertical profile of the normalized geopotential height anomalies, 1 time per day is used to reduce the download load. The difference between a climatology with 4 times per day and a climatology with 1 time per day is exemplarily calculated for 15 February. With a range between 1.5 gpm and 3.25 gpm difference between the two climatologies, the use of only 1 time per day to calculate this specific climatologies is justified.

3.3.2 Calculation of S2S Climatologies

In case of the S2S data set, a separate climatology for each initialization date needs to be calculated. The climatology is computed from all perturbed reforecasts with the same initialization date of every available year. Due to the limited available data, the year which is investigated is excluded from the climatology. At first, the ensemble mean of every year is calculated. Then, the multi-year daily mean is computed and afterwards, a 7-day running mean is performed to guarantee comparability with the ERA-Interim climatologies. As the reforecasts have a maximum length of 46 days, the missing values due to the running mean are substituted manually by taking the first, respectively the last, available value and pasting it to beginning and end of the climatology. This has to be kept in mind when analyzing the first and last three values of climatologies or anomalies.

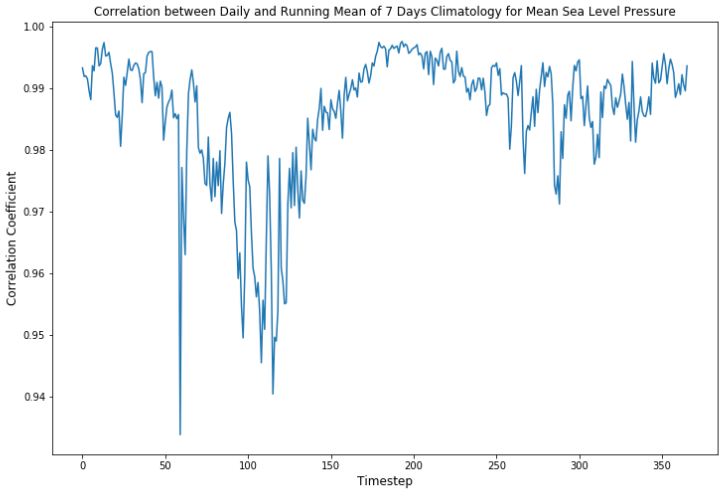

Figure 3.1: **Differences between Climatologies Based on ERA-Interim (1979-2019).** Correlation of the daily climatology and the 7-day running mean climatology for the mean sea level pressure. The time step on the x-axis of the figure corresponds to the day of year.

3.4 Downward Propagation of Standardized Geopotential Height Anomalies

Standardized geopotential height anomalies are frequently used to show the downward propagation of stratospheric signals to the surface (e.g. Karpechko et al., 2018). Anomalies in wind and temperature are also visible in the geopotential height, making it to a useful tool to show not only the downward propagation of signals but also their influence on a fixed pressure level. Usually the geopotential height anomalies in respect to the temporal climatology are used to detect positive anomalies induced by SSW events (e.g. Figure 5.1). The standardization of these anomalies is used for an easy comparison between the strength of different events. Also wave structures can be seen in the geopotential height and in its anomalies when using the anomalies from the zonal-mean geopotential height ((e.g. Figure 5.2); Lim and Wallace, 1991). It has to be kept in mind that waves with different wavenumbers can be superposed, making a clear statement concerning upward or downward propagation difficult. In general, westward with height tilted structures show upward propagating baroclinic waves (Lim and Wallace, 1991). So downward propagating baroclinic waves feature an eastward with height tilted structures. When the structures are not tilted with height, they show barotropic features (Lim and Wallace, 1991). For both, barotropic and baroclinic wave structures, coupling between the troposphere and stratosphere is possible (Attard and Lang, 2019). The structures can also be identified when looking at the geopotential height and, for example, on temperature (e.g. Figure 5.4). When the geopotential height isolines and the temperature isolines intersect each other, a baroclinic structure is present (Holton, 2010). Otherwise, the structure is barotropic. When looking at several pressure levels, vertical changes in baroclinic or barotropic structures can be determined as well as the vertical tilt and twist of structures.

3.5 Sudden Stratospheric Warming Indices

SSW indices are defined in various ways, usually for the months November to March (Butler et al., 2015). SSW events occurring during this period are sometimes also called „midwinter warmings“ in literature (Butler et al., 2015).
Based on the used definition, the number of detected SSW events per year changes significantly (Butler et al., 2015). One of the most used definitions is based on the reversal of the zonal-mean 10 hPa zonal wind at 60°N (Butler et al., 2015; Charlton and Polvani, 2007). It is argued though that it would be better to look at a reference latitude of 65°N rather than 60°N because the latter is located in the so called surf-zone, where local reversals of the zonal-mean zonal wind can occur due to wave breaking. Those wind-reversals are not associated with the dynamics of the polar vortex. Butler et al- (2015) found that using 65°N instead of 60°N in the SSW index definition gives about 10% less events in the period from 1958 to 2015.
Another wind-based definition uses the zonal-mean zonal wind averaged over the polar cap, 60°N to 90°N. By this SSW index, 30% more events are detected in the period from 1958 to 2015.
All wind-based SSW index definitions call the first day when the wind speed reaches 0 ms^{-1} or becomes negative the central date of a major SSW (Karpechko et al., 2018; Charlton and Polvani, 2007). This implicitly defines which weak polar vortex events are classified as major SSW events. For the separation of two events, the zonal-mean zonal wind has to turn westerly again for at least 20 consecutive days (Butler et al., 2015, Charlton and Polvani, 2007). These 20 days correspond to the time of two radiative damping time-scales at 10 hPa, leaving enough time for the polar vortex to recover through radiative processes (Charlton and Polvani, 2007). Wind reversals at the end of winter are not classified as SSW events and called „final warmings“ instead (Butler et al., 2015; Charlton and Polvani, 2007). A wind-reversal is classified as a final warming when the zonal-mean zonal wind at 10 hPa does not return westerly in 10 consecutive days before 30 April (Butler et al., 2015; Charlton and Polvani, 2007). Final warmings occur at the end of every winter due to the seasonal reversal of zonal wind, caused by the increasing radiative heating due to the rising sun (Butler et al., 2015).
In addition to the purely wind-based indices, a combination of the meridional temperature gradient, averaged over the polar cap, and the reversal of the zonal-mean 10 hPa zonal wind at 60°N is calculated in this thesis (Butler et al., 2015; Yu et al., 2018). A major SSW event is detected when the wind reverses to easterlies and the meridional temperature gradient turns negative in 10 consecutive days as well. According to Charlton and Polvani (2007) the inclusion of the meridional temperature gradient in the definition of the SSW index makes little difference in the number of detected SSWs.
The fifth computed index in this thesis is a temperature-based SSW index. It detects a major SSW event when the temperature between 100 hPa and 10 hPa at any grid point northward of 60°N increases more than 40 K in one week. This index does not differentiate between SSWs and final warmings (Butler et al., 2015).

3.5.1 Comparison of Sudden Stratospheric Warming Indices for the Winters of 1999/2000 to 2018/2019

The SSW index by Charlton and Polvani (2007) (CP07) detects 17 SSW events in 14 out of the 20 winters which are investigated in this thesis (Table 3.1). Twelve of those SSWs are also detected by the wind- and temperature-based SSW index (U&T). The modification of the CP07 index which uses 65°N instead of 60°N as reference latitude (U65) detects 20 events in the same 14 winters. The central dates of the SSWs detected by both wind-based indices vary up to 8 days. This increase in the number of SSW events when using 65°N as reference latitude instead of 60°N is contrary to the findings of Butler et al. (2015). A possible explanation of this dissent is the different considered time period.

The third wind-based SSW index which uses the meridional mean between 60°N and 90°N as reference latitude (U6090) detects 26 SSW events in 18 of the 20 available winters (Table 3.1). The increase of detected SSW events detected by this index in comparison to CP07 is consistent with the findings of Butler et al. (2015).

The purely temperature based SSW index (TMP) does not detect any SSWs in the winters of 1999/2000 to 2018/2019 (Table 3.1). Therefore, this index is not used to detect SSW events in this thesis. The U&T index is also excluded because it is more computing-intensive than the purely wind-based indices and does not support necessary additional information.

Concerning the wind-based indices, all three indices are taken into consideration, with U65 used for the detailed analysis (e.g. Figure 5.3). It is calculated for the ERA-Interim data using all available times per day to include important daily fluctuations in the 10 hPa zonal-mean zonal wind. The classification of SSW events is done analogous to Charlton and Polvani (2007) but taking the period of 13 days prior and 18 days after the central date of the SSW obtained by U65 into consideration. This is done to account for the maximum variation of the central dates obtained by CP07 and U65.

Table 3.1: **Detection of SSW Events by Different SSW Indices for the Winters 1999/2000 to 2018/2019.** The SSW index by Charlton and Polvani (2007) („CP07“) is compared to its modified versions regarding the reference latitude („U65“ and „U6090“) and its combination with a meridional temperature gradient („U&T“). Furthermore a purely temperature-based index („TMP“) is used. If an SSW event is detected, the central date of this event is given, otherwise there is a dash.

Winter	CP07	U&T	U65	U6090	TMP
1999/2000	20 Mar	-	20 Mar	20 Mar	-
2000/2001	11 Feb	√	23 Nov, 3 Feb	22 Nov, 2 Feb	-
2001/2002	30 Dec, 17 Feb	√, -	29 Dec, 16 Feb	29 Dec, 16 Feb	-
2002/2003	18 Jan	√	17 Jan, 17 Feb	16 Jan, 17 Feb	-
2003/2004	4 Jan	√	3 Jan	29 Dec	-
2004/2005	-	-	-	12 Mar	-
2005/2006	20 Jan	√	21 Jan	12 Jan	-
2006/2007	24 Feb	√	23 Feb	22 Feb	-
2007/2008	22 Feb	√	22 Feb	22 Feb	-
2008/2009	24 Jan	√	24 Jan	24 Jan	-
2009/2010	28 Jan, 23 Mar	√, √	25 Jan	23 Jan, 20 Mar	-
2010/2011	-	-	-	-	-
2011/2012	-	-	-	14 Jan, 14 Feb	-
2012/2013	6 Jan	-	6 Jan	6 Jan	-
2013/2014	-	-	-	4 Feb	-
2014/2015	-	-	-	3 Jan, 2 Feb	-
2015/2016	-	-	-	-	-
2016/2017	2 Feb	√	24 Nov, 1 Feb, 24 Feb	24 Nov, 31 Jan, 24 Feb	-
2017/2018	11 Feb, 19 Mar	√, -	11 Feb, 22 Mar	11 Feb	-
2018/2019	1 Jan	-	31 Dec	29 Dec	-

3.6 Blocking Index

In literature, many approaches to define blocking indices are found. Rex (1950) proposes a subjective criterion based on 500 hPa geopotential height anomaly maxima and Dole (1978) extends this criterion by adding a mandatory persistence of the pattern. Okland and Lejenäs (1987) also focus on blocking persistence and define a climatological probability that a specific blocking pattern lasts at least for a certain number of days. These subjective blocking indices are compared by Liu (1994).

An objective blocking index based on the meridional gradient of the 500 hPa geopotential height

field is developed by Tibaldi and Molteni (1990). They calculate a northern meridional gradient, GHGN, between 60°N and 80°N and a southern gradient, GHGS, between 60°N and 40°N:

$$GHGN = \frac{Z(\Phi_n) - Z(\Phi_0)}{\Phi_n - \Phi_0},$$

$$GHGS = \frac{Z(\Phi_0) - Z(\Phi_s)}{\Phi_0 - \Phi_s},$$

where Z is the 500 hPa geopotential height at a specific latitude Φ. The latitude Φ is thereby varied as follows:

$$\Phi_n = 80°\text{N} + \Delta,\ \Phi_0 = 60°\text{N} + \Delta,\ \Phi_s = 40°\text{N} + \Delta,\ \Delta = -4°,\ 0° \text{or } 4°.$$

Hereby is Φ_0 called the „central latitude“. For the occurrence of blocking, GHGN needs to be smaller than -10 m/° latitude and GHGS greater than 0. For the detection of blocking, it is sufficient if GHGS and GHGN fulfill their criteria for one central latitude Φ_0. Therefore, the maximal values of GHGS, as this needs to be >0, and the minimal values for GHGN, as this need to be <-10 m/° latitude, are computed for each longitude. If blocking is detected, GHGS, which is a proxy for the blocking strength, is shown for the ERA-Interim reanalysis in a Hovmöller plot with the 500 hPa geopotential height field in the background (e.g. Figure5.6). A region is considered as blocked, if 3 adjacent grid points are blocked.
A 2-dimensional extension of the index by Tibaldi and Molteni (1990) is developed by Scherrer et al. (2006). This index is computed in a similar way with GHGS and GHGN but the central latitude varies from 35°N to 75°N. In this thesis, the central latitude is varied between 34.5°N and 75°N with a latitude step of 1.5° due to the model resolution. This is also done by Quinting and Vitart (2019). Δ is set constantly to 0:

$$\Phi_n = \Phi_0 + 15°$$

$$\Phi_s = \Phi_0 - 15°$$

$$\Phi_0 = 35°\text{N to } 75°\text{N in } 1.5°\text{steps},\ \Delta = 0°.$$

In this approach, a field of the blocking index is calculated and not only a single value per latitude as done by Tibaldi and Molteni (1990). If both, GHGS and GHGN, fulfill their criterion, blocking is detected and GHGS plotted. For the ERA-Interim reanalysis data set, these plots also show the 500 hPa geopotential height field in the background to illustrate ridges and troughs and therefore the type of blocking (e.g. Figure 5.7). Scherrer et al. (2006) additionally include a 5 day persistence criterion, which is not used in this thesis because in the Hovmöller plot showing the blocking index by Tibaldi and Molteni (1990) the persistence of the blocking pattern can be detected easily and applied to the 2-dimensional extension by Scherrer et al. (2006).
For the S2S data, the 500 hPa geopotential height anomalies, averaged between 70°W and 30°E as well as 40-80°N, are shown instead of the Hovmöller diagrams (e.g. Figure 6.12). This is done because Hovmöller diagrams are disadvantageous when having large ensemble spreads, such as at the end of the reforecasts' lead time. Then, the overlap of the different GHGS values for the

ensemble members makes it difficult to determine single blocking patterns. For the same reason, in the 2-dimensional 500 hPa geopotential height field only the 5600 gpm isoline is drawn for the ensemble members and the ERA-Interim reanalysis (e.g. Figure 6.14).
Other blocking indices found in literature are based on the potential temperature. These indices include wave breaking in their criteria, which is an important factor of blocking (Pelly and Hoskins, 2003). As the potential temperature is only available in the ERA-Interim data set but not in the S2S data set, indices based on potential temperature are not used in this thesis.

3.7 Position of the Mid-Latitude Jet Stream

For the position of the jet stream, the 850 hPa zonal-mean zonal wind is displayed in a Hovmöller diagram with latitude and time on its axes (e.g. Figure 5.8). The wind-maxima, which indicate the position of the jet stream, are marked additionally with lines. To filter out synoptic-scale events such as cyclones, a Lanczos filter with a 61-day moving window and a cutoff-frequency of 1/10 days is applied (Woollings et al., 2010; Duchon, 1979). The truncated weight function of the filter can be written as:

$$w(k) = \sigma_1 \cdot \sigma,\ w(n) = w(-n) ... = 2 \cdot \text{cutoff-frequency},\ k \in [-n, n],$$

where $w(k)$ is the truncated weight function with k being the step and σ the so-called σ-factor developed by Lanczos (Duchon, 1979). The weight function is symmetric around $k = 0$. The total number of steps n is computed depending on the length of the moving window:

$$n = \frac{(\text{length moving window } - 1)}{2} + 1.$$

It is half the length of the moving window, creating a symmetric weight function which is essentially a centered running mean multiplied by a factor σ. This σ-factor is dependent on the steps and the total number of steps:

$$\sigma = \frac{\sin\left(\frac{\pi k}{n}\right) \cdot n}{\pi k}.$$

It is a sinc-function, showing only values $\neq 0$ inside a window between the negative and positve cutoff-frequency. The first σ-factor σ_1 is given with:

$$\sigma_1 = \frac{\sin\left(2\pi k \cdot \text{ cutoff-frequency}\right)}{\pi k}.$$

This Lanczos filter is basically a 10-day lowpass-filter combined with a 61-day running mean. This leads to 31 days at the beginning and end of the used time series which are affected by boundary conditions and therefore uncertain. The same filtering method is applied to the 850 hPa zonal-mean zonal wind climatology to determine the position of the jet stream relative to its climatological mean.

3.8 North Atlantic Oscillation Indices

There is not a unique definition of the NAO index in literature but there is a sign convention. A positive index corresponds to a strengthening difference between the Icelandic low and the Azores' high, a negative index corresponds to a weakening difference between the Icelandic low and the Azores' high (Blessing et al., 2005). According to Leckebusch et al. (2008) the traditional way to calculate the NAO index is the use of the difference of standardized mean sea level pressure anomalies between Lisbon and a station on Iceland, typically Stykkishólmur or Reykjavik. This is also called the Lisbon-Iceland index.
To take the movement of the NAO centers into consideration, the EU Index uses two latitude circles, one at 35°N and one at 65°N, which are averaged over the sector between 20°W and 40°E. The difference of the standardized mean sea level pressure anomaly of the southern and northern circle is then called the EU Index. One possible issue with this approach is the choice of the longitude sector, which is positioned to a great extent over continental Europe, but the NAO itself is defined over the northern Atlantic ocean basin.
The Zonal Index is defined in a region closer over the North Atlantic ocean by using a longitudinal sector between 0°W and 40°W. It also uses a latitudinal sector creating two regions, in which the mean sea level pressure anomalies are then averaged separately and standardized. The southern area is located between 35°N and 50°N, the northern area between 55°N and 70°N. The difference between the southern and the northern area creates the Zonal Index.
Instead of using standardized mean sea level pressure anomalies, standardized geopotential height anomalies can also be used for the calculation of the NAO index in different heights (Jung et al., 2011). This approach is tested for the standardized 500 hPa geopotential height anomalies and the regions defined by the Zonal Index.
Beside the gridpoint-based indices, indices based on empirical orthogonal functions are used frequently (Jia et al., 2007). But according to Jia et al. (2007) gridpoint-based indices represent the difference between the two NAO phases better than indices based on empirical orthogonal functions. Therefore, only the former are used in this thesis.

3.8.1 Comparison of North Atlantic Oscillation Indices

The comparison of the different definitions of the NAO index is done exemplarily for the winter 2017/2018. The differences between the various NAO indices are found to be not negligible and sometimes even varying in sign (Figure 3.2 left). As the Lisbon-Iceland Index does not consider movements of the NAO centers, the other indices are preferred (https://climatedataguide.ucar.edu/climate-data/hurrell-north-atlantic-oscillation-nao-index-station-based, last viewed 26 August 2019). For the same reason, the Zonal Index is prefered over the EU Index, as the latter only considers longitudinal movements of the NAO centers. Except for the magnitude, the surface based Zonal Index and the 500 hPa geopotential height based Zonal Index show a similar behaviour (Figure 3.2 left and right). To include the analysis of dynamics on the surface, the mean sea level pressure based Zonal Index in this thesis. The standardization of the index is done with the multi-year temporal standard deviation of the mean sea level pressure.
As daily values of the NAO index are computed to show the influence of the SSW events on the pattern, the results are sensitive to the used climatology. The difference for the Zonal Index cal-

culated once with a daily climatology and once with a 7-day running mean climatology varies between ± 0.25 standard deviations during November to May (not shown). For consistency in this thesis, the 7-day running mean climatology is used to calculate the Zonal Index. To exclude synoptic-scale events of the considered winter, a 7-day running mean of the Zonal Index is calculated afterwards and plotted together with the daily NAO index (e.g. Figure 5.9; e.g. Baldwin and Dunkerton, 1999).

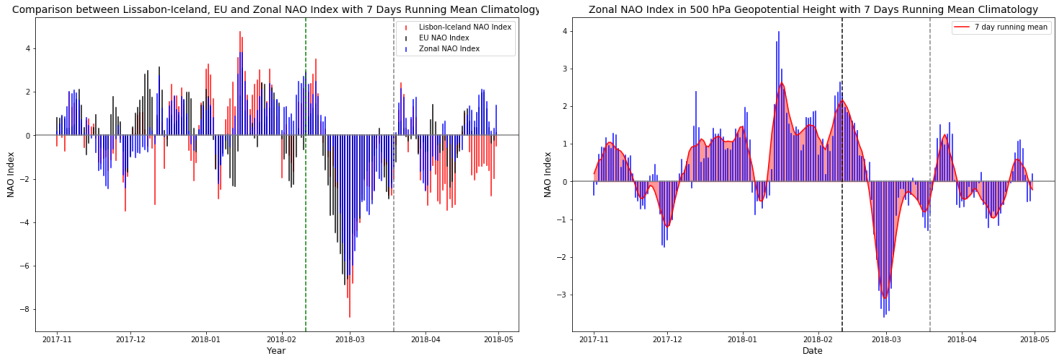

Figure 3.2: **Comparison of Different NAO Indices.** Comparison between the mean sea level pressure based Lisbon-Iceland, EU and Zonal Index computed with a 7-day running mean climatology (left) and the Zonal Index in 500 hPa geopotential height also computed with a 7-day running mean climatology (right) for the winter 2017/2018. The green respectively black dashed line shows the central date of the first major SSW in this winter, the gray dashed line the date of the second major SSW.

3.9 Definition of Cold Waves

In literature, a unique definition of cold waves cannot be found. Garfinkel et al. (2017) define a cold snap as the 2 metre temperature anomalies below 1 K under the climatological value. Although for the cold wave itself there is not a persistence criterion, the separation of events is clearly done with demanding at least 3 consecutive days between two events. This definition is adapted for the ERA-Interim reanalysis and the S2S-reforecast data and calculated for the European mean and regional means for different European regions (Figure 3.3). To spare the duration criterion, a 7-day running mean of the daily anomalies is calculated afterwards. The days which fulfill the criterion for cold waves are marked (e.g. Figure 4.11). The term „European cold wave“ describes in this thesis a period of consecutives days which fulfill the criterion for cold waves in the European mean. This description is adapted for the different European regions.

In addition to this definition, the definition of cold waves by Smid et al. (2019) is used for the ERA-Interim reanalysis. This definition is based on the 2 metre daily minimum temperature and defines a cold snap as those days which are colder than the lowest 10 percentile of the climatology. The climatology is calculated for the period of 1999-2019 with a 31-day moving window. The minimum duration of a cold wave is given with 3 consecutive days. The definition by Smid et al. (2019) is also calculated for the European mean and the different European regions (Figure 3.3). The term „European cold waves“ is used in the same way as done for the definition of cold waves based on the 7-day running mean of the 2 metre temperature anomalies.

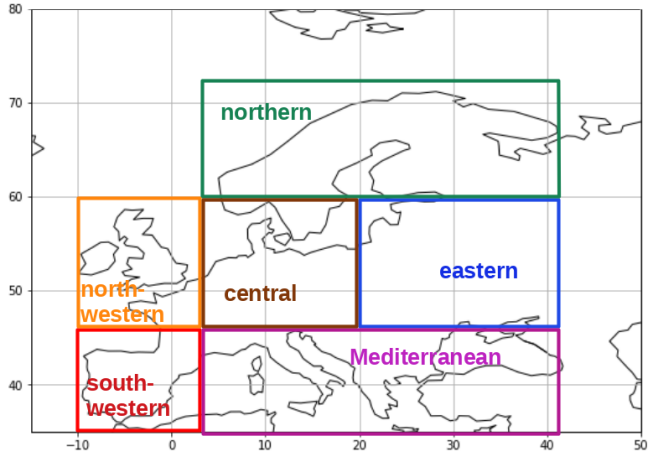

Figure 3.3: **Regions for the Detection of Cold Waves.** The European mean is calculated by averaging between 10°W to 42°E and 35°N to 72°N. The anomalies for north-western Europe between 10°W to 3°E and 45°N to 60°N, for south-western Europe between 10°W to 3°E and 35°N to 45°N, for eastern Europe between 20°E to 42°E and 45°N to 60°N, for northern Europe between 3°E to 42°E and 60°N to 72°N, for central Europe between 3°W to 20°E and 45°N to 60°N and for the Mediterranean between 3°E to 42°E and 35°N to 45°N.

3.10 Selection of Case Studies

The selection of case studies is done subjectively with the aim to show the high case-to-case variability of the SSW events itself and their possible influence on European cold waves on the subseasonal to seasonal time scale. As a first case study the winter 2008/2009 is selected. This winter features the strongest and longest-lasting SSW event of the past 20 years (Table 3.2). Easterly winds reach values up to -36 ms^{-1} and a total duration of 34 days in the middle stratosphere. According to Afargan-Gerstman and Domeisen (2020) this SSW does not influence surface weather over Europe. Thus, the SSW event should not have an effect on the predictability of European cold waves and the winter 2008/2009 is only analyzed with the ERA-Interim reanalysis.
The winter 2009/2010 is selected as a second case study. This winter is appealing because it features besides a strong and long-lasting SSW event in January 2010 another reversal of the 10 hPa zonal-mean zonal wind at the end of March 2010. The U65 index classifies this wind reversal already as the final warming but the CP07 and U6090 index detect a second SSW here (Table 3.1). The SSW detected by all indices features maximum easterly winds up to -20 $m^{-1}s$ which last 32 days in the middle stratosphere. According to Jung et al. (2011) and Santos et al. (2013) the SSW plays only a minor role in the maintenance of the following surface weather pattern. Therefore, this winter is only analyzed with the ERA-Interim reanalysis.
As a third case study, the winter 2000/2001 is selected. It features two very different SSW events (Table 3.2). The first SSW is a rather weak and short-lasting D-type warming at the end of November. Easterly winds with a maximum amplitude of -4 ms^{-1} are present for 4 days in the middle stratosphere. The second SSW is a S-type warming in the beginning of February. It features maximum easterly winds with -16 ms^{-1} and a duration of easterly winds for 20 days in the middle atmosphere. To the knowledge of the author, the first SSW of the winter 2000/2001 is not analyzed in studies concerning its impact on surface weather. A reason for this might be that it is not

detected by the often used SSW index by Charlton and Polvani (2007) which uses the reversal of the 10 hPa zonal-mean zonal wind at 60°N as a measure of major SSWs. This makes the first SSW event of the winter 2000/2001 suitable for a detailed analysis with the S2S reforecasts in addition to the ERA-Interim reanalysis.

Table 3.2: **Features of the Major SSW events of the Winters 1999/2000 to 2018/2019.** The reversal of the 10 hPa zonal-mean zonal wind at 65°N is used for the detection of events (Butler et al., 2015). The case studies selected for further analysis are printed in bold.

Winter	Central Date SSW	Type	Max. Easterly Wind Speed	Duration Easterlies
1999/2000	20 Mar	D	-11 ms^{-1}	2 d
2000/2001	**23 Nov**	**D**	**-3 ms^{-1}**	**4 d**
2000/2001	**3 Feb**	**S**	**-16 ms^{-1}**	**20 d**
2001/2002	29 Dec	D	-5 ms^{-1}	18 d
2001/2002	16 Feb	D	-5 ms^{-1}	4 d
2002/2003	17 Jan	S	-3 ms^{-1}	2 d
2002/2003	17 Feb	S	-5 ms^{-1}	20 d
2003/2004	3 Jan	D	-12 ms^{-1}	33 d
2004/2005	-	-	-	-
2005/2006	21 Jan	D	-28 ms^{-1}	27 d
2006/2007	23 Feb	D	-18 ms^{-1}	5 d
2007/2008	22 Feb	D	-21 ms^{-1}	33 d
2008/2009	**24 Jan**	**S**	**-36 ms^{-1}**	**34 d**
2009/2010	**25 Jan**	**S**	**-20 ms^{-1}**	**32 d**
2010/2011	-	-	-	-
2011/2012	-	-	-	-
2012/2013	6 Jan	S	-21 ms^{-1}	23 d
2013/2014	-	-	-	-
2014/2015	-	-	-	-
2015/2016	-	-	-	-
2016/2017	24 Nov	D	-2 ms^{-1}	1 d
2016/2017	1 Feb	D	-5 ms^{-1}	1 d
2016/2017	24 Feb	D	-5 ms^{-1}	19 d
2017/2018	11 Feb	S	-34 ms^{-1}	16 d
2017/2018	22 Mar	D	-6 ms^{-1}	8 d
2018/2019	31 Dec	S	-15 ms^{-1}	26 d

3.10.1 Selection of S2S Reforecasts and Representative Members

The selection of reforecasts for analysis of the first SSW event of the winter 2000/2001 is based on the SSW index, which is only defined between November and March. Therefore, the earliest useful initialization date of the S2S reforecasts is 31 October 2000. At this date, 1 ensemble member predicts the central date of the first SSW in the winter 2000/2001 correctly, 1 member too early and 9 members show only westerly winds (Table 3.3). The SSW event is considered to be predicted correctly when the ensemble member predicts the reversal of the 10 hPa zonal-mean zonal wind in the time-range of 3 days around the central date of the SSW event obtained from the ERA-Interim renalysis (Karpechko et al., 2018). At this early time of initialization, the correct prediction of the SSW event could be coincidence but the reforecast initialized 4 days later also features 1 member which predicts the SSW's central date correctly. This might be an indicator for an early predictability of the SSW. The reforecast initialized on 31 October 2000 is therefore subject to further analysis.

So is the reforecast initialized on 7 November 2000 which features 4 members predicting the SSW correctly and 5 members, which do not predict easterly winds during at all (Table 3.3). This case looks very promising to detect the differences in reforecasts with and without SSWs. The reforecasts initialized after 7 November 2000 show an increasing number of ensemble members which predict the SSW correctly. Firstly on 18 November 2000, 5 days prior to the central date of the SSW, all ensemble members predict the SSW correctly. The closest initialization date after the central date of the SSW is 25 November 2000. This reforecast is not only the closest to the central date of the SSW, but also the last one with all members being initialized as easterly winds (Table 3.3). Thus, this reforecast is also investigated further.

For the selected reforecasts which are initialized prior to the central date of the SSW, the representative members are chosen based on the SSW index. From all members which predict the SSW correctly the ensemble mean is calculated. This is done also for all member which do not show easterlies at all during the reforecast period. For every cluster, the representative member is the one which shows the smallest root mean square error to the ensemble mean. Ensemble members which predict the SSW too early or too late are excluded. This guarantees a clear distinction between members being influenced by the SSW event and those which are not.

For the selected reforecast initialized after the central date of the SSW, the choice of the representative members is based on the 100 hPa standardized geopotential height anomalies. The ensemble member closest to the ensemble mean of all ensemble members showing only values >0.5 standard deviation from the mid-December onwards is selected as the representative member with prevailing standardized geopotential height anomalies >0.5 standard deviation. As it follows the ERA-Interim reanalysis in sign, it is also called the member with the correct prediction of the atmospheric state. It has to be kept in mind though that this only applies to the sign but not the magnitude of anomalies. The ensemble member closest to the ensemble mean of all ensemble members showing only values <0.5 standard deviation from the beginning of December onwards is selected as the representative member with prevailing standardized geopotential height anomalies <0.5 standard deviation.

Table 3.3: **Selection of Reforecasts for the Analysis of the Winter 2000/2001.** In the table, the number of ensembles members which predict the central date correctly („Central Date“), too early or too late („Earlier or Later Easterlies“) or not at all („Only Westerlies“) are listed. The reforecasts which are analyzed further are written in bold and marked by a tick.

Initialization	Selected	Central Date	Earlier or Later Easterlies	Only Westerlies
31 Oct 2000	√	1	1	9
4 Nov 2000	-	1	1	9
7 Nov 2000	√	4	2	5
11 Nov 2000	-	8	2	1
14 Nov 2000	-	10	0	1
18 Nov 2000	-	11	0	0
21 Nov 2000	-	11	0	0
25 Nov 2000	√	11	0	0
28 Nov 2000	-	0	0	11

4 Winter 2008/2009

4.1 Troposphere-Stratosphere Coupling

The winter 2008/2009 shows a strongly positive normalized geopotential height anomaly up to 3.0 standard deviations at the stratospause between mid-January and mid-February 2009 (Figure 4.1). This is the only time when normalized geopotential height anomalies >1.0 standard deviation are present at the stratospause. Especially striking is the sharp gradient of geopotential height anomalies at the beginning of the structure indicating a sudden change of the stratospheric circulation at that time (Figure 4.1). The positive geopotential height anomalies show values >1.0 standard deviation in the stratosphere during the whole time but only between 11 and 16 February 2009 positive anomalies are found continuously from the stratopause to the surface (Figure 4.1). When looking at the deviation from the geopotential height from the zonal-mean in the stratosphere at the same time, a strongly westward tilted with height structure of continuously positive geopotential height anomalies in the troposphere and stratosphere is found (Figure 4.2 bottom). This indicates the upward propagation of tropospheric baroclinic waves in the stratosphere (Lim and Wallace, 1991). In the troposphere, the structure is not tilted with height indicating a barotropic state. Besides this prominent structure of positive geopotential height anomalies over the North Atlantic-European sector, another structure is visible in the troposphere over North America (Figure 4.2 bottom). The westward tilted with height structure is also associated with an upward propagation of tropospheric baroclinic waves (Lim and Wallace, 1991). This leads to a wavenumber 2 flow in the troposphere whereas a wavenumber 1 circulation is present in the stratosphere. The same circulation pattern is present between 5 and 6 November 2008 (Figure 4.2 top). The wavenumber 2 flow in the troposphere is characterized by a barotropic structure with positive geopotential height anomalies over the North Atlantic-European sector and another barotropic structure over North America. In the stratosphere, only the latter structure is visible showing a slightly westward tilt with height. This indicates the upward propagation of baroclinic tropospheric waves (Lim and Wallace, 1991). Polar-cap averaged positive normalized geopotential height anomalies >1.0 standard deviation are visible up to heights of 2.5 hPa during this time (Figure 4.1).

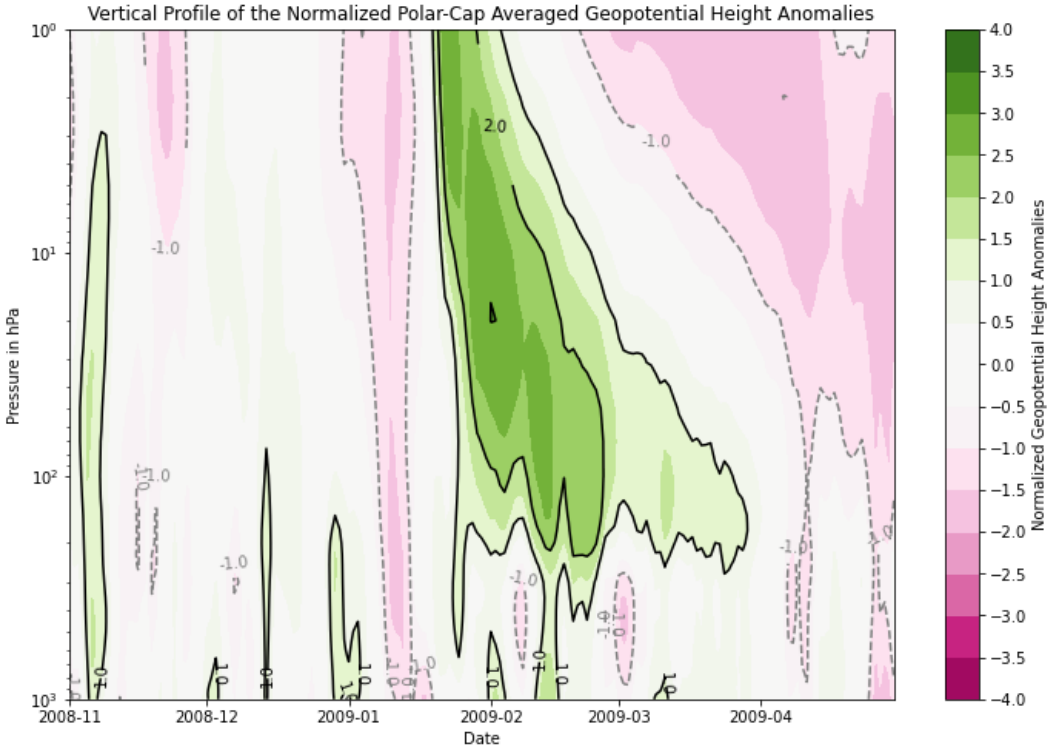

Figure 4.1: **Vertical Profile of the Polar-Cap Averaged Normalized Geopotential Height Anomalies during the Winter 2008/2009 based on ERA-Interim.** The green structure starting at 1 hPa is an indicator of a possible SSW event.

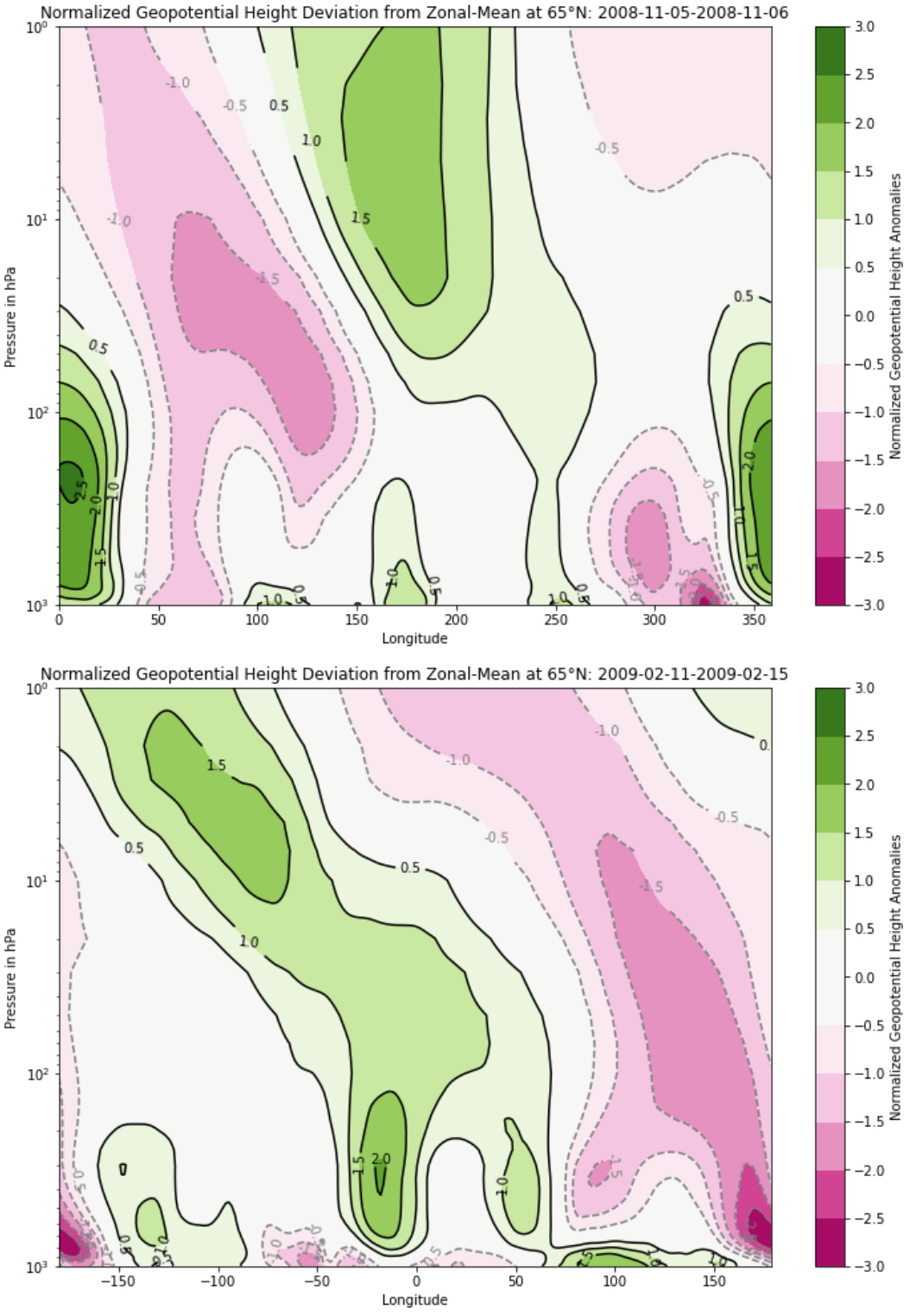

Figure 4.2: **Normalized Geopotential Height Deviations from Zonal-Mean in the Winter 2008/2009 based on ERA-Interim.** The top plot is averaged over the positive polar-cap averaged normalized geopotential height anomalies at the surface, the bottom plot around the time of the largest positive standard deviations of the normalized geopotential height anomalies associated with the SSE event at the surface.

4.2 Sudden Stratospheric Warming Signals in the Middle Stratosphere

As the presence of the normalized geopotential height anomalies >1.0 standard deviation at the stratopause already suggest, there is only one SSW event occurring in the winter 2008/2009 (Figure 4.1 and 4.3). This event is detected by all three wind-based SSW indices with its central date on 24 January 2009 (Table 3.1). Until roughly 1 month before the SSW event, the 10 hPa zonal-mean zonal wind varies between approximately 20 ms^{-1} and 40 ms^{-1} while the polar-cap averaged 10 hPa temperature is steadily below 215 K (Figure 4.3). The polar vortex is stable during this time with the exception of an elongation on 8 December 2008 (Figure 4.4 left column, top). This is may caused by an anomalously wavenumber 1 tropospheric wave forcing observed at the same time (Manney et al., 2009). In 10 hPa height, the strong polar vortex is slightly elongated and shows a split of the 28750 gpm isoline. In 30 hPa and 50 hPa height only less pronounced separated geopotential height contours are seen (Figure 4.4 left column, middle and bottom). The temperatures are down to 190 K in all three heights and the polar vortex is in a slightly baroclinic state. Interestingly, polar-cap averaged normalized geopotential height anomalies >1.0 standard deviation are not found in the stratosphere at that time (Figure 4.1). In mid-December 2008 the stratospheric polar night jet accelerates until 11 January 2009 when it reaches its winter-maximum with 68 ms^{-1} (Figure 4.3). The 10 hPa polar-cap averaged temperature is below 205 K at that time, just a few degrees above its wintertime-minimum in early January 2009. In all three displayed heights, the polar vortex is centered over the pole (Figure 4.5 left column). In 10 hPa height, it has an oval shape with minimum geopotential height values around 28000 gpm showing a slight baroclinicity while in lower heights the baroclinicity increases and the shape of the polar vortex is more concentric. From 11 January 2009 onwards the 10 hPa zonal-mean zonal wind decelerates rapidly (Figure 4.3). On 19 January 2009 the polar vortex is clearly elongated in 10 hPa, 30 hPa and 50 hPa height reaching far south into North America and Asia (Figure 4.4 middle column). In 10 hPa height the polar vortex is clearly in a baroclinic state with temperatures reaching locally already up to 260 K (Figure 4.4 middle column, top). In lower heights, the polar vortex is in a more barotropic state with temperatures staying below 240 K (Figure 4.4 middle column, middle and bottom). At the central date of the SSW the 10 hPa polar-cap averaged temperature reaches its wintertime-maximum with 252 K (Figure 4.3). Until this date, the temperature increased approximately 50 K in roughly 2 weeks. Locally temperatures up to 290 K are found over Grenland in 10 hPa, making this SSW event to one of the strongest SSW events (Figure 4.4 left column, top; Schneidereit et al., 2017). The polar vortex is clearly split at the central date of the SSW into two parts with minimum geopotential height values around 29500 gpm and 29250 gpm in 10 hPa height where it features strong baroclinic characteristics. In 30 hPa height the split of the polar vortex is also visible as well as the baroclinic structure (Figure 4.4 right column, middle). Temperatures stay here, and in 50 hPa height, below 240 K. In 50 hPa height the polar vortex is only elongated but not split and in a less baroclinic state than in the upper levels (Figure 4.4 right column, bottom).

On 29 January 2009 the SSW index reaches its winter-minimum with -36 ms^{-1} (Figure 4.3). In the last 3 weeks the stratospheric polar night jet changed its wind speed by 104 ms^{-1} which is again characterizing the SSW of the winter 2008/2009 as an especially strong one. The polar vortex is

now clearly split in all three displayed heights and in a baroclinic state (Figure 4.5 middle column, top, middle and bottom). Temperatures are still high in 10 hPa reaching locally values up to 270 K (Figure 4.5 middle column, top). In the lower heights, temperatures do not reach values above 250 K (Figure 4.5 middle column, middle and bottom). From 29 January 2009 onwards the 10 hPa zonal-mean zonal wind accelerates again and turns westerly on 25 February 2009 after 34 days with easterly winds (Figure 4.3). Concurrently with the acceleration of the stratospheric polar night jet the 10 hPa polar-cap averaged temperature decreases again. It reaches values slightly below 210 K on 9 March 2009, the time when the polar vortex in 10 hPa is restored (Figure 4.3). It is in a nearly barotropic state again showing a rather concentric shape, centering a little south of the pole (Figure 4.5 right column, top). According to Manney et al. (2009) this recovery of the polar vortex is not significant in lower heights showing again the large impact of the SSW event on the circulation in the stratosphere. In these lower heights the polar vortex is in a more baroclinic state with a less concentric shape, centering more southward with decreasing height (Figure 4.5 right column, middle and bottom). It is the only time when a clear tilt of the polar vortex with height is seen in the winter 2008/2009.

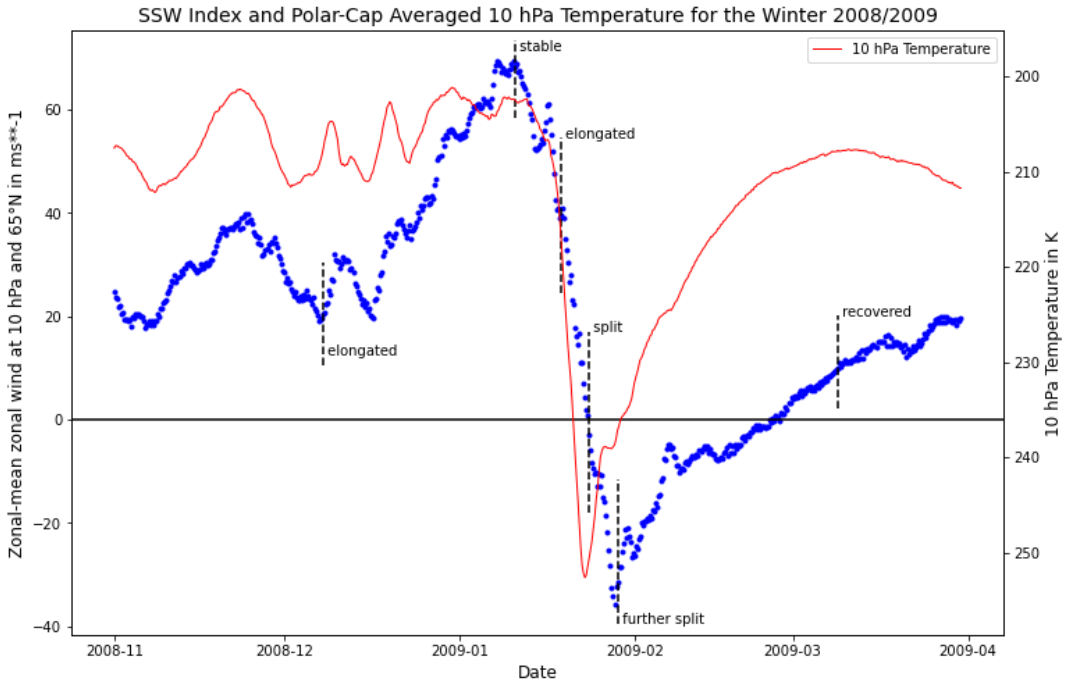

Figure 4.3: **SSW Index and Polar-Cap Averaged 10 hPa Temperature for the Winter 2008/2009 based on ERA-Interim.** The blue dots show the modified SSW index by Charlton and Polvani (2007) with 65°N instead of 60°N as reference latitude. The red line shows the polar-cap averaged 10 hPa temperature. Days with distinctive shapes of the polar vortex in the 10 hPa geopotential height field are marked.

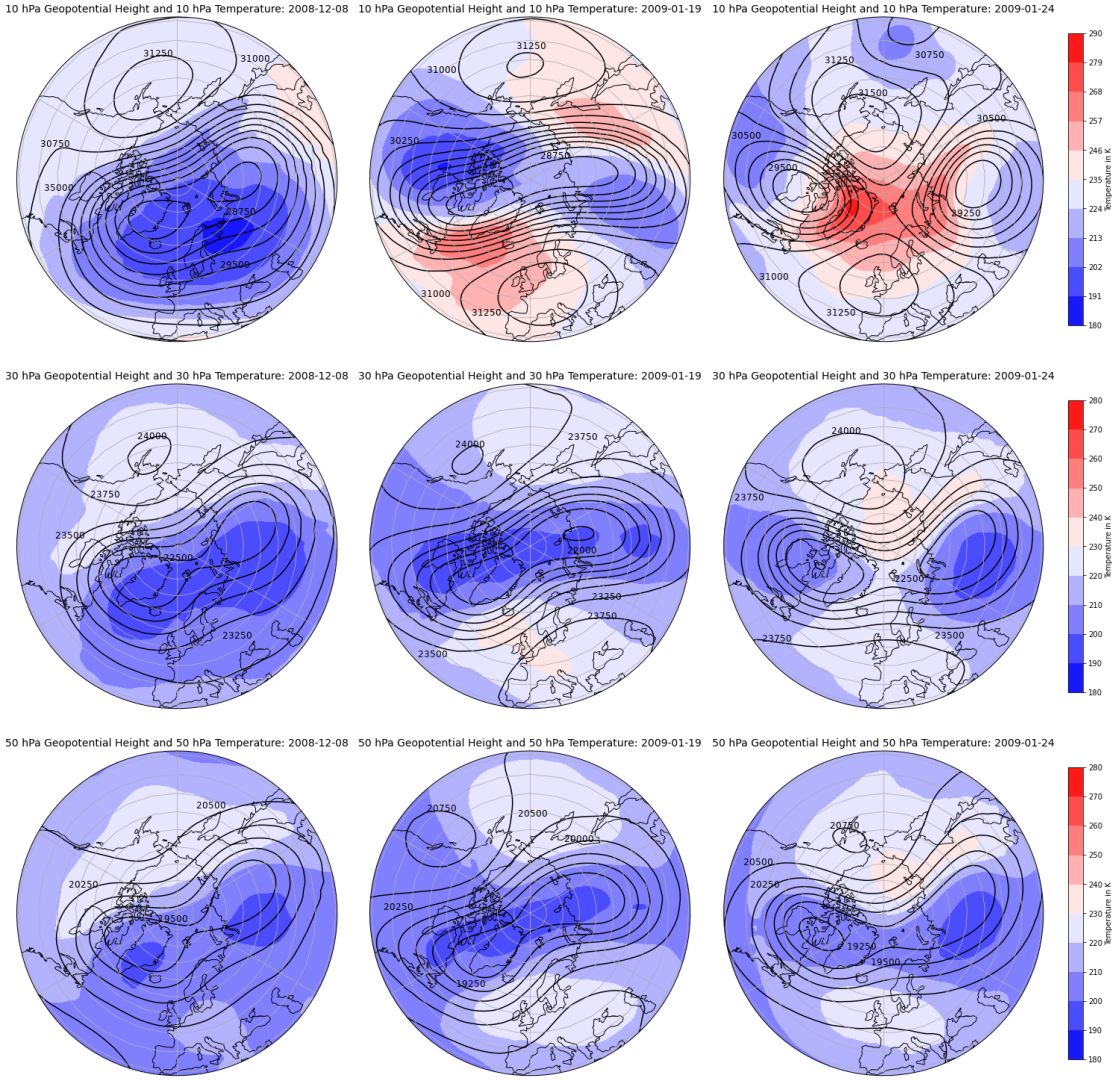

Figure 4.4: **Geopotential Height and Temperature in the Middle Stratosphere on 8 December 2008, 19 January 2009 and 24 January 2009 based on ERA-Interim.** The geopotential height and temperature are shown in 10 hPa (top row), 30 hPa (middle row) and 50 hPa (bottom row) for 8 December 2008 (left column), 19 January 2009 (middle column) and 24 January 2009 (right column). All plots have the same color-scale except the plot on the top right (the color-scale for this plot is given next to it).

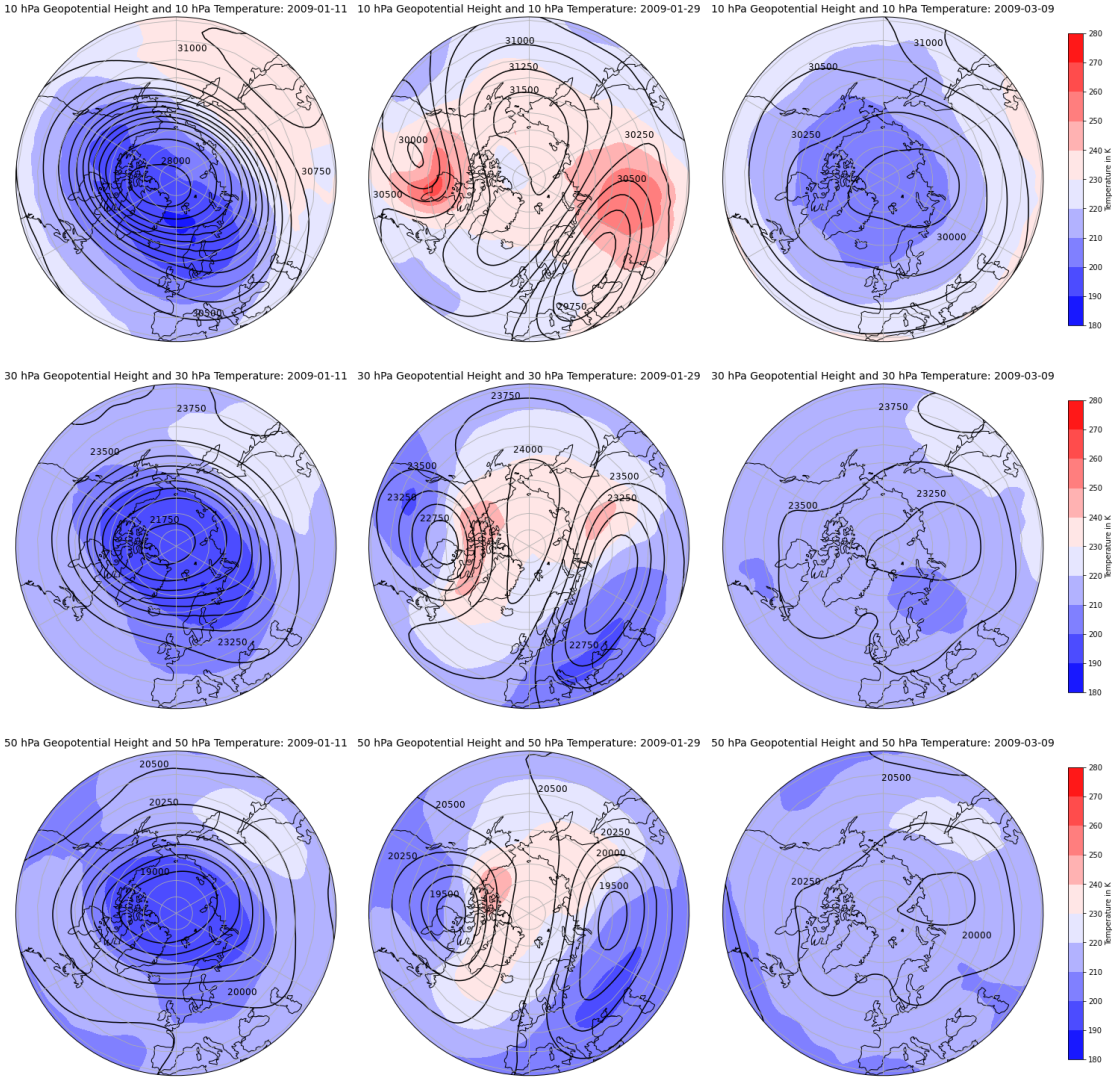

Figure 4.5: **Geopotential Height and Temperature in the Middle Stratosphere on 11 January 2009, 29 January 2009 and 9 March 2009 based on ERA-Interim.** The geopotential height and temperature are shown in 10 hPa (top row), 30 hPa (middle row) and 50 hPa (bottom row) for 11 January 2009 (left column), 29 January 2009 (middle column) and 9 March 2009 (right column).

4.3 Blocking in the Middle Troposphere

The winter 2008/2009 is characterized by a wavy zonal flow in the middle troposphere, shown for the time between the beginning of December and mid-February (Figure 4.6). Already on 5 November 2008 four ridges are found in the northern hemisphere, partly with blocking embedded (Figure 4.7 top). At the ridges over the Euro-Atlantic sector, North America and eastern Asia, an upward propagation of tropospheric waves is detected (Figure 4.2 top). The normalized geopotential height anomalies >1.0 standard deviation of this upward propagation reach up to 3 hPa height and lead to a small temperature increase and deceleration of the stratospheric polar night jet in 10 hPa (Figure 4.1 and 4.3). The elongation of the polar vortex on 8 December 2008 coincides also with the occurrence of pronounced ridges over the Euro-Atlantic sector and western North America but at that time, large blocking patterns are absent (Figure 4.6). According to Manney et al. (2009) an anomalously strong wavenumber 1 tropospheric wave forcing is present in the stratosphere around this time. This is may caused by the upward propagation of planetary-scale waves at one of the detected ridges.

From 8 December 2008 onwards until 11 January 2009, four pronounced blocking patterns are detected over the Euro-Atlantic sector and the North Pacific (Figure 4.6). These lead, according to Schneidereit et al. (2017) to an anomalously upward propagation of wavenumber 2 tropospheric waves into the stratosphere (Figure 4.6). Its causes may be found in the presence of moderate La Niña conditions which lead to a stronger than usual anticyclonic circulation over Alaska and Scandinavia (Schneidereit et al., 2017). According to Schneidereit et al. (2017) the MJO also plays a role in maintaining the Alaskan ridges. This beneficial phasing of ENSO and MJO conditions in the winter 2008/2009 may dominates over the hindering influence of the QBO west phase and the present number of sunspots on the development of an SSW event. Nevertheless, this is not the only driver of the SSW event.

During this time of enhanced upward propagation of tropospheric waves, the stratospheric polar night jet accelerates to its winter-maximum, the polar-cap 10 hPa temperatures drop below 205 K and the polar vortex stabilizes until 11 January 2009 (Figure 4.3). From this date onwards, the polar night jet rapidly decelerates and the polar-cap averaged 10 hPa temperature increases (Figure 4.3). At the same time a pronounced Scandinavian ridge develops and only small blocking patterns are observed over the northern hemisphere (Figure 4.6). The large and long-lasting blocking pattern before 11 January 2009 might be a precursor of the following SSW event, however, in the stratosphere only normalized geopotential height anomalies <1.0 standard deviations are present at that time (Figure 4.1). Additionally, the largely negative geopotential height anomalies at the stratopause in the beginning of January 2009 support rather the theory of a resonant excitation of the polar vortex in mid-January than the theory of the vortex disturbance by anomalously strong upward propagating tropospheric waves caused by blocking patterns (Figure 4.1; Albers and Birner, 2014).

Positive normalized geopotential height anomalies >1.0 standard deviation at both, the stratopause and the surface, are found firstly between 2 and 5 February 2009 (Figure 4.1). During this time blocking is detected over the eastern North Atlantic ocean and parts of Europe (Figure 4.6). The resulting strong meridional flow component features four pronounced ridges (Figure 4.7 middle). The only time when positive normalized geopotential height anomalies are present continuously

from the stratopause to the surface is between 11 and 16 February 2009 (Figure 4.1). At this time, only small blocking patterns are observed over North America and the Euro-Atlantic sector which coincide with the upward propagation of tropospheric waves at these locations (Figure 4.6 and 4.2 bottom). Especially over western Asia and the eastern North Atlantic, two pronounced ridges are found where tropospheric waves propagate upward into the stratosphere (Figure 4.7 bottom and 4.2 bottom). The time after 16 February 2009 is not investigated further since only normalized geopotential height anomalies <1.0 standard deviations are present at surface making an influence of the SSW event less likely than in the time between 11 and 16 February 2009 (Figure 4.1). The only exception are a few days in mid-March which show normalized geopotential height anomalies >1.0 standard deviations from the surface to roughly 800 hPa height.

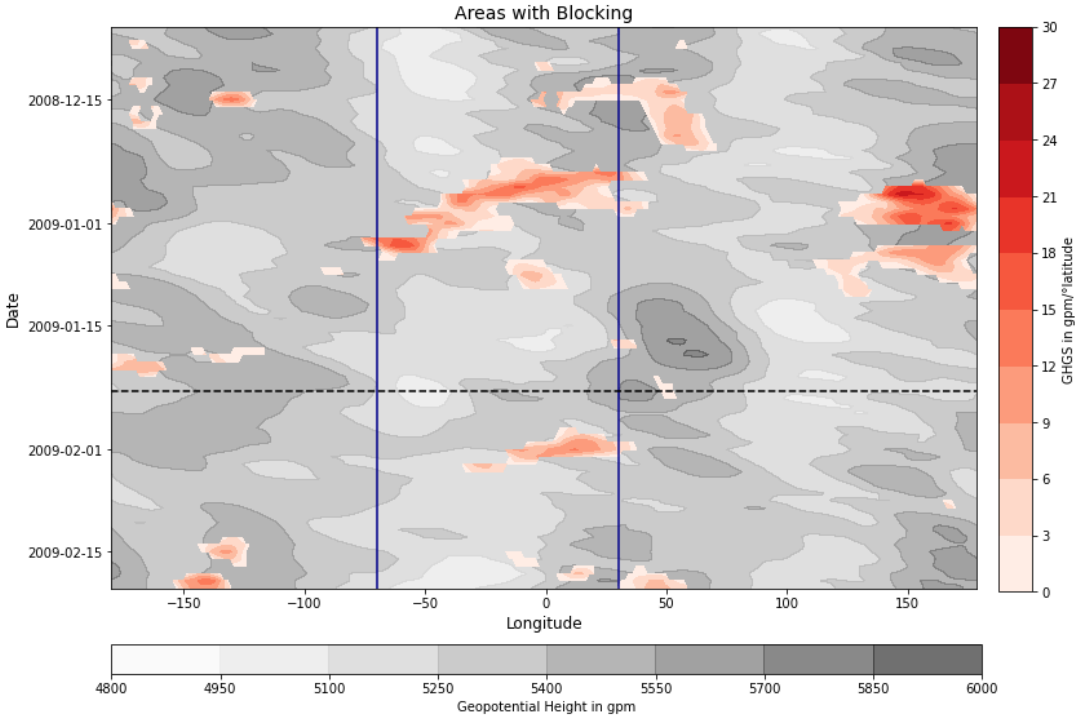

Figure 4.6: **Blocking Situation between December 2008 and February 2009 based on ERA-Interim.** The Hovmöller diagram shows the 500 hPa geopotential height, averaged between 40°N and 80°N, as grey shading. The GHGS component of the blocking index by Tibaldi and Molteni (1990) is shown in red. The horizontal black dashed lines mark the central date of the SSW event. The area between the solid blue lines refers to the Euro-Atlantic sector, 70°W to 30°E.

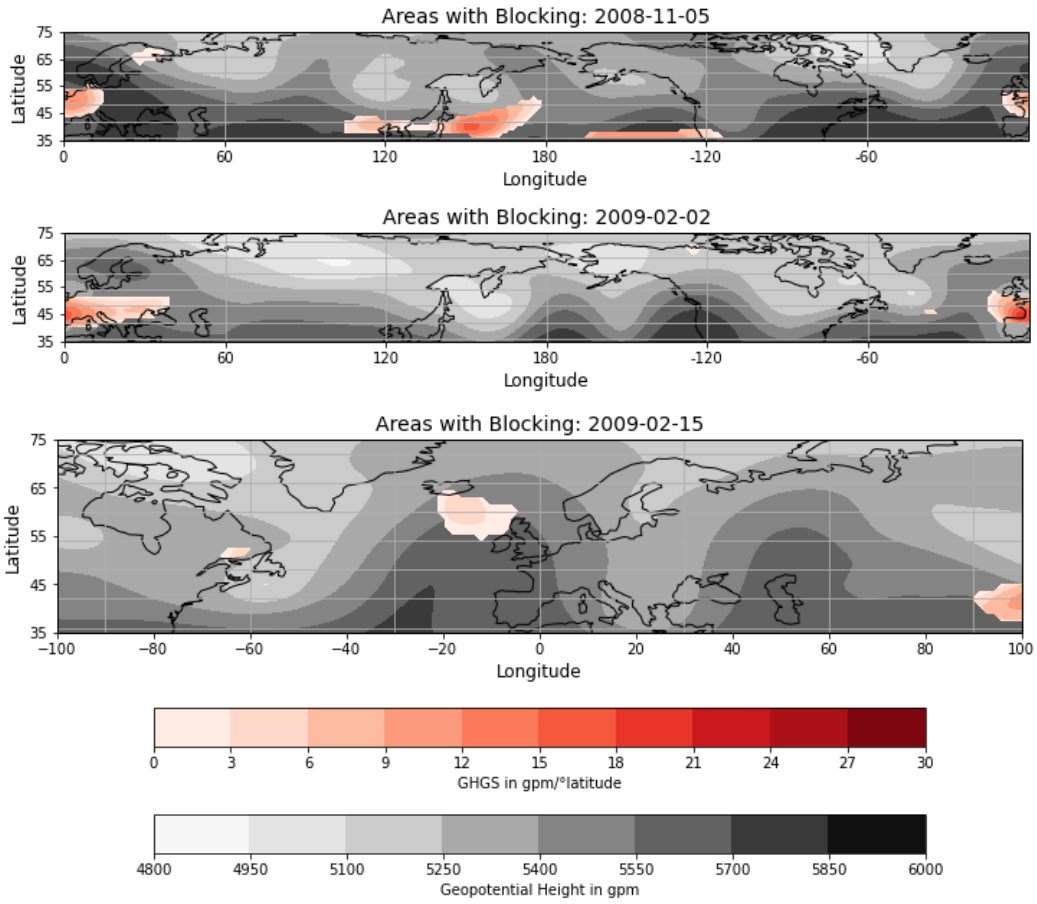

Figure 4.7: **Distinctive Blocking Patterns in the Middle Troposphere in the Winter 2008/2009 based on ERA-Interim.** Selected days, 5 November 2008 (top), 2 February 2009 (middle) and 15 February 2009 (bottom) with blocking patterns are shown. The 500 hPa geopotential height is shown as grey shading and the GHGS component of the blocking index by Scherrer et al. (2006) in red.

4.4 Position of the Mid-Latitude Jet Stream in the Lower Troposphere

In the beginning of the winter 2008/2009, the mid-latitude jet stream is located at its climatological position, thus not indicating the upward propagation of tropospheric baroclinic waves occurring at the same time (Figure 4.8 and 4.2 top). Here it is important to note that the wind data in November is prone to boundary effects of the filtering and that the strongest upward propagation of baroclinic waves occurs over the North Pacific and not over the North Atlantic ocean. Coinciding with the elongation of the polar vortex on 8 December 2008, the mid-latitude jet stream over the North Atlantic ocean is displaced poleward from its climatological position (Figure 4.8). This is may caused by the occurring ridges in the North Atlantic region (Figure 4.6). The following long-lasting and strong blocking situation in the Euro-Atlantic sector may cause either a split of the mid-latitude jet stream or a rapid shift from high latitudes to 35°N at the end of December 2009 (Figure 4.6 and 4.8; Martius et al., 2009).

From mid-January onwards, coincinding with the deceleration of the 10 hPa zonal-mean zonal

wind, the position of the jet stream varies between its climatological position and 35°N (Figure 4.8 and 4.3). Between 11 and 16 February 2009 when positive normalized geopotential height anomalies are present continuously from the stratopause to the surface, the mid-latitude jet stream is displaced poleward and maybe split for a short time period (Figure 4.1 and 4.8). Since large blocking patterns are absent over the North Atlantic ocean at that time, a split of the jet stream is rather unlikely but cannot be excluded with the methods used in this thesis (Figure 4.6). The poleward shift of the North Atlantic mid-latitude jet stream indicates according to Afargan-Gerstman and Domeisen (2020) an surface influence of the SSW event over the Pacific ocean. This is not confirmed by the deviation of the geopotential height from the zonal-mean which shows an upward propagation of tropospheric waves over the Pacific ocean, at least at 65°N (Figure 4.2 bottom). The SSW event of the winter 2008/2009 is therefore not associated with the poleward displacement of the mid-latitude jet stream in mid-February 2009.
Until April 2009, the jet stream is located constantly in the region around its climatological position and 10°latitude above it (Figure 4.8). The equatorward displacement in the beginning of April is already more than 60 days after the central date of the SSW and therefore not associated with it (Baldwin et al., 2003).

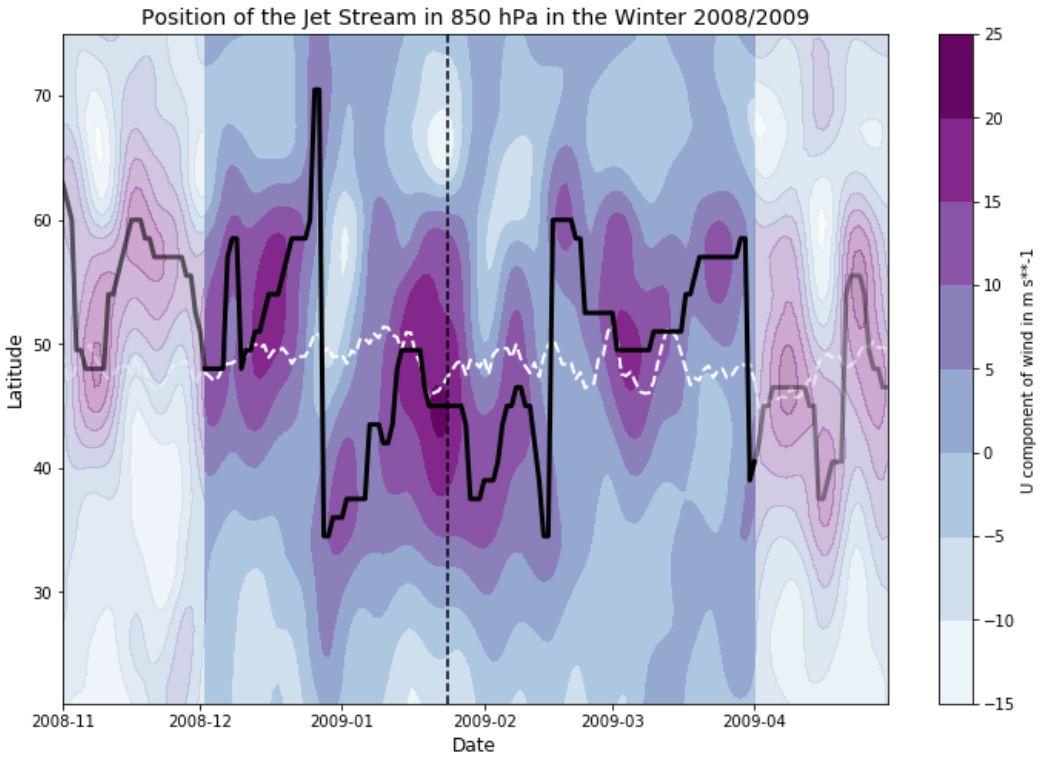

Figure 4.8: **Zonal Wind Speed Anomalies during the Winter 2008/2009 based on ERA-Interim.** The zonal-wind anomalies in 850 hPa, averaged over 60°W to 0°E are shown as shading in the Hovmöller diagram. The anomalies are filtered using a Lanczos filter with a moving window of 61 days and a cutoff-frequency of 1/10 days. Data on the edges of the timeseries are prone to boundary effects due to the filtering and therefore, shown paler than the unaffected data. The wind maxima are shown as a black solid line. The white dashed line shows the climatological position of the mid-latitudes jet stream. The central date of the SSW is marked with the vertical black dashed line.

4.5 North Atlantic Oscillation Index at the Surface

The winter 2008/2009 shows a frequent change of the NAO phases (Figure 4.9). Two of the five NAO- phases in this winter reach values below -3.5 standard deviations in the 7-day running mean of the standardized NAO index. The first strongly negative NAO phase occurs between 23 December 2008 and 8 January 2009 (Figure 4.9). It co-occurs with an equatorward shift of the mid-latitude jet stream and a long-lasting strong blocking pattern over the North Atlantic-European sector (Figure 4.8 and 4.6). Although the polar vortex is elongated on 8 December 2008, a downward influence of the weak polar vortex is not detected by the methods used in this thesis (Figure 4.4 left column, top).

On 9 January 2009, about 2 weeks prior to the central date of the SSW, a positive phase of the NAO establishes (Figure 4.9). Only at 3 consecutive days in this time, on 13 and 15 January 2009, the daily NAO index turns negative coinciding with negative polar-cap averaged geopotential height anomalies at the surface (Figure 4.9 and 4.1). This is not reflected in the 7 day running mean of the NAO index.

On 28 January 2009, coinciding with positive polar-cap averaged geopotential height anomalies at the surface, the NAO index turns negative until 17 February 2009 (Figure 4.9 and 4.1). This comprises the time when positive geopotential height anomalies >1.0 standard deviation associated with the SSW, are present at surface (Figure 4.1). Nevertheless, the NAO- phase is not associated with a downward influence of the SSW event since during this time, an upward propagation of tropospheric waves is only present over the North Atlantic ocean, at least at 65°N (Figure 4.2 bottom). A possible trigger of this NAO- phase is a long-lasting blocking pattern over the North Atlantic-European sector which is detected at the same time as the NAO- phase starts (Figure 4.6; Santos et al., 2013). Two short blocking situations in mid-February may maintain it (Figure 4.6 and 4.9). It is noteworthy that the NAO- pattern is shifted eastward over Europe instead of being centered over the North Atlantic ocean between the end of January and mid-February 2009 (Figure 4.10 top row).

The following NAO- phase in March 2009 could theoretically be influenced by a downward propagation of stratospheric anomalies caused by the SSW as it occurs less than 2 month after the central date of the SSW event (Figure 4.9; Baldwin et al., 2003). It coincides indeed with positive normalized geopotential height anomalies >1.0 standard deviation at the surface but the roughly climatological position of the mid-latitude jet stream at that time does not indicate a downward influence of the SSW event on the troposphere (Figure 4.1 and 4.8). A downward influence of the SSW event during this time is therefore not suggested.

The following two NAO- phases occur after 2 month after the central date of the SSW and are therefore not associated with it (Figure 4.9; Baldwin et al., 2003).

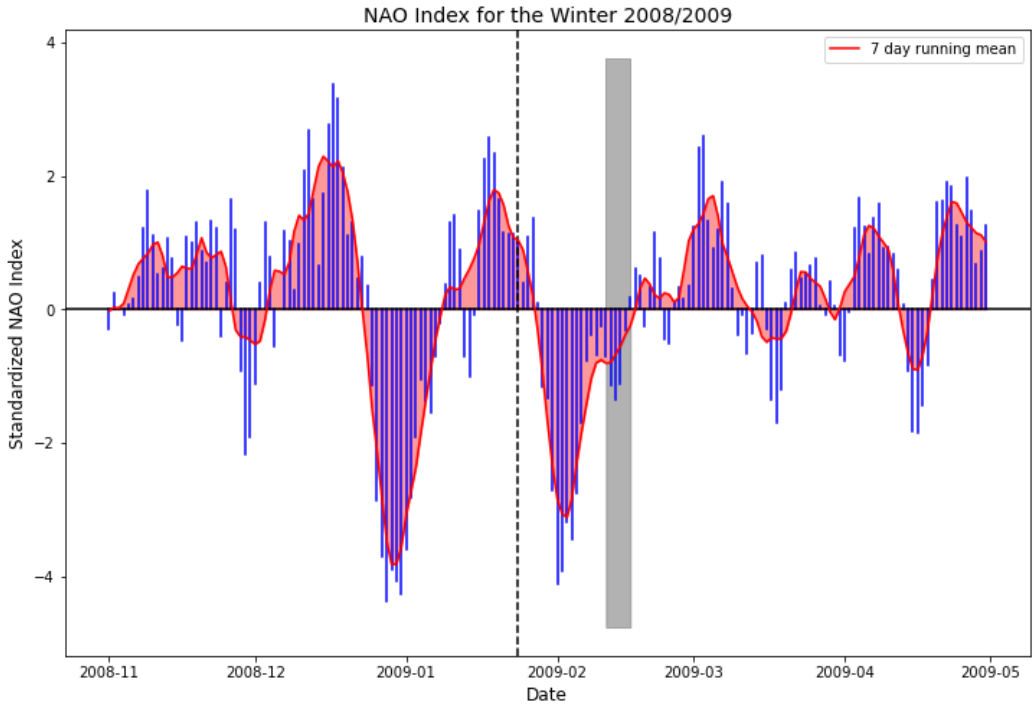

Figure 4.9: **NAO Index during the Winter 2008/2009 based on ERA-Interim.** Shown is the Zonal Index which is calculated as the standardized mean sea level pressure anomaly difference between a southern box, averaged over 40°W to 0°E and 35°N to 50°N, and a northern box, averaged over 40°W to 0°E and 55°N to 70°N (Leckebusch et al., 2008). The black dashed line marks the central date of the SSW. The period with normalized geopotential height anomalies >1.0 standard deviation associated with the SSW which are present continuously from the stratosphere to the surface, is shaded in dark grey.

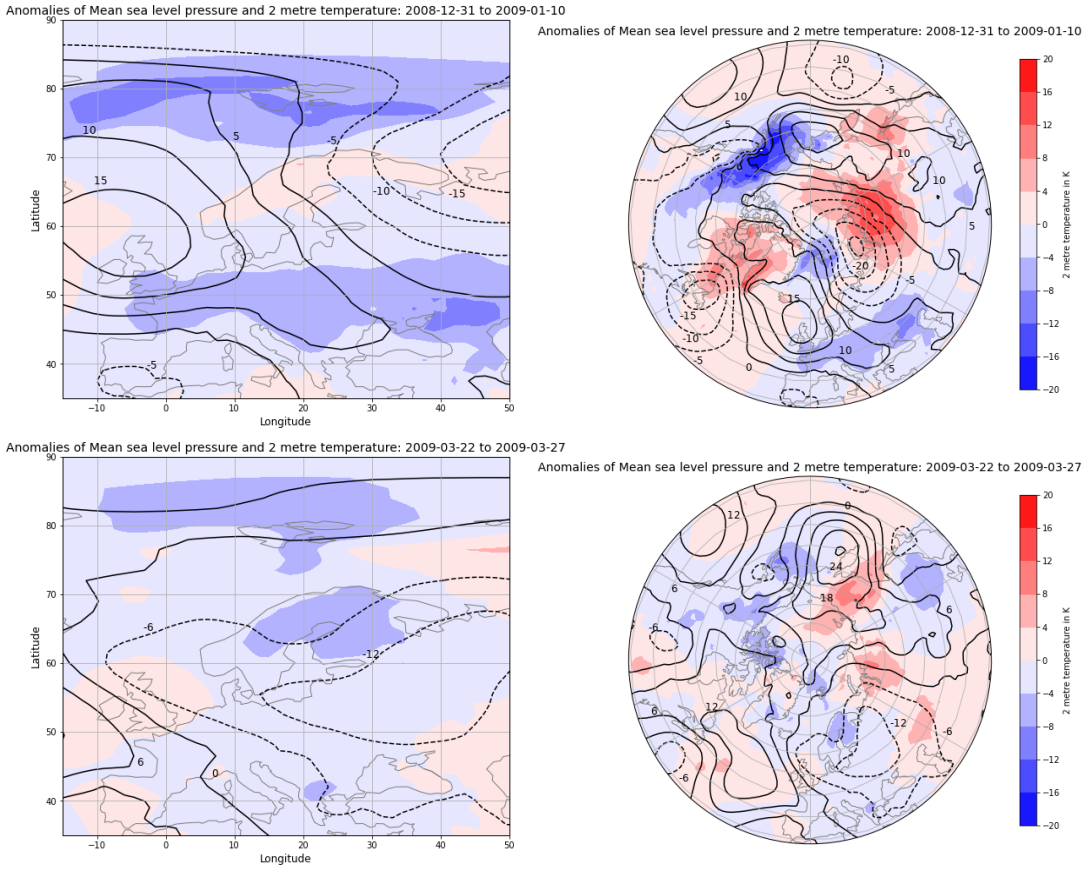

Figure 4.10: **Mean Sea Level Pressure Anomalies and 2 Metre Temperature Anomalies for Two European Cold Waves based on ERA-Interim.** Shown is the European cold wave between end of December 2008 and beginning of January 2009 (top row) and the European cold wave in the end of March 2009 (bottom row). The dashed contours show negative mean sea level pressure anomalies, the solid contours show positive mean sea level anomalies. The 2 metre temperature anomalies are plotted as shading.

4.6 European Cold Waves at the Surface

When looking at the 2 metre temperature anomalies of the winter 2008/2009 only two European cold waves are detected and only one of them is confirmed by the approach of Smid et al. (2019) (Figure 4.11 and 4.12). The cold wave detected by both approaches coincides roughly with the NAO- phase occurring between 23 December 2008 and 9 January 2009 (Figure 4.9). The coldest temperatures are found over eastern Europe reaching mean values up to 6 K and locally up to 12 K below the climatology (Figure 4.11 and 4.10 top row). All European regions, except south-western Europe according to the approach by Smid et al. (2019) experience colder than usual 2 metre temperatures. Since this cold wave happens before the SSW event, it cannot be associated with it.

During the time when positive normalized geopotential height anomalies associated with the SSW event are found continuously from the stratopause to the surface, a mean European cold wave is not detected although the Mediterranean, central and northern Europe experience unusually cold temperatures (Figure 4.11 and 4.12). This is surprising as the co-occurring NAO- phase often leads to colder than usual temperatures in large parts of Europe (Butler et al., 2015). Since an upward propagation of tropospheric waves over the Euro-Atlantic sector is observed during this time, an influence of the SSW on European temperatures is not suggested (Figure 4.2 bottom).

The cold wave occurring between 22 and 27 March 2009 is only detected in the 7-day running mean of the 2 metre temperature anomalies (Figure 4.11). It is strongest over northern Europe with temperature anomalies up to 4 K below the climatology (Figure 4.10 bottom row). Since the SSW event occurs almost exactly 2 month before the cold wave, it may have triggered but not maintained it (Figure 4.3). The poleward shift of the mid-latitude jet stream and the change between NAO- and NAO+ at that time also not support the idea of the SSW triggering the cold wave (Figure 4.8 and 4.9). Therefore, it is not associated with the SSW.

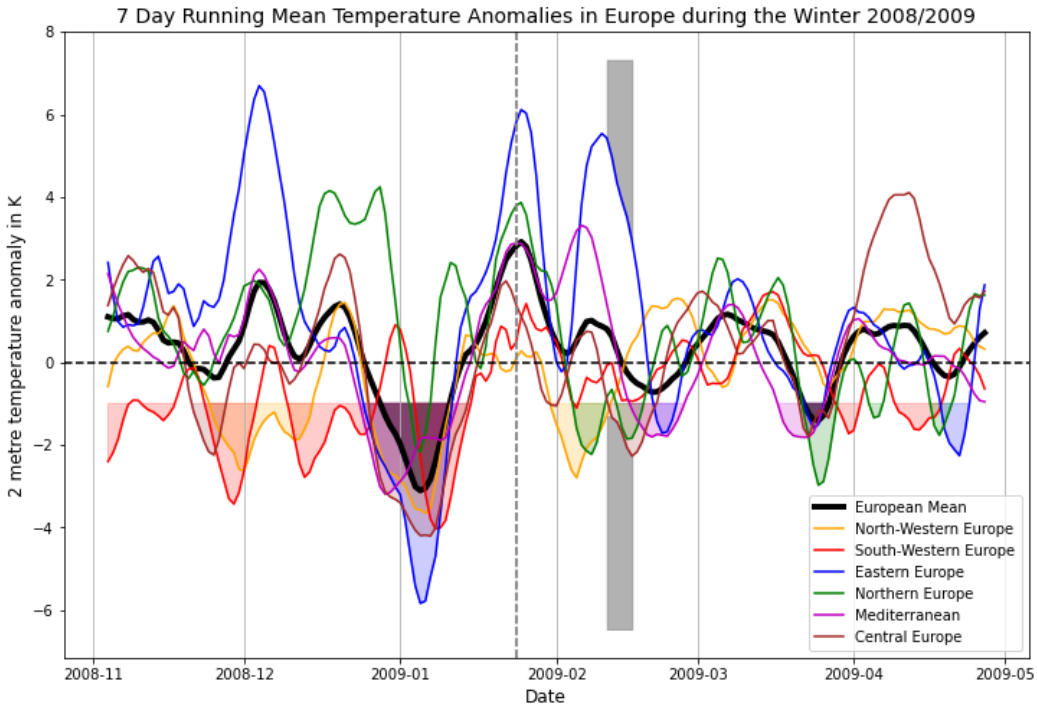

Figure 4.11: **2 Metre Temperature Anomalies during the Winter 2008/2009 based on ERA-Interim.** Periods of cold waves are defined using 1 K below the climatological mean as the warm temperature threshold for cold waves (Garfinkel et al., 2017). The days with cold waves are marked as shading in the respective color. The vertical black dashed line marks the central date of the SSW in the winter 2008/2009. The period with normalized geopotential height anomalies >1.0 standard deviation associated with the SSW which are present continuously from the stratosphere to the surface, is shaded in dark grey. The European mean is calculated by averaging between 10°W to 42°E and 35°N to 72°N. The anomalies for north-western Europe between 10°W to 3°E and 45°N to 60°N, for south-western Europe between 10°W to 3°E and 35°N to 45°N, for eastern Europe between 20°E to 42°E and 45°N to 60°N, for northern Europe between 3°E to 42°E and 60°N to 72°N, for central Europe between 3°W to 20°E and 45°N to 60°N and for the Mediterranean between 3°E to 42°E and 35°N to 45°N.

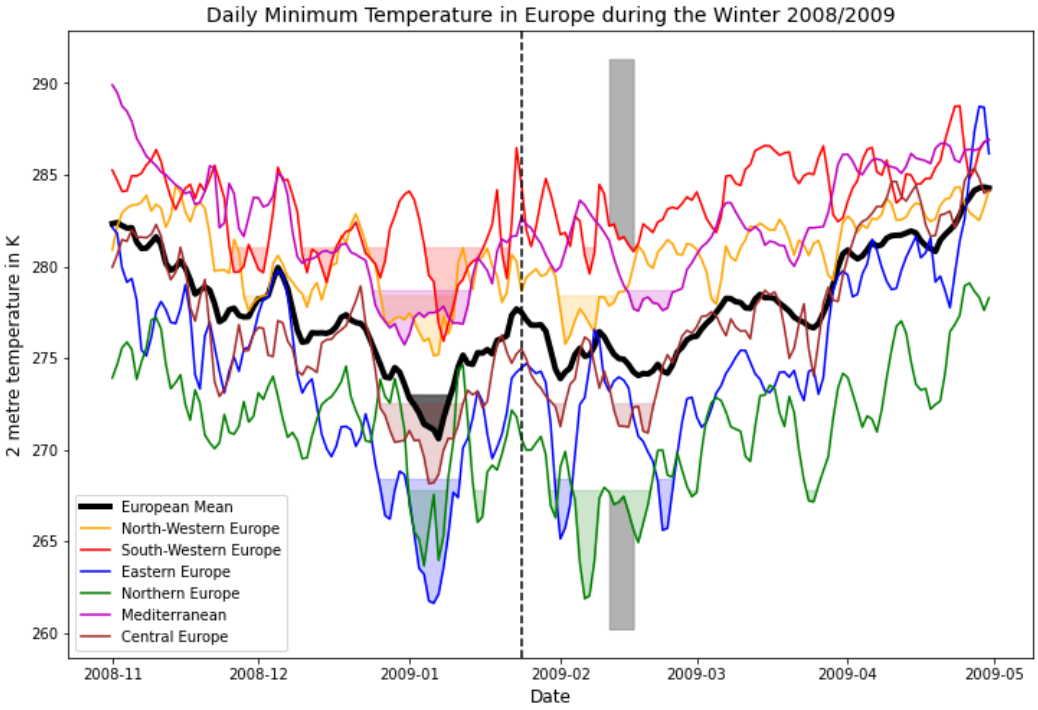

Figure 4.12: **2 Metre Daily Minimum Temperature during the Winter 2008/2009 based on ERA-Interim.** Periods of cold waves are defined as at least 3 consecutive days with daily minimum temperatures below the 10^{th} percentile of the climatological daily minumum temperature (Smid et al., 2019). The climatology is calculated for the period between 1999 and 2019 with a 31 day running mean. The days with cold waves are marked as shading in the respective color. The vertical black dashed line marks the central date of the SSW.The period with normalized geopotential height anomalies >1.0 standard deviation associated with the SSW which are present continuously from the stratosphere to the surface, is shaded in dark grey. The European mean is calculated by averaging between 10°W to 42°E and 35°N to 72°N. The anomalies for north-western Europe between 10°W to 3°E and 45°N to 60°N, for south-western Europe between 10°W to 3°E and 35°N to 45°N, for eastern Europe between 20°E to 42°E and 45°N to 60°N, for northern Europe between 3°E to 42°E and 60°N to 72°N, for central Europe between 3°W to 20°E and 45°N to 60°N and for the Mediterranean between 3°E to 42°E and 35°N to 45°N.

4.7 Concluding Remarks

The winter 2008/2009 features the longest-lasting SSW event with the strongest easterly winds in the middle stratosphere of the past 20 years (Table 3.2). In roughly 2 weeks, the 10 hPa polar-cap averaged temperature increases by approximately 50 K while the 10 hPa zonal-mean zonal wind decreases 104 ms^{-1} in total. However, this S-type event is not associated with a downward influence on European surface weather. Positive normalized geopotential height anomalies are present continuously from the stratosphere to the surface between 11 and 16 February 2010 and associated with an upward propagation of tropospheric baroclinic waves over the Euro-Atlantic sector (Figure 4.1 and 4.2 bottom). Although the NAO is in its negative phase and the mid-latitude jet stream is displaced equatorward, unusually low 2 metre temperatures are found only in central and northern Europe but not in the European mean (Figure 4.9, 4.8, 4.11 and 4.12). A possible explanation herefore is the occurrence of a pronounced ridge over the eastern North Atlantic ocean with embedded blocking (Figure 4.7 bottom). This may lead to a meridional transport of polar air at its eastern flank which is located over central Europe. The only European mean cold wave after the central date of the SSW occurs between 22 and 27 February 2009 (Figure 4.11). Interestingly, this cold wave is only detected by the 7-day running mean of the 2 metre temperature anomalies but not when using the lowest 10^{th} percentiles of the 2 metre minimum temperatures (Figure 4.12). By the latter approach, only a small cold wave over northern Europe is detected. The late start of the European cold wave roughly 2 months after the central date of the SSW is one reason why it is unlikely that the cold temperature anomalies are linked to the SSW event (Baldwin et al., 2003). The other reasons are the poleward displacement of the mid-latitude jet stream and the shift from the negative to the positive phase of the NAO during this time (Figure 4.8 and 4.9).

5 Winter 2009/2010

5.1 Troposphere-Stratosphere Coupling

During the winter 2009/2010, three structures with positive normalized geopotential height anomalies >1.0 standard deviation are visible in the stratopause region around 1 hPa (Figure 5.1). Two of these structures show continuous normalized geopotential height anomalies >1.0 standard deviation from the stratopause to the surface. In case of the first structure, these anomalies are present continuously at the surface between 9 December 2009 and 11 January 2010. The coupling of the troposphere with the stratosphere is nearly instantaneous at the beginning of December 2009 but around 2 weeks later positive normalized geopotential height anomalies >1.0 standard deviation are only detected below the lower stratopause region (Figure 5.1). A coupling between the troposphere and stratosphere can be excluded in early January as negative geopotential height anomalies are present in the upper and middle stratosphere above the positve anomalies detected in the troposphere. When looking at the deviation of the normalized geopotential height anomalies from the zonal-mean, the structure with continuous positive geopotential height anomalies >1.0 standard deviation in the troposphere and stratosphere shows a westward tilt with height (Figure 5.2 top). This indicates an upward propagation of baroclinic waves (Lim and Wallace, 1991). At the same time, an upward propagation of baroclinic waves into the lower stratosphere is present over Scandinavia. This upward propagation of tropospheric waves continuous as long as positive geopotential height anomalies are still present at the surface (Figure 5.1). A possible reasons for the stop of the troposphere-stratosphere coupling in mid-December 2009 might be the establishment of strong westerly winds in the tropopause region caused for example by tropospheric internal variability. As only positive geopotential height anomalies can be associated with SSW events (Karpechko et al., 2018), negative geopotential height anomalies are not investigated further in this thesis. Positive normalized geopotential height anomalies >1.0 standard deviation belonging to the second structure with continuous positive normalized geopotential height anomalies >1.0 standard deviation from the stratosphere to the troposphere are found at the surface between 30 January 2010 and 27 February 2010 (Figure 5.1). The coupling of the troposphere and the stratosphere is again nearly instantaneous. In the deviation of normalized geopotential height from the zonal-mean, the structure with positive anomalies over the Pacific is not tilted with height from the surface to 3 hPa height and then slightly tilted to the east with height (Figure 5.2 bottom). This mostly barotropic feature indicates a downward propagation of stratospheric signals to the surface, although the positive geopotential height deviation near the surface shows only positive values <1.0 standard deviation (Figure 5.2 bottom; Lim and Wallace, 1991). Another strongly positive geopotential height structure at the surface over Scandinavia shows a westward tilt with height, indicating the upward propagation of tropospheric waves over that region (Lim and Wallace, 1991).

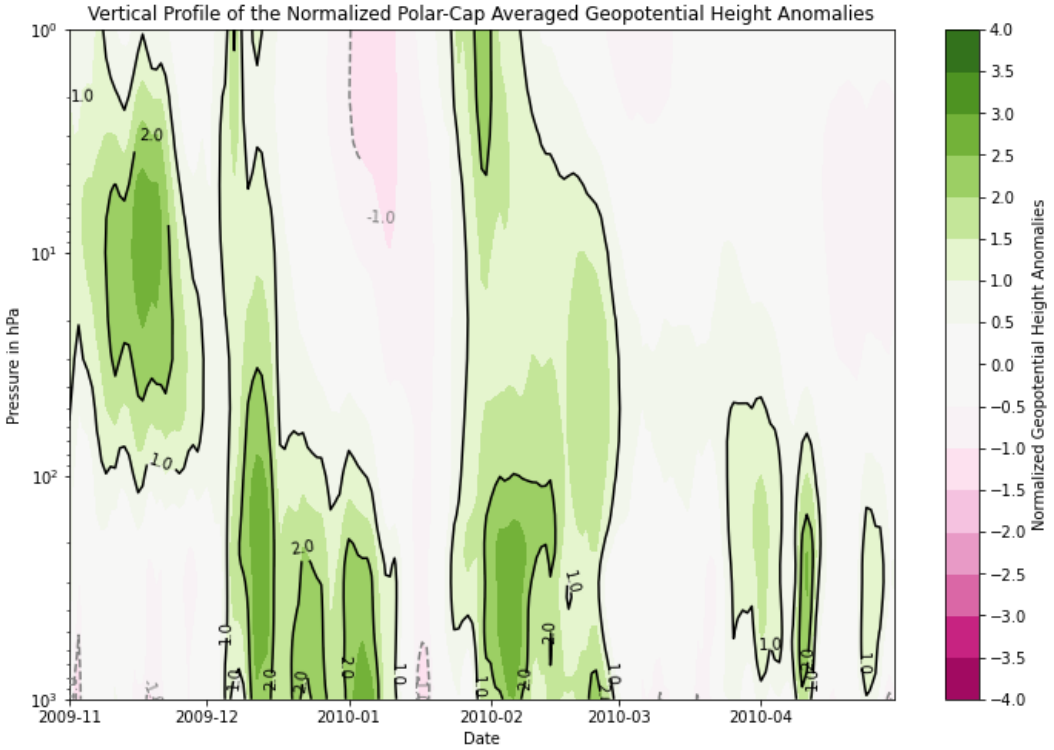

Figure 5.1: **Vertical Profile of the Polar-Cap Averaged Normalized Geopotential Height Anomalies during the Winter 2009/2010 based on ERA-Interim.** The green structures starting at 1 hPa are an indicator of possible SSW events.

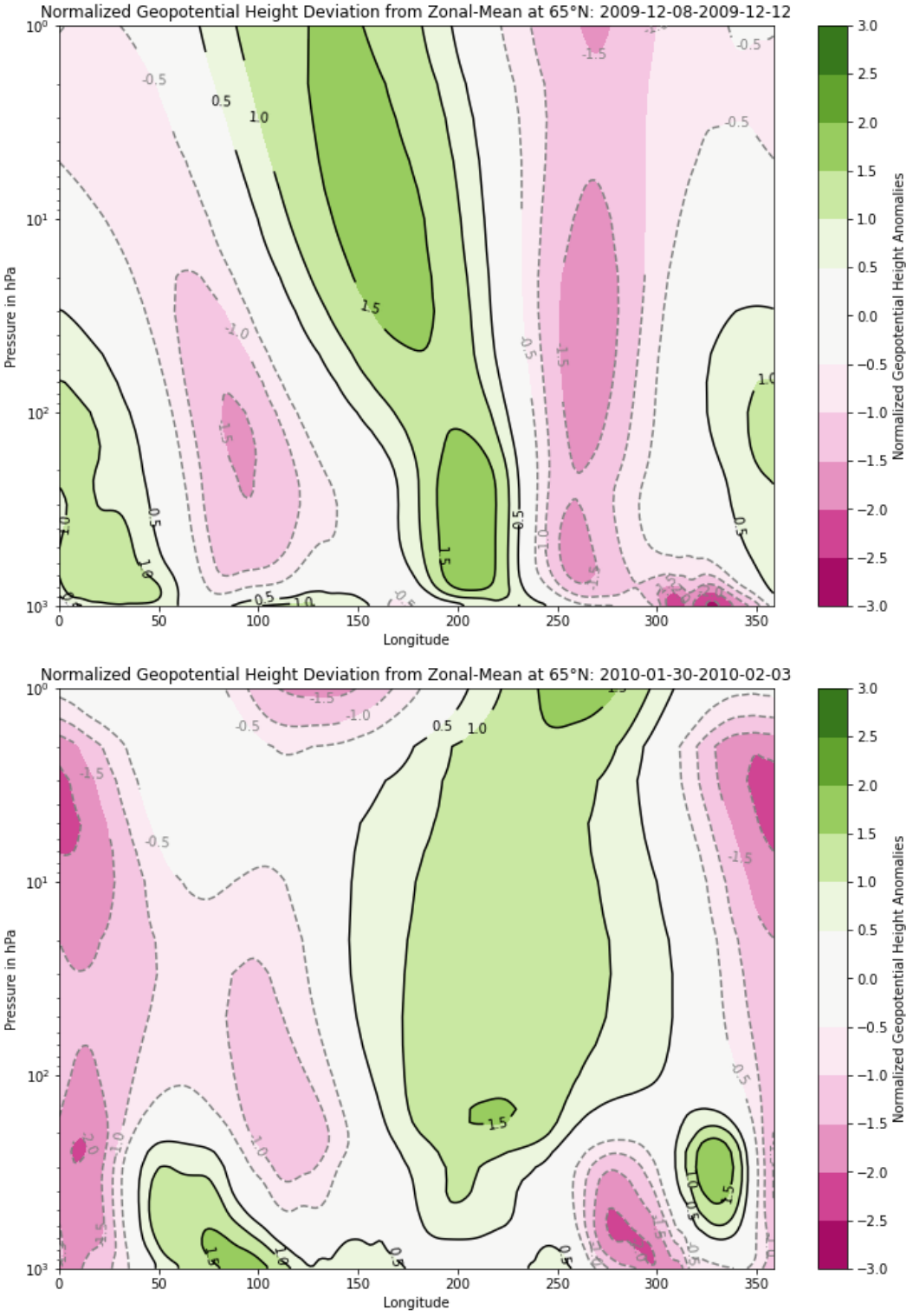

Figure 5.2: **Normalized Geopotential Height Deviations from Zonal-Mean after the SSW Events of the Winter 2009/2010 based on ERA-Interim.** The time for averaging is the time around the largest positive standard deviations of the normalized geopotential height anomalies at the surface, associated with positive geopotential height anomalies >1.0 standard deviation at the stratopause (top plot) and from the beginning of positive normalized geopotential height anomalies >1.0 standard deviation at the surface associated with the second structure of positive normalized geopotential height anomalies >1.0 standard deviation at the stratopause (bottom).

5.2 Sudden Stratospheric Warming Signals in the Middle Stratosphere

The three structures with positive normalized positive geopotential height anomalies >1.0 standard deviation at the stratopause lead to the suggestion that three SSW events occur in the winter 2009/2010 (Figure 5.1). This is not confirmed by the SSW index which only detects one SSW event in this winter (Figure 5.3). The detected event with its central date on 25 January 2010 is associated with the third structure with positive normalized geopotential height anomalies >1.0 standard deviation at the stratopause. The structure with positive normalized positive geopotential height anomalies >1.0 standard deviation at the beginning of the winter coincides with a deceleration of the 10 hPa zonal-mean zonal wind at 65°N (Figure 5.1 and 5.3). This clearly shows a weakened polar vortex but the event is not classified as an SSW because the zonal-mean zonal wind is still westerly. At the end of November 2009, the polar jet is strengthening again reaching values slightly below 40 ms^{-1} in the beginning of December. Until this time, the polar-cap averaged 10 hPa temperature is below 210 K, but rises about 5 K in the days before 12 December 2009 (Figure 5.3). At this date, positive normalized positive geopotential height anomalies >1.0 standard deviation are present at the stratospause for the second time in this winter (Figure 5.1). This structure shows positive anomalies continuously from the stratosphere to the surface and is associated with an upward propagation of baroclinic waves over the Pacific ocean (Figure 5.2 top). The upward propagation of tropospheric signals is also visible in the shape of the polar vortex (Figure 5.4 left column). In 50 hPa height, the polar vortex is split clearly in two parts of comparable size. Temperatures are below 230 K over the whole northern hemisphere (Figure 5.4 left column bottom). In 30 hPa height, the polar vortex is split, too but in this height temperatures between 230 K and 240 K are visible over the Sea of Okhotsk and parts of south-eastern Russia (Figure 5.4 left column middle). The region of the warm temperatures is the same region, where the upward propagating baroclinic waves are detected which indicates the breaking of these waves in that region (Figure 5.2 top; Matsuno, 1971). In 10 hPa height, the regions with temperatures above 230 K are the same as the regions where the upward propagating baroclinic waves are detected, too (Figure 5.4 left column top and 5.2 top). This supports the idea of wave breaking in this region. The polar vortex itself is elongated in 10 hPa height with the beginning formation of two smaller vortex parts inside the elongated vortex filament. The baroclinicity which is seen in the geopotential height deviation from the zonal-mean is also seen in the different heights (Figure 5.2 top and 5.4 left column). Although the polar vortex is split in 30 hPa and 50 hPa height, all three wind-based SSW indices do not detect an SSW event (Table 3.1). The U65 index shows minimal westerly wind speeds of 17 ms^{-1} while the 10 hPa polar-cap averaged temperatures are around 210 K (Figure 5.3). After this split of the polar vortex, the two vortex parts reunite and form a stable polar vortex with 28000 gpm at its core and maximum westerly wind-speeds of 59 ms^{-1} on 10 January 2010 (Figure 5.3). The 10 hPa polar-cap temperature is with roughly 205 K on the lowest state of the winter 2009/2010. The polar vortex has a concentric shape centered over the pole in all three displayed heights and features a barotropic structure (Figure 5.5 left column). After this strong polar vortex state, the 10 hPa zonal-mean zonal wind at 65°N decelerates rapidly and reverses on 25 January 2010 (Figure 5.3). This is a typical behaviour observed before SSW events (Charlton and Polvani, 2007). The polar-cap averaged temperature in 10 hPa increases up to 238 K

until 1 February 2010. On 27 January 2010, 2 days after the central date of the major SSW, the polar vortex is displaced from the pole and clearly elongated in all three displayed heights (Figure 5.5 middle column). The vortex split is observed on 4 February 2010, coinciding with large positive normalized geopotential height anomalies at the surface belonging to the third strucure with positive normalized geopotential height anomalies >1.0 standard deviation at the stratopause (Figure 5.3 and 5.1). Although the SSW index is positive at that time, the polar vortex is clearly split with its remnants located at the same position in all three displayed heights (Figure 5.4 middle column and 5.3). The stronger part with 29000 gpm is located over the North Atlantic ocean and the weaker part with 30250 gpm over the North Pacific ocean. In 10 hPa height, temperatures up to 260 K are found over eastern Scandinavia and locally over central Asia (Figure 5.4 middle column top). The structure of the polar vortex is baroclinic, whereas in 30 hPa the structure of the polar vortex is barotropic (Figure 5.4 middle column top and middle). This is also seen in the geopotential height deviation from the zonal-mean at 65°N (Figure 5.2 bottom). In 30 hPa height, the warmest temperatures up to 250 K are located over north-western Russia (Figure 5.4 middle column middle). In 50 hPa height, the warmest temperatures do not reach 240 K and are located further southward (Figure 5.4 middle column middle and bottom). The polar vortex is again in a barotropic state (Figure 5.4 bottom). Around 10 February 2010, the SSW index reaches its winter minimum with -20 ms^{-1}, roughly a week later than the temperature maximum of the winter is reached (Figure 5.3). On 19 February 2010 the whole northern hemisphere in 10 hPa is still clearly warmed over eastern Europe and western Asia with temperatures up to 257 K (Figure 5.4 right column top). Meanwhile three remants of the polar vortex show a baroclinic structure with the strongest remnants located over Hudson bay. The weaker remnants are located over central Europe and western Asia. In 30 hPa as well as in 50 hPa height, the vortex remants located over Hudson Bay and western Asia stay in the same position (Figure 5.4 right column middle and bottom). In the lower heights, the northern hemispheric temperatures are cooler, reaching maximum below 250 K in 30 hPa height and below 240 K in 50 hPa height. In addition to the colder temperatures in 50 hPa height, the two weaker remnants of the polar vortex are not split and the filament is located completely over Asia (Figure 5.4 right column bottom). In the following two and a half weeks, the polar vortex is strenghtening again, featuring westerly winds from 26 February onwards, 2 days before only normalized geopotential height anomalies <1.0 standard deviation are found at the surface (Figure 5.3 and 5.1). This ends the 32 day lasting SSW event. At the end of March 2010, the polar night jet turns again to easterlies. This marks the onset of the final warming of the winter 2009/2010 according to the U65 index (Figure 5.3). The other two wind-based SSW indices, CP07 and U6090, classify this wind-reversal as a second SSW of the winter 2009/2010 (Table 3.1). The polar vortex is displaced off the pole and shows barotropic features in all three displayed heights (Figure 5.5 right column). In 10 hPa height it shows the typical „comma-“shape of a D-type event (Figure 5.5 right column top; Charlton and Polvani, 2007). Temperatures up to 250 K are found over southern central Asia. In 30 hPa and 50 hPa height, the polar vortex has a less distince „comma-“shape (Figure 5.5 right column middle and bottom). The maximum temperatures are below 220 K over the whole northern hemisphere at both pressure levels (Figure 5.5 right column middle and bottom). After this phase of easterly winds, the polar night jet accelerates again but does not reach westerly wind-speeds >5 ms^{-1} until the final warming of the winter 2009/2010 which changes the stratospheric zonal-mean zonal winds to easterlies again

(not shown). The standardized geopotential height anomalies at the stratopause are constantly <1.0 standard deviation during that time (Figure 5.1). This indicates a rather gradual than abrupt change of the stratospheric circulation. In addition to that, the polar vortex does not recover to a stable, concentric shape centered over the pole. Thus, this wind-reversal event is considered to be part of the final warming of the winter 2009/2010, as classified by the U65 index, and therefore, not investigated further in this thesis.

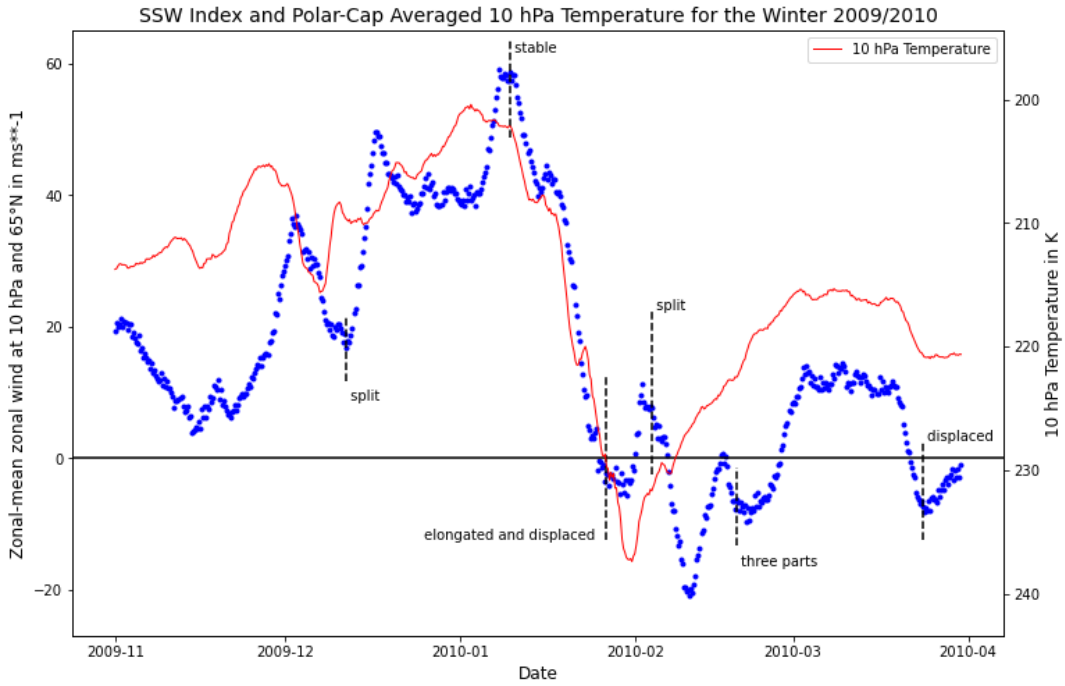

Figure 5.3: **SSW Index and Polar-Cap Averaged 10 hPa Temperature for the Winter 2009/2010 based on ERA-Interim.** The blue dots show the modified SSW index by Charlton and Polvani (2007) with 65°N instead of 60°N as reference latitude. The red line shows the polar-cap averaged 10 hPa temperature. Days with distinctive shapes of the polar vortex in the 10 hPa geopotential height field are marked.

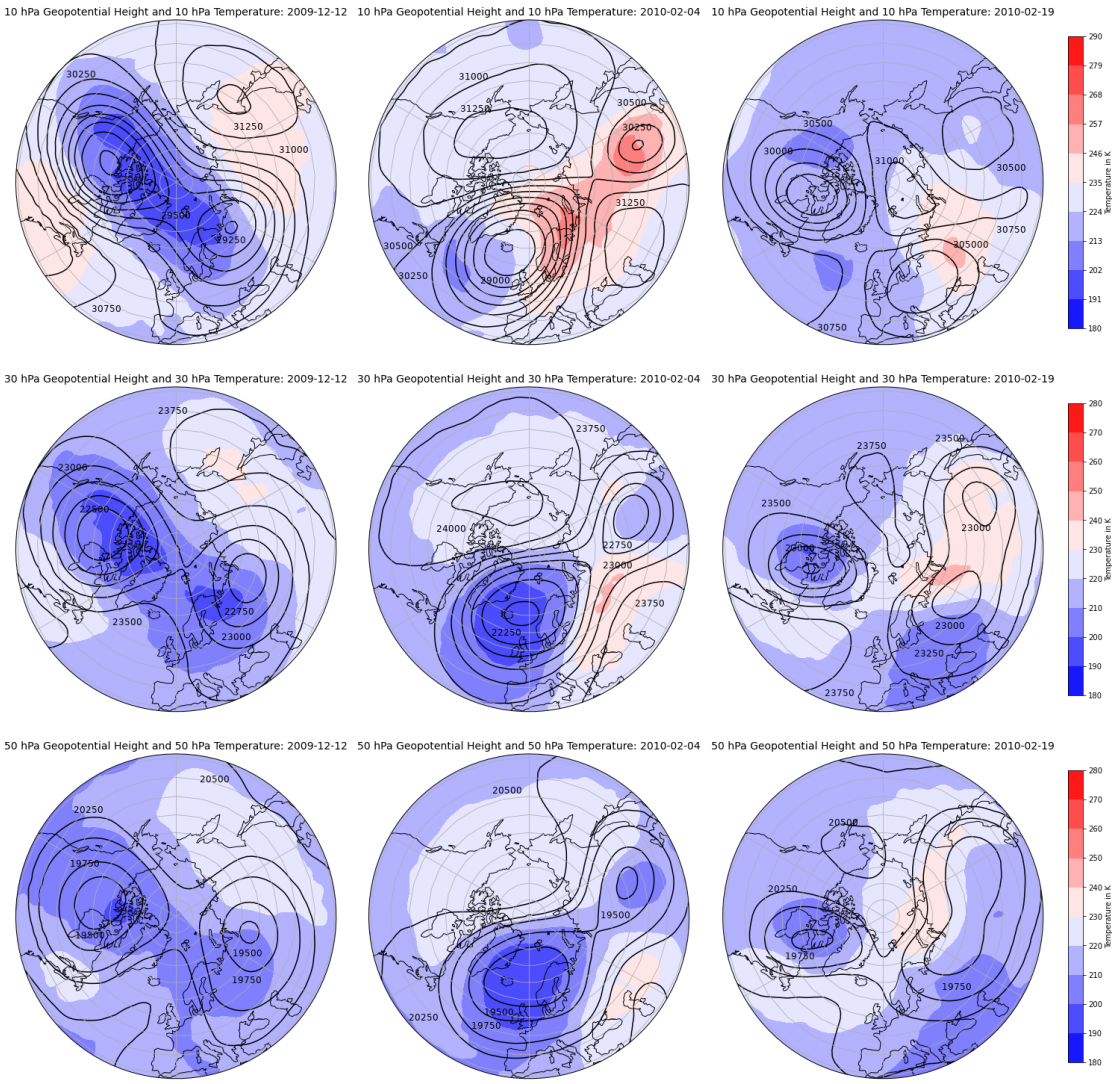

Figure 5.4: **Geopotential Height and Temperature in the Middle Stratosphere on 12 December 2009, 4 February 2010 and 19 February 2010 based on ERA-Interim.** The geopotential height and temperature are shown in 10 hPa (top row), 30 hPa (middle row) and 50 hPa (bottom row) for 12 December 2009 (left column), 4 February 2010 (middle column) and 19 February 2010 (right column). All plots have the same color-scale except the plot on the top right (the color-scale for this plot is given next to it).

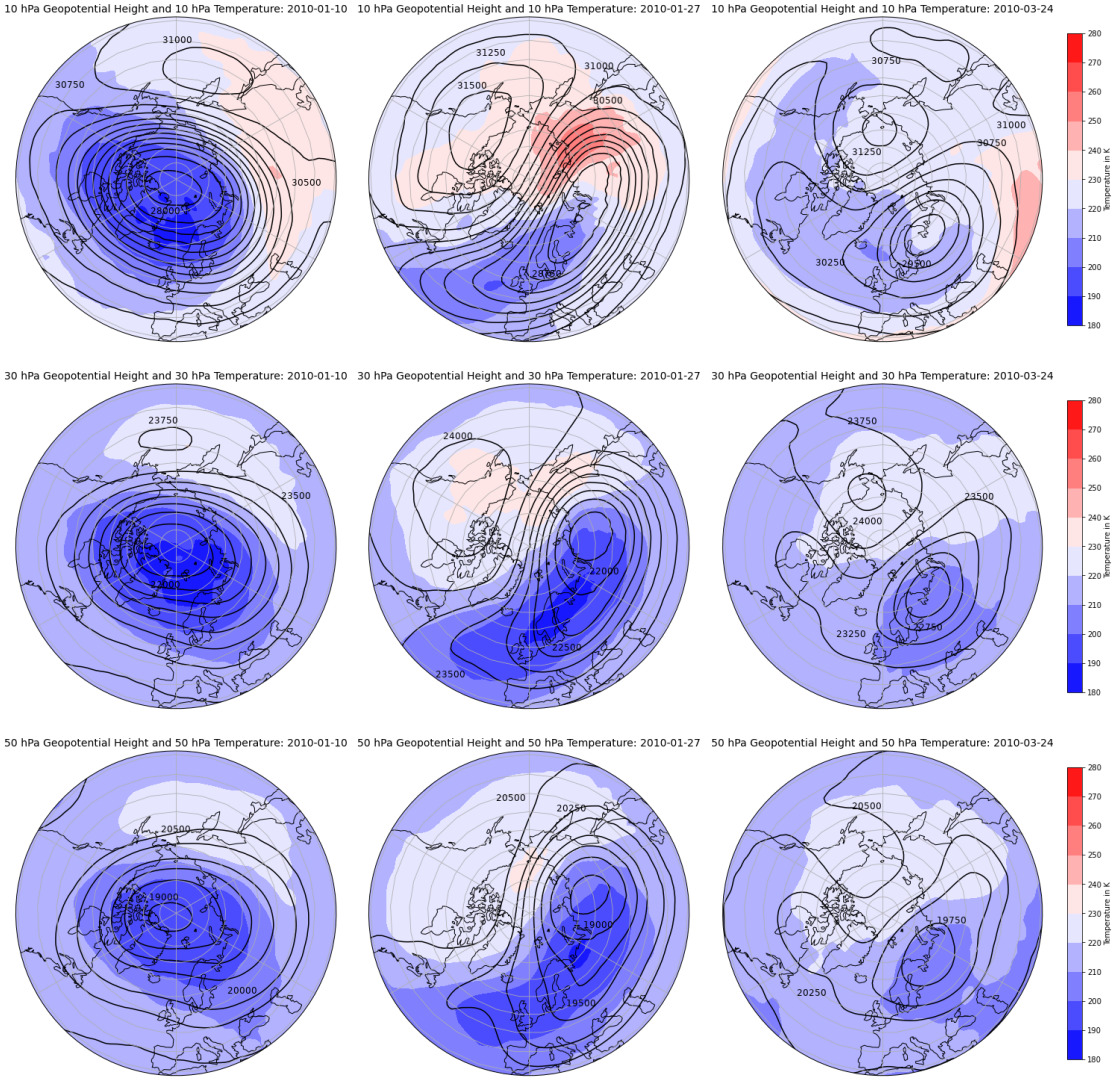

Figure 5.5: **Geopotential Height and Temperature in the Middle Stratosphere on 10 January 2010, 27 January 2010 and 24 March 2010 based on ERA-Interim.** The geopotential height and temperature are shown in 10 hPa (top row), 30 hPa (middle row) and 50 hPa (bottom row) for 10 January 2010 (left column), 27 January 2010 (middle column) and 24 March 2010 (right column).

5.3 Blocking in the Middle Troposphere

During the time of possible upward propagation of tropospheric signals with positive geopotential height anomalies into the stratosphere, 9 December 2009 to 11 January 2010, four long-lasting blocking patterns are detected over the Pacific and Atlantic sectors (Figure 5.6 top). On 9 December 2009, a strong „Ω“-blocking over Alaska occurs concurrently with a pronounced ridge over Scandinavia (Figure 5.7 top). This is a typical situation of a wavenumber 2 tropospheric wave forcing, which may penetrates into the stratosphere (Tripathi et al., 2015). The roughly 1.5 weeks lasting blocking event is followed by a 2 weeks lasting blocking event over the North Atlantic ocean (Figure 5.7 top). According to Tripathi et al. (2016) a sequence of North Pacific blocking followed by North Atlantic blocking is typical for upward propagating planetary waves which lead to a break-up of the polar vortex. Although an SSW event is not detected at that time, the polar night jet is disrupted and splits on 12 December 2009 (Figure 5.3, 5.2 top and 5.4 left column). From this date onwards, the 10 hPa polar night jet accelerates again which indicates the absence of planetary waves in that height (Figure 5.3). As the wave forcing induced by the frequent blocking situations is constantly high, a plausible explanation for the stop of the troposphere-stratosphere coupling is the formation of a layer with easterly winds in the tropopause region (Figure 5.6 top; Matsuno, 1971). In the days before the central date of the SSW event Alaskan blocking is detected (Figure 5.6 bottom). Since nearly instantaneous coupling between the troposphere and stratosphere is observed, this blocking situation may is a precursor block of the SSW (Figure 5.1). During the time of positive standardized gepotential height anomalies associated with the SSW at the surface a long-lasting blocking pattern over the Atlantic ocean is observed besides several small blocking patterns (Figure 5.6 bottom). It is a complex structure, featuring a „high-over-low“ blocking type over the western Atlantic, an „Ω “ block over the eastern Atlantic and an amplified ridge over western Asia, leading to a highly wavy and meridional circulation in the middle troposphere (Figure 5.7 bottom).

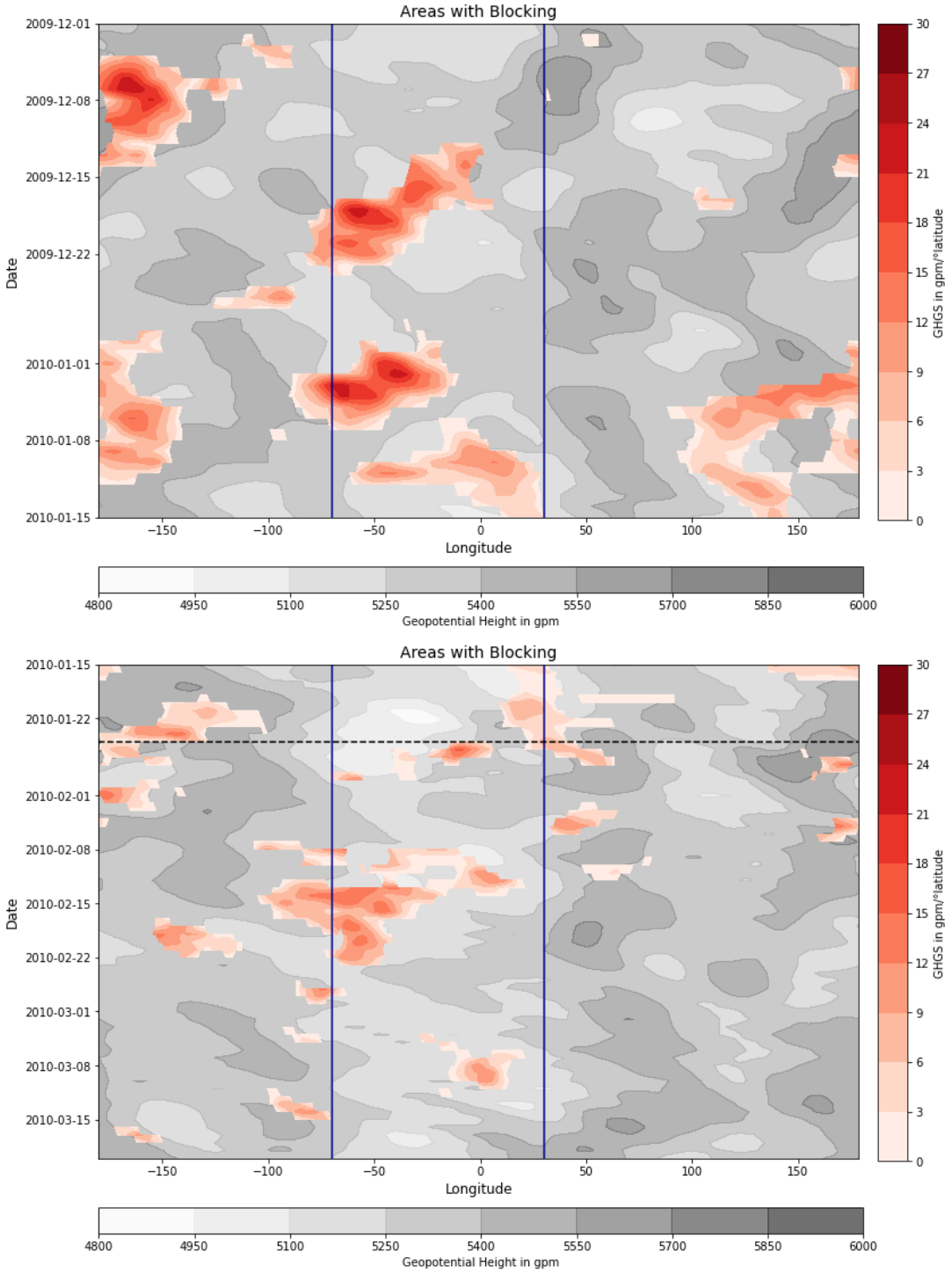

Figure 5.6: **Blocking Situation between December 2009 and March 2010 based on ERA-Interim.** The Hovmöller diagrams show the 500 hPa geopotential height between December and mid-January (top) as well as mid-January and mid-March (bottom). It is averaged between 40°N and 80°N and shown as grey shading. The GHGS component of the blocking index by Tibaldi and Molteni (1990) is shown in red. The horizontal black dashed lines mark the central date of the SSW event. The area between the solid blue lines refers to the Euro-Atlantic sector, 70°W to 30°E.

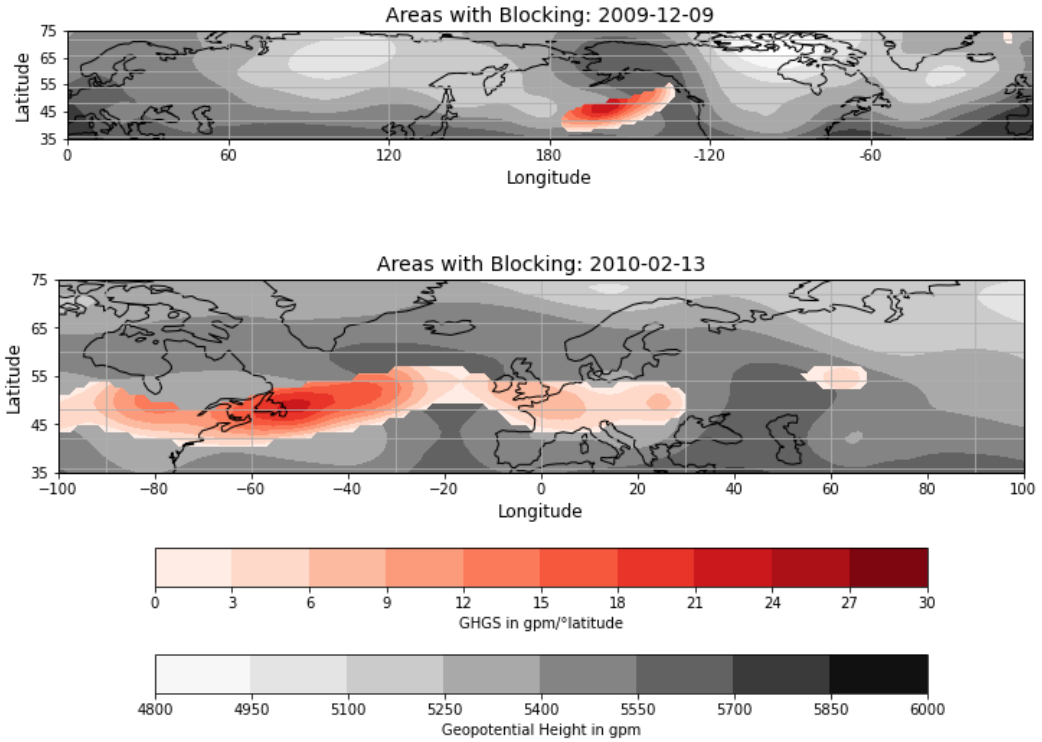

Figure 5.7: **Distinctive Blocking Patterns in the Middle Troposphere in the Winter 2009/2010 based on ERA-Interim.** Selected days, 9 December 2009 (top) and 13 February 2010 (bottom) with blocking patterns are shown. The 500 hPa geopotential height is shown as grey shading and the GHGS component of the blocking index by Scherrer et al. (2006) in red.

5.4 Position of the Mid-Latitude Jet Stream in the Lower Troposphere

From mid-December 2009 until mid January 2010, the 850 hPa jet stream is located up to 20° south of the climatological position of the jet stream (Figure 5.8). This is a typical feature observed after SSW events (Charlton-Perez et al., 2018; Domeisen, 2019). Although the equatorward displacement of the mid-latitude jet stream coincides with the split of the polar vortex on 12 December 2009, it is not associated with it. The reason herefore is the upward instead of downward propagation of positive geopotential height anomalies associated with frequent and long-lasting blocking situations over the North Pacific and North Atlantic ocean (Figure 5.2 top and 5.6 top). These blocking patterns themselves may lead to the southward displacement of the midlatitude-jet. In the days before the central date of the SSW, the jet stream moves poleward again to roughly 60°N which coincides with negative standardized geopotential height anomalies in the lower troposphere (Figure 5.8 and 5.1). Shortly after 25 January 2010, the central date of the SSW, the mid-latitude jet stream is displaced southward again and positive normalized geopotential height anomalies are observed in the whole stratosphere and troposphere (Figure 5.8 and 5.1). Already in the beginning of February 2010 it is located at latitudes about 20° south of its climatological position. Since a downward propagation of positive geopotential height anomalies caused by the SSW is present only over the Pacific ocean, the equatorward shift of the jet stream over the North

Atlantic ocean is not associated directly with the SSW (Figure 5.2 bottom). It is either caused by the internal tropospheric variability or maybe by a teleconnection between the Pacific/North American (PNA) pattern and the North Atlantic storm track which is not analyzed further in this thesis (Pinto et al., 2011; Afargan-Gerstman and Domeisen, 2020). The persistent southward displacement of the mid-latitude jet stream leads to a weak zonal flow and frequent blocking patterns caused by cyclonic Rossby-wave breaking (Santos et al., 2013). These blocking patterns can lead to a split of the jet stream (Martius et al., 2009). The jump in the jet stream latitude in the beginning of March 2010 may shows such a split of the mid-latitude jet stream, perhaps caused by the Atlantic blocking happening at the same time (Figure 5.8 and 5.6). Another possible split of the jet stream is visible in mid-April 2010 after a poleward displacement of it (Figure 5.8). As the positive standardized geopotential height anomalies associated with the SSW event only last until 17 March 2010 in the lower troposphere, this development of the mid-latitude jet stream is not analyzed further (Figure 5.1). Additionally it has to be kept in mind that the wind data in April is prone to boundary effects due to the applied filtering.

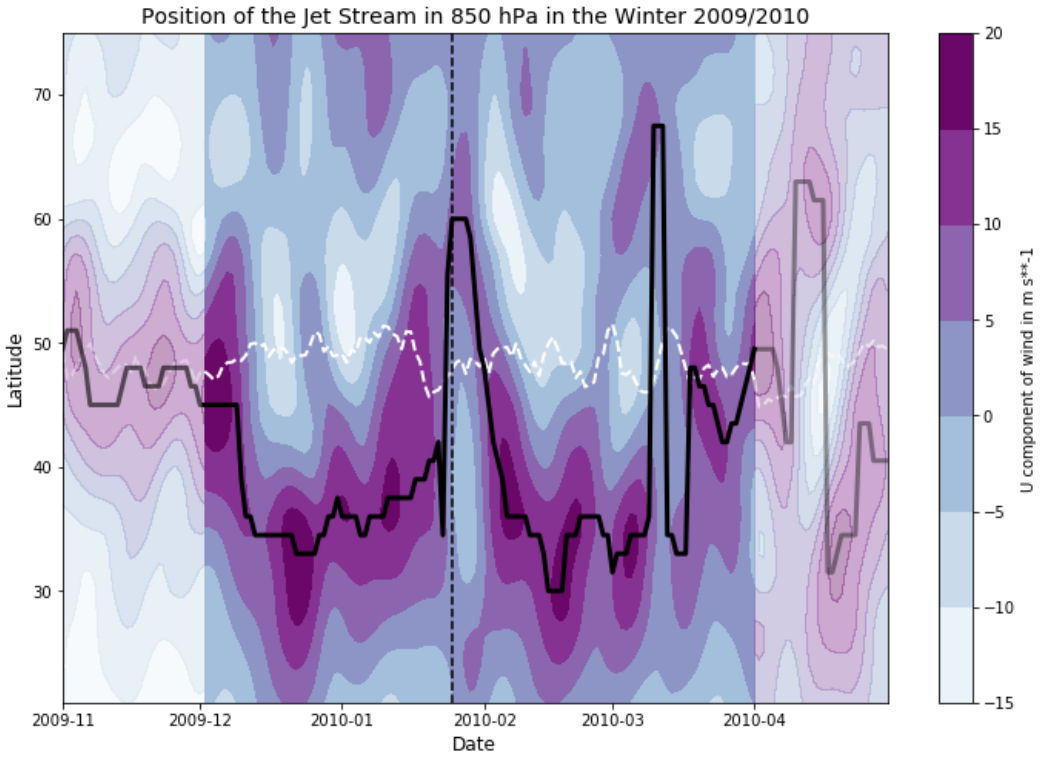

Figure 5.8: **Zonal Wind Speed Anomalies during the Winter 2009/2010 based on ERA-Interim.** The zonal-wind anomalies in 850 hPa, averaged over 60°W to 0°E are shown as shading in the Hovmöller diagram. The anomalies are filtered using a Lanczos filter with a moving window of 61 days and a cutoff-frequency of 1/10 days. Data on the edges of the timeseries are prone to boundary effects due to the filtering and therefore, shown paler than the unaffected data. The wind maxima are shown as a black solid line. The white dashed line shows the climatological position of the mid-latitudes jet stream. The central date of the SSW is marked with the vertical black dashed line.

5.5 North Atlantic Oscillation Index at the Surface

It is striking that most of the winter 2009/2010 is characterized by a strongly negative NAO phase, lasting from 7 December 2009 until 19 March 2010 considering the 7-day running mean of the NAO index (Figure 5.9). One possible explanation of this long-lasting NAO- phase is the presence of moderate to strong El Niño conditions in the winter 2009/2010 which favor the teleconnection between ENSO and the negative phase of the NAO index (https://www.cpc.ncep.noaa.gov/products/analysis_monitoring/ensostuff/detrend.nino34.ascii.txt, last viewed 2 June 2020; Lee et al., 2019). Other factors which may contribute to the long-lasting NAO- phase are the QBO east phase and the anomalously snow cover extent over the northern hemisphere (https://www.geo.fu-berlin.de/en/met/ag/strat/produkte/northpole/index.html, last viewed 4 June 2020; Jung et al., 2011). According to Jung et al. (2011) and Santos et al. (2013) though, these external forcings are neither the dominant cause nor maintainer of the NAO- phase.

On 9 December 2009, the daily NAO index turns negative (Figure 5.9). This coincides with the start of positive geopotential height anomalies at the surface which are associated with an upward propagation of tropospheric baroclinic waves (Figure 5.1 and 5.2 top). These waves are may excited by a blocking pattern over the North Pacific ocean, lasting from 3 to 15 December 2009 (Figure 5.6). At the same time, upward propagation of tropospheric waves over Scandinavia is observed (Figure 5.2 top). According to Jung et al. (2011) the internal atmospheric variability which includes blocking pattern, is probably the cause of the NAO- phase. With an exception of 1 week at the end of December 2009, the North Atlantic ocean is constantly featuring blocking patterns until 14 January 2010 (Figure 5.6). Santos et al. (2013) state that cyclonic wave breaking causing the blocking pattern over the North Atlantic-European sector is relevant for the formation and maintenance of the negative phase of the NAO.

Between 14 and 25 January, blocking is detected over western Europe but not over the North Atlantic ocean (Figure 5.6). The NAO index increases to values >-1 during that time but stays negative in the 7-day running mean (Figure 5.9). The fact that it decreases in the following 3 days when blocking occurs again over the North Atlantic ocean supports the idea that the North Atlantic blocking patterns maintain this NAO- phase (Figure 5.9 and 5.6). From 30 January until 8 February 2010, blocking patterns are again absent over the North Atlantic ocean (Figure 5.6). This time though, the NAO index continuous to decrease (Figure 5.9). At the same time, positive geopotential height anomalies at the surface associated with the SSW event on 25 January 2010 are detected (Figure 5.1). Due to the absence of North Atlantic blocking, the decrease of the NAO index during this time can may be explained by the downward influence of the SSW event, if there is for example a teleconnection between the PNA and the NAO, keeping in mind that a varying strength of external forcings such as the possible teleconnection with ENSO may plays a role as well. During the time of positive geopotential height amomalies at the surface, associated with the SSW event, the NAO index stays negative with maximum values around -4 in the 7-day running mean (Figure 5.9). Besides the influence of the SSW on the NAO during this time, a 2 weeks lasting North Atlantic blocking pattern in February may helps to maintain this strongly negative NAO- phase (Figure 5.6). While in February a typical NAO- pattern with a strong pressure gradient between Iceland and the Azores is observed, in March the NAO- pattern is shifted southwards with the positive mean sea level pressure anomaly being displaced eastward and the negative mean

sea level pressure anomaly displaced westwards (Figure 5.10 right column top and bottom). This results in a less negative NAO index in the beginning of March 2010 which is perhaps maintained by a roughly 1 week lasting blocking pattern in March (Figure 5.9 and 5.6). Though normalized positive geopotential heights >1.0 standard deviation associated with the SSW event are not present at the surface, a possible influence of the SSW on the NAO cannot be excluded for the times with less extreme positive geopotential height anomalies at the surface (Figure 5.1).
On 19 March 2010 the NAO index turns positive until 24 March 2010 when considering the daily NAO index (Figure 5.9). According to Baldwin et al- (2003) SSW events influence surface weather up to 60 days after their central date, which is in the case of the winter 2009/2010 up to 25 March 2010. Although the SSW event cannot be excluded as being part of the triggering mechanism of this NAO- phase, it is suggested to play a negligible role. The last NAO- phase of the winter 2009/2010 occurs more than 2 months after the central date of the SSW event and is therefore not associated with it (Baldwin et al., 2003; Tripathi et al., 2015).

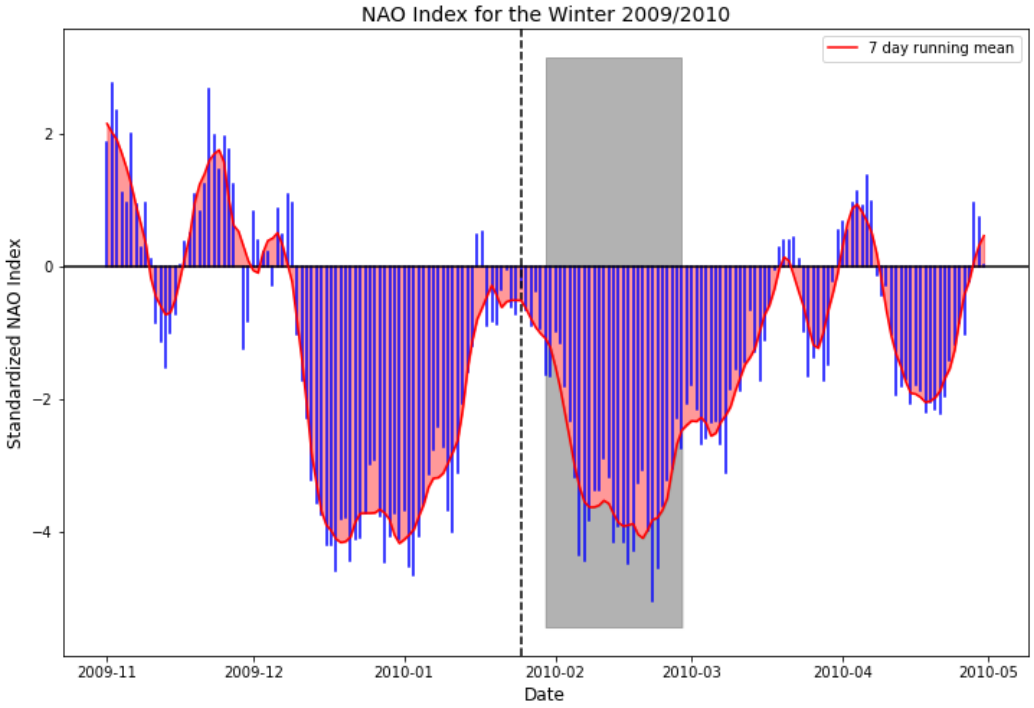

Figure 5.9: **NAO Index during the Winter 2009/2010 based on ERA-Interim.** Shown is the Zonal Index which is calculated as the standardized mean sea level pressure anomaly difference between a southern box, averaged over 40°W to 0°E and 35°N to 50°N, and a northern box, averaged over 40°W to 0°E and 55°N to 70°N (Leckebusch et al., 2008). The black dashed line marks the central date of the SSW. The period with normalized geopotential height anomalies >1.0 standard deviation associated with the SSW at surface is shaded in dark grey.

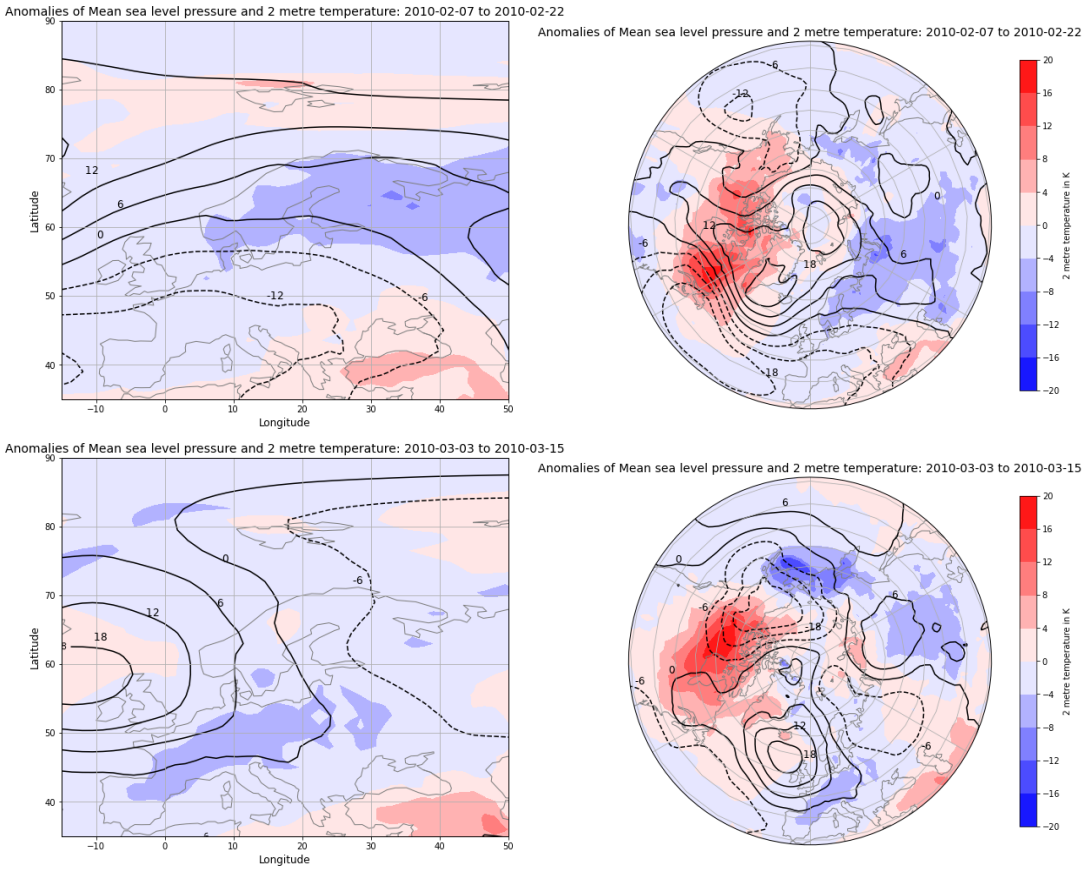

Figure 5.10: **Mean Sea Level Pressure Anomalies and 2 Metre Temperature Anomalies for Two European Cold Waves based on ERA-Interim.** Shown is the European cold wave in February 2010 (top row) and in March 2010 (bottom row). The dashed contours show negative mean sea level pressure anomalies, the solid contours show positive mean sea level anomalies. The 2 metre temperature anomalies are plotted as shading.

5.6 European Cold Waves at the Surface

During the time of the negative NAO phase, several cold waves occur in Europe (Figure 5.11). According to the index by Smid et al. (2019) the cold waves in Europe exclusively happen in the time, when the NAO index shows negative values. During this time, every region experiences between 2 and 5 periods with unusually low 2 metre minimum temperatures (Figure 5.12). This is also true for the 7-day running mean of the 2 metre temperature anomalies, except for 2 short cold waves over eastern Europe in the beginning and end of the winter 2009/2010 (Figure 5.11). The first two European mean cold waves occur during the time when positive geopotential height anomalies >1.0 standard deviation are present at surface (Figure 5.11 and 5.2). Since these anomalies are associated with an upward propagation of tropospheric waves, a stratospheric influence on European 2 metre temperatures is not suggested in this case (Figure 5.2 top). A possible trigger of the European cold waves are the frequent blocking situations occurring over the North Atlantic-European sector in the same time (Figure 5.6). According to Woollings et al. (2018) the frequent blocking patterns are an important reason for the cold European weather in the winter 2009/2010. The European cold wave comprising the central date of the SSW event, coincides with block-

ing over central Europe (Figure 5.11 and 5.6). This might be the reason why eastern Europe is especially strongly affected by this cold wave, featuring temperatures up to 11 K below the climatology in the 7-day running mean 2 metre temperature anomalies (Figure 5.11). During the time when positive geopotential height anomalies associated with the SSW are present on surface, one European cold wave is detected in the 7-day running mean 2 metre temperature anomalies (Figure 5.11). The cold wave happening between 5 and 10 February 2010 with European mean temperature anomalies around 2 K below the climatology is detected by both approaches to classify cold waves (Figure 5.11 and 5.12). Longest affected is northern Europe during the cold wave but the most extreme temperatures are found in eastern, central and south-western Europe with 2 metre temperatures around 4 K below the climatological mean (Figure 5.10 top left and 5.11). The only not-affected area when looking at the 2 metre temperature anomalies is the Mediterranean. This is not confirmed when looking at the lowest 10 percentiles of the daily minimum temperatures. When using this approach, all European regions experience unusual cold temperatures, with the strongest cold waves detected in south-western and north-western Europe (Figure 5.12). As the NAO- phase coinciding with the European cold wave is maybe influenced indirectly by the SSW, the European cold wave is, too. An indication of the downward propagation of stratospheric anomalies caused by the SSW is the strong positive temperature anomaly over western Greenland and northern North America, reaching values up to 20 K above the climatological mean locally (Figure 5.10 top right; Hinssen et al., 2011). At the time of the second European cold wave, happening between 3 and 15 March 2010, largely positive anomalies over southern Greenland and Canada are again an indication of the downward propagation of stratospheric signals (Figure 5.10 right bottom; Hinssen et al., 2011). Since negative geopotential height anomalies are present at the surface during this time, the European cold wave is not associated with the SSW (Figure 5.1). This cold wave affects in the mean central Europe the strongest with 2 metre temperatures up to 8 K below the climatology (Figure 5.10 left bottom). All European regions except the Mediterranean are affected by this cold wave detected by the 7-day running mean of the 2 metre temperature anomalies (Figure 5.11). The approach by Smid et al. (2019) does not detect the European mean cold wave (Figure 5.12). Only eastern, north-western and south-western Europe show cold waves in this approach with the strongest one detected over south-western Europe.

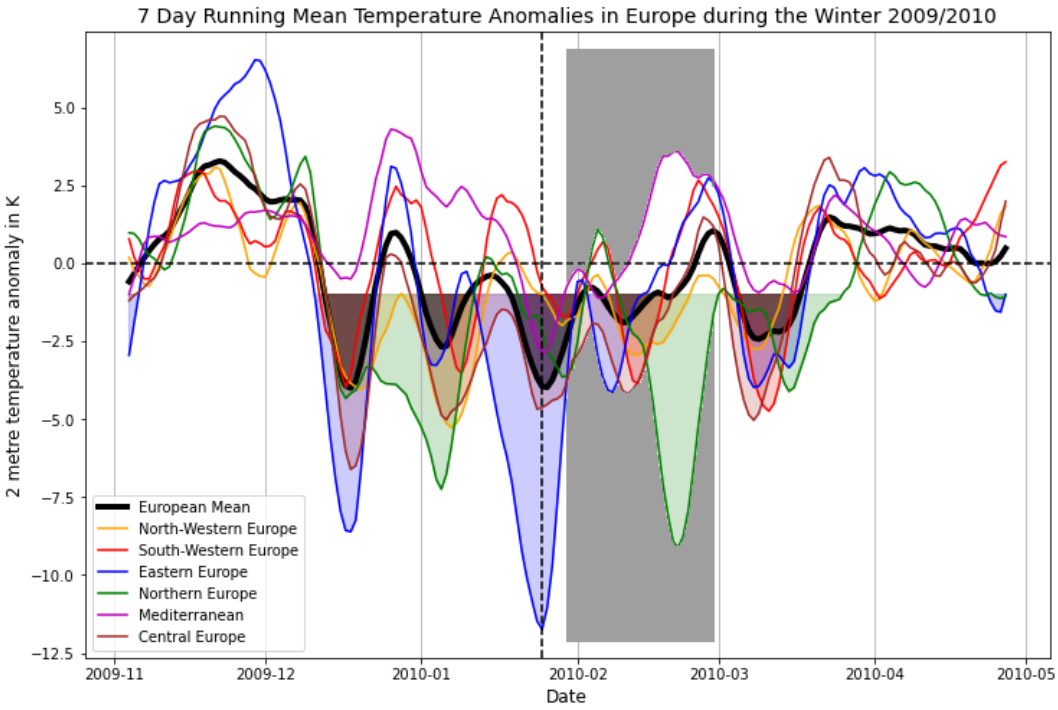

Figure 5.11: **2 Metre Temperature Anomalies during the Winter 2009/2010 based on ERA-Interim.** Periods of cold waves are defined using 1 K below the climatological mean as the warm temperature threshold for cold waves (Garfinkel et al., 2017). The days with cold waves are marked as shading in the respective color. The vertical black dashed line marks the central date of the SSW in the winter 2009/2010. The period with normalized geopotential height anomalies >1.0 standard deviation associated with the SSW at surface is shaded in grey. The European mean is calculated by averaging between 10°W to 42°E and 35°N to 72°N. The anomalies for north-western Europe between 10°W to 3°E and 45°N to 60°N, for south-western Europe between 10°W to 3°E and 35°N to 45°N, for eastern Europe between 20°E to 42°E and 45°N to 60°N, for northern Europe between 3°E to 42°E and 60°N to 72°N, for central Europe between 3°W to 20°E and 45°N to 60°N and for the Mediterranean between 3°E to 42°E and 35°N to 45°N.

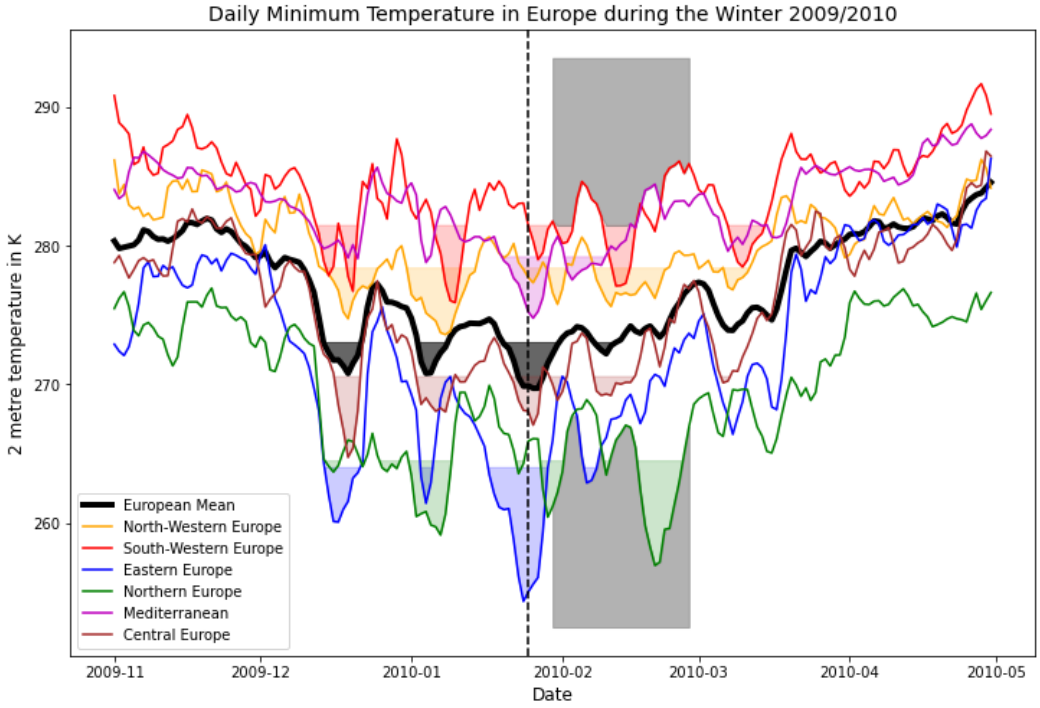

Figure 5.12: **2 Metre Daily Minimum Temperature during the Winter 2009/2010 based on ERA-Interim.** Periods of cold waves are defined as at least 3 consecutive days with daily minimum temperatures below the 10^{th} percentile of the climatological daily minumum temperature (Smid et al., 2019). The climatology is calculated for the period between 1999 and 2019 with a 31 day running mean. The days with cold waves are marked as shading in the respective color. The vertical black dashed line marks the central date of the SSW. The period with normalized geopotential height anomalies >1.0 standard deviation associated with the SSW at surface is shaded in grey for the SSW of the winter 2009/2010. The European mean is calculated by averaging between 10°W to 42°E and 35°N to 72°N. The anomalies for north-western Europe between 10°W to 3°E and 45°N to 60°N, for south-western Europe between 10°W to 3°E and 35°N to 45°N, for eastern Europe between 20°E to 42°E and 45°N to 60°N, for northern Europe between 3°E to 42°E and 60°N to 72°N, for central Europe between 3°W to 20°E and 45°N to 60°N and for the Mediterranean between 3°E to 42°E and 35°N to 45°N.

5.7 Concluding Remarks

The most striking feature of the winter 2009/2010 is the long-lasting negative NAO phase between December 2009 and April 2010 (Figure 5.9). It can be divided into 2 parts with a strongly negative NAO index reaching values around -4, separated by a short time period when the NAO index shows values around -1. Between 30 January and 27 February 2010, coinciding with the second part of the strongly negative NAO index and an equatorward shift of the mid-latitude jet stream, positive normalized geopotential height anomalies are found at the surface (Figure 5.1). These anomalies are associated with a downward propagation of stratospheric signals caused by the S-type SSW event with its central date on 25 January 2010 (Figure 5.2 bottom). Usually an equatorward shift of the mid-latitude jet stream over the North Atlantic ocean and the negative phase of the NAO are indicators of a downward influence of the SSW on surface (Afargan-Gerstman and Domeisen, 2020; Charlton-Perez et al., 2018). However, the downward propagation of the geopotential height anomalies caused by the SSW is located over the North Pacific ocean and, not as expected from the behaviour of the jet stream and the NAO, over the North Atlantic ocean (Figure 5.2 bottom). This leads to the suggestion that the shift of the jet stream and the NAO- phase may arise from internal tropospheric variability such as blocking situations or possibly from teleconnections. Due to the absence of blocking patterns over the North Atlantic-European sector at the end of January 2010, the decrease of the NAO index and the equatorward shift of the mid-latitude jet stream may therefore be linked to some kind of teleconnection (Figure 5.6). An example for a possible teleconnection is the influence of the PNA on the North Atlantic storm track and therefore the NAO (Pinto et al., 2011; Afargan-Gerstman and Domeisen, 2020). Since the downward propagation of stratospheric anomalies caused by the SSW occurs over the North Pacific ocean, an influence of the SSW on the PNA is likely. Assuming that there is a teleconnection between the PNA and NAO in the winter 2009/2010, the equatorward shift of the mid-latitude jet stream, the NAO- phase and the concurrent European cold wave may be linked to the SSW. It has to be kept in mind though that according to Jung et al. (2011) and Santos et al. (2013) external forcings, such as the SSW event, are not the primary cause and maintainer of the NAO- phase.

Under the assumption of a nearly instantaneous coupling between the North Pacific and North Atlantic ocean, the first European cold wave occurring during this second strongly negative NAO phase of the winter 2009/2010 can be associated with the SSW event (Figure 5.11). Another factor which contributes to the European cold wave is blocking over the North Atlantic-European sector which coincides also with the anomalously low 2 metre temperatures over Europe (Figure 5.6; Woollings et al., 2018). The cold waves occurring in the first strongly negative NAO- phase cannot be associated with a stratospheric influence. Although the polar vortex is split in the middle stratosphere on 12 December 2009, stratospheric signals seem not to propagate downward (Figure 5.4 left column, 5.1 and 5.2 top). The steady upward propagation of tropospheric waves is associated with frequent blocking situations over the Pacific and North Atlantic ocean (Figure 5.6). The latter are together with the strong NAO- phase likely the reason for the European cold waves occurring before 30 January 2010.

All European cold waves, except for two short ones over eastern Europe at the beginning and end of the winter 2009/2010, coincide with the long-lasting negative NAO phase. The short eastern European cold wave in the beginning of the winter 2009/2010 occurs simultaneously with positive

geopotential height anomalies at the stratopause but at least the anomalies >1.0 standard deviation do not enter the troposphere (Figure 5.11 and 5.1). These anomalies indicate a weak stratospheric polar vortex state starting before November 2009. Since the SSW index is only defined from November onwards, this weak stratospheric polar vortex state is not detected as an SSW. The stratospheric temperatures stay below 215 K and the 10 hPa zonal-mean zonal wind at 65°N does not reverse (Figure 5.3).

At the end of April, another eastern European cold wave occurs, roughly 1 month after a reversal of the 10 hPa zonal-mean zonal wind at 65°N. While the U65 index classifies this wind-reversal already as the final warming, the CP07 and U6090 index detect a second SSW in the winter 2009/2010 (Table 3.1). The polar vortex shows the typical features of a D-type SSW event but only in 10 hPa height (Figure 5.5 right column). As standardized geopotential height anomalies >1.0 standard deviation are not found in the stratosphere at that time, the wind-reversal is associated with the gradual final warming of the winter 2009/2010 (Figure 5.1).

6 Winter 2000/2001

6.1 Troposphere-Stratosphere Coupling

The winter 2000/2001 shows 4 structures with positive normalized geopotential height anomalies >1.0 standard deviation in the troposphere and stratosphere (Figure 6.1). Two of these anomalies are present at 1 hPa. This indicates that these normalized geopotential height anomalies are induced by SSW events. The other two structures show a bottom-up development and are therefore not investigated further. The first possible SSW event is characterized by a large normalized geopotential height anomaly up to 4.0 standard deviations and an almost instantaneous downward propagation of the anomaly. Positive normalized geopotential height anomalies are present at surface between 10 December 2000 and 3 January 2001, containing a few days with slightly less positive values (Figure 6.1). During the time of the largest positive normalized geopotential height anomalies, an eastward tilted with height structure of the positive normalized geoptential height deviation from the zonal-mean is observed (Figure 6.2 top). This is an indicator for a downward propagation of stratospheric anomalies induced by the SSW to the surface with the largest geopotential height deviations located over the North Atlantic ocean (Figure 6.2 top; Lim and Wallace, 1991). The second possible SSW event is indicated by positive normalized geopotential height anomalies smaller than 2.5 standard deviations (Figure 6.1). Especially at the stratopause-level around 1 hPa the normalized geopotential height anomalies are less extreme than the ones of the first possible sudden stratospheric event of the winter 2000/2001. The downward propagation of the anomalies is also different to the first possible SSW, showing a clear time-lag of about 3 weeks between positive normalized geopotential height anomalies >1.0 standard deviation at 1 hPa and the tropopause region (Figure 6.1). At the surface, positive normalized geopotential height anomalies >1.0 standard deviation are present between 22 February and 6 March 2001, interrupted by a few days with slightly less positive normalized geopotential height anomalies. The normalized geopotential height deviations from the zonal-mean at 65°N show two slightly westward tilted with height structures of positive deviations over the North Pacific sector and the North Atlantic ocean (Figure 6.2 bottom). This leads to the suggestion that both structures develop at the surface and propagate upward.

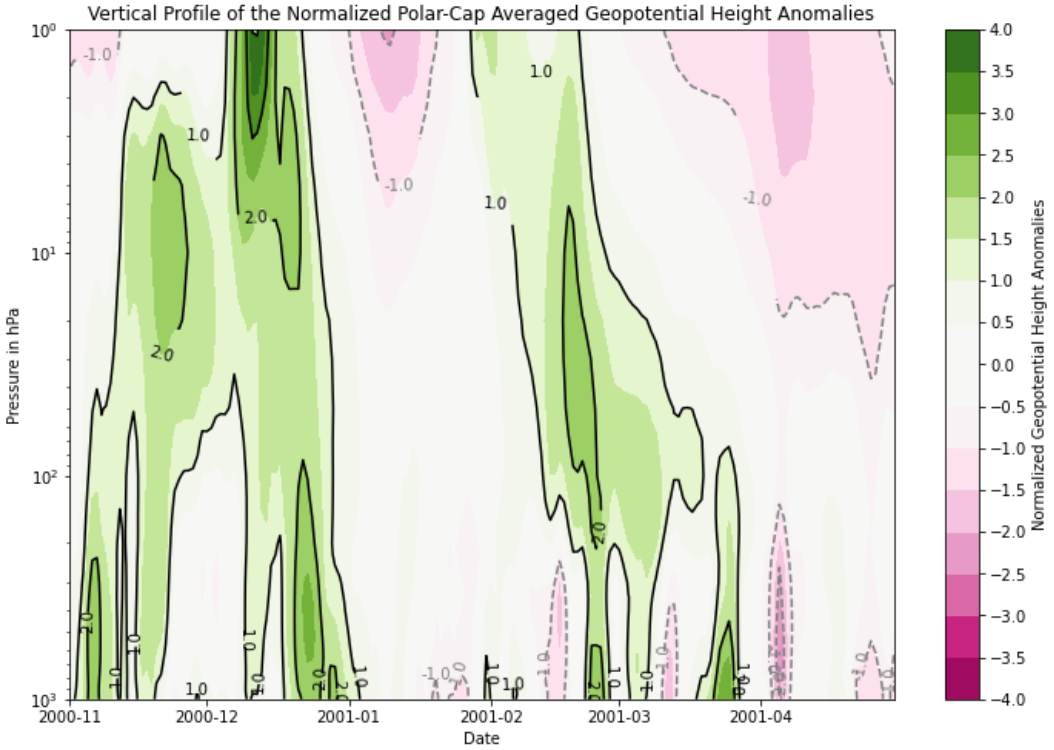

Figure 6.1: **Vertical Profile of the Polar-Cap Averaged Normalized Geopotential Height Anomalies during the Winter 2000/2001 based on ERA-Interim.** The green structures starting at 1 hPa are associated with SSW events.

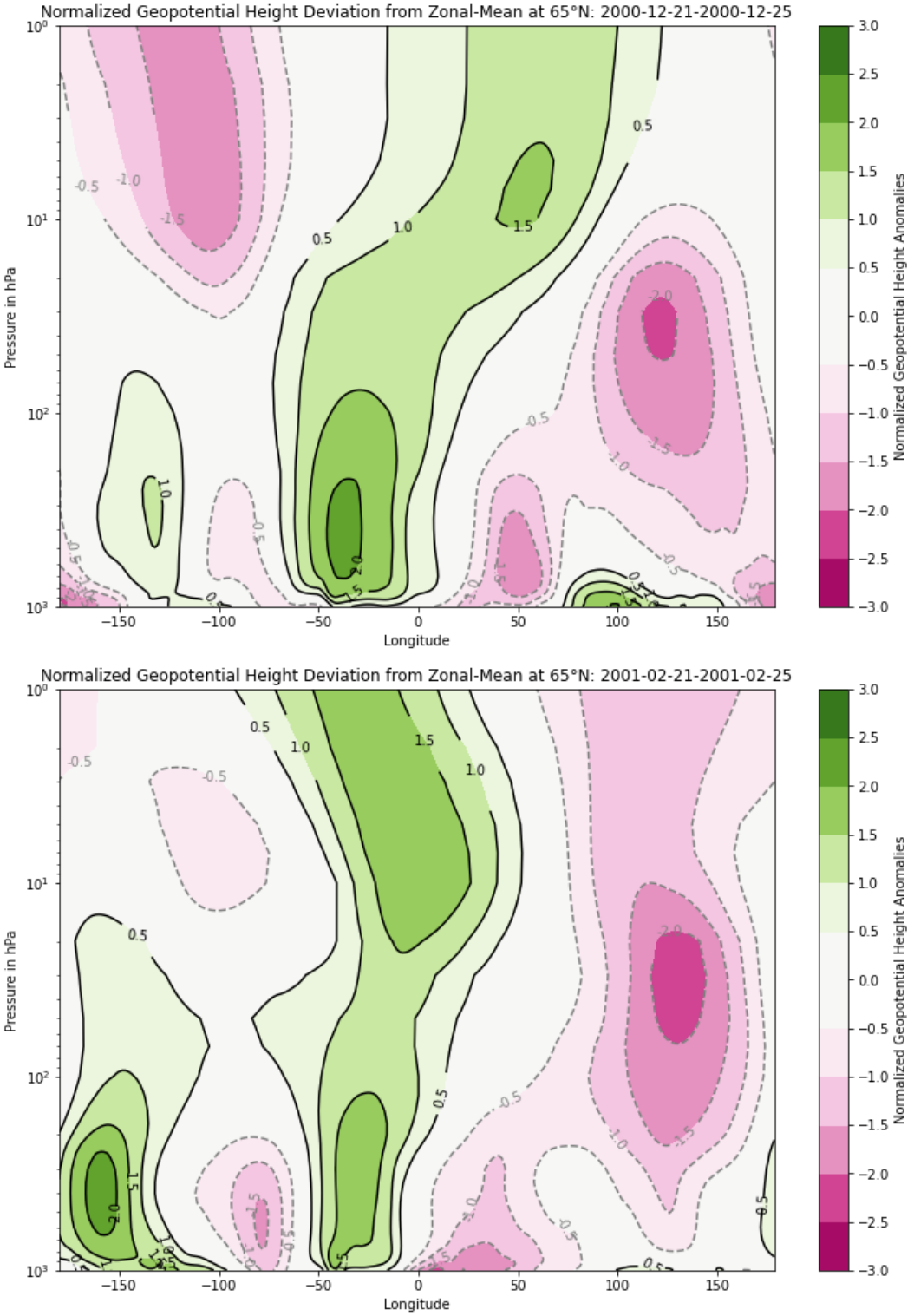

Figure 6.2: **Normalized Geopotential Height Deviations from Zonal-Mean after the SSW Events of the Winter 2000/2001 based on ERA-Interim.** The time for averaging is the time around the largest positive standard deviations of the normalized geopotential height anomalies associated with the preceding SSW at surface.

6.2 Sudden Stratospheric Warming Signals in the Middle Stratosphere

The U65 index confirms the two SSW events suggested by the positive normalized geopotential height anomalies >1.0 standard deviation at the stratopause in the winter 2000/2001 (Figure 6.1 and 6.3). So does the U6090 index but not the CP07 index which detects only one SSW event with its central date on 11 February 2001 (Table 3.1). According to the U65 index, the central date of the first SSW is on 23 November 2000 and the central date of the second event on 3 February 2001 (Figure 6.3). Referring to Manney et al. (2001) the first SSW of the winter 2000/2001 is triggered by a wavenumber-1 amplification. The polar vortex in the middle atmosphere shows the typical „comma-shape“ classifying the warming as a D-type event (Figure 6.4 left column; Charlton and Polvani, 2007). The polar vortex is at a nearly constant location in the whole middle atmosphere. The coldest temperatures down to 190 K are found inside the polar vortex in 10 hPa, 30 hPa and 50 hPa height. This barotropic structure in the stratosphere is an indicator of a downward propagation of stratospheric signals into the troposphere (Attard and Lang, 2019). The polar-cap averaged temperature increases by about 10 K during this warming event in 10 hPa height, in the lower stratosphere by 15 K (Figure 6.3; Manney et al., 2001). The maximum easterly wind speed in 10 hPa is reached on 26 November 2000 with -3 ms^{-1} (Figure 6.3). Easterly winds persist there for 4 days (Figure 6.3). According to Manney et al. (2001) this SSW has, despite its relatively small temperature increase and little weakening of the 10 hPa polar vortex, a substantial impact on the further development of the polar vortex. From the beginning of December 2000 to mid-January 2001, the polar vortex strengthens again with an intermediate weakening at the end of December. At the same time, the polar-cap averaged 10 hPa temperature curve shows a local maximum with temperatures around 222 K. According to Manney et al. (2001) the 10 hPa polar vortex is stronger than average and the lower stratospheric polar vortex weaker than average at this time. In mid-January 2001 the 10 hPa wind reaches its winter-maximum with 43 ms^{-1}. At the same time, the 10 hPa polar-cap averaged temperature reaches its winter minimum around 200 K (Figure 6.3). The polar vortex is stabilizing until the 23 January 2001, reaching values beneath 28250 gpm and a near concentric shape, centered north-east of Greenland (Figure 6.5 left column). The coldest temperatures down to 190 K are found inside the polar vortex, while warm temperatures up to 260 K are found over northern Asia in all three displayed heights, showing again a barotropic structure of the middle stratosphere. The polar vortex is located further northward in the lower heights leading to a slightly twisted vortex structure with height. In the following days the polar vortex is displaced southward and starts to elongate as the polar-cap averaged 10 hPa temperature rapidly rises (Figure 6.3). On 31 January 2001 the polar vortex features values up to 1500 gpm less in geopotential height than on 23 January 2001, showing a clear weakening of the stratospheric polar-night jet (Figure 6.5 middle column). The lowest 10 hPa temperatures of about 200 K are found on the western flank of the elongated jet, while the warmest temperatures up to 260 K are found on the north-eastern flank of it. In 30 hPa and 50 hPa height, the coldest temperatures are found inside the polar vortex and the warmest are centered north-west of it. In all three levels, baroclinicity is observed and the polar vortex is slightly twisted with height. On 9 February 2001, 6 days after the central date of the SSW, the polar vortex is clearly elongated and displaced off the pole, covering northern UK, Scandinavia and parts of northern Russia

(Figure 6.4 middle column). The lowest temperatures are found again inside the polar vortex filament, reaching values down to 210 K. The warmest temperatures of about 250 K are seen on the north-eastern flank of the elongated polar vortex. In all three levels, baroclinicity is again observed. The polar vortex is roughly located at the same position in all three levels, showing only a small northward displacement in lower heights. Maximum polar-cap averaged 10 hPa temperatures are reached with 235 K a few days before, ending the rapid temperature increase of more than 35 K in less than 1 week (Figure 6.3). Maximum easterly winds with -16 ms^{-1} are reached on 18 February 2001. The polar vortex is already split a day earlier, featuring a stronger western than eastern part (Figure 6.3 and Figure 6.5 right column). Both parts are clearly weakened, showing geopotential height values greater than 30000 gpm. The SSW event is therefore classified as a S-type. Warm temperatures higher than 230 K are found almost everywhere over Europe and Asia in 10 hPa height with maximum temperatures up to 268 K over eastern Europe (Figure 6.5 right column). The middle stratosphere shows a baroclinic structure with a strongly twisted polar vortex. Easterly winds prevail in 10 hPa height for 20 days until 23 February 2001 (Figure 6.3). On 28 March 2001 the polar vortex in the middle atmosphere is restored again but profoundly weaker than before the SSW (Figure 6.4 left and right column). The 10 hPa polar-cap averaged temperature is with 215 K more than 15 K higher than before the warming, showing minimum values down to 200 K in the middle of the polar vortex (Figure 6.3 and 6.4 left and right column). Also in 30 hPa and 50 hPa low temperatures and a barotropic structure are present again.

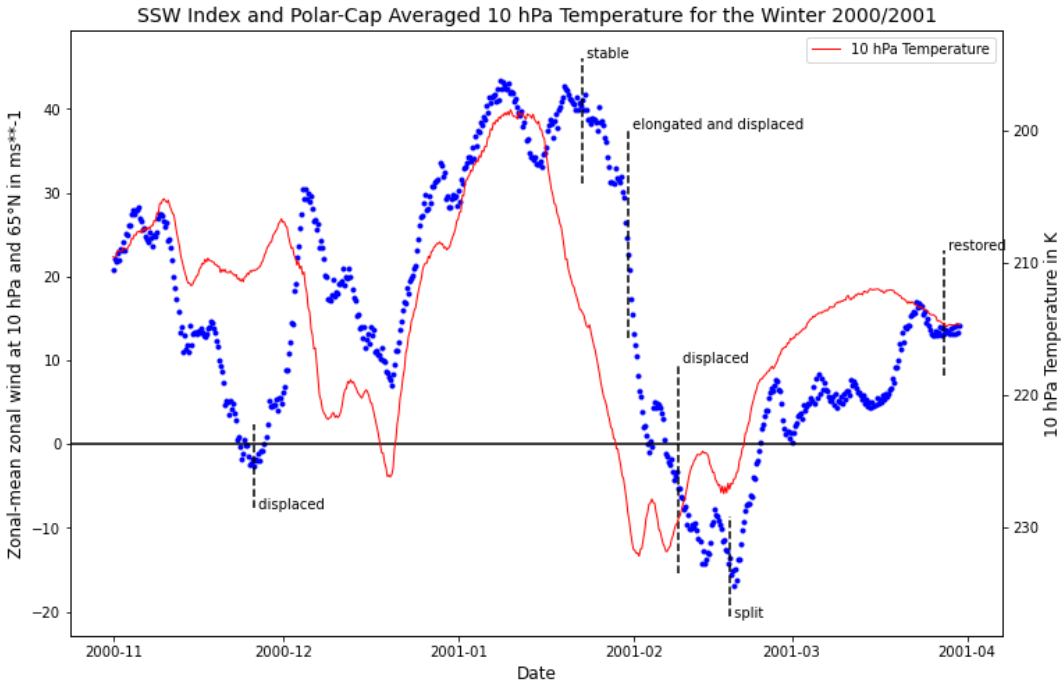

Figure 6.3: **SSW Index and Polar-Cap Averaged 10 hPa Temperature for the Winter 2000/2001 based on ERA-Interim.** The blue dots show the modified SSW index by Charlton and Polvani (2007) with 65°N instead of 60°N as reference latitude. The red line shows the polar-cap averaged 10 hPa temperature. Days with distinctive shapes of the polar vortex in the 10 hPa geopotential height field are marked.

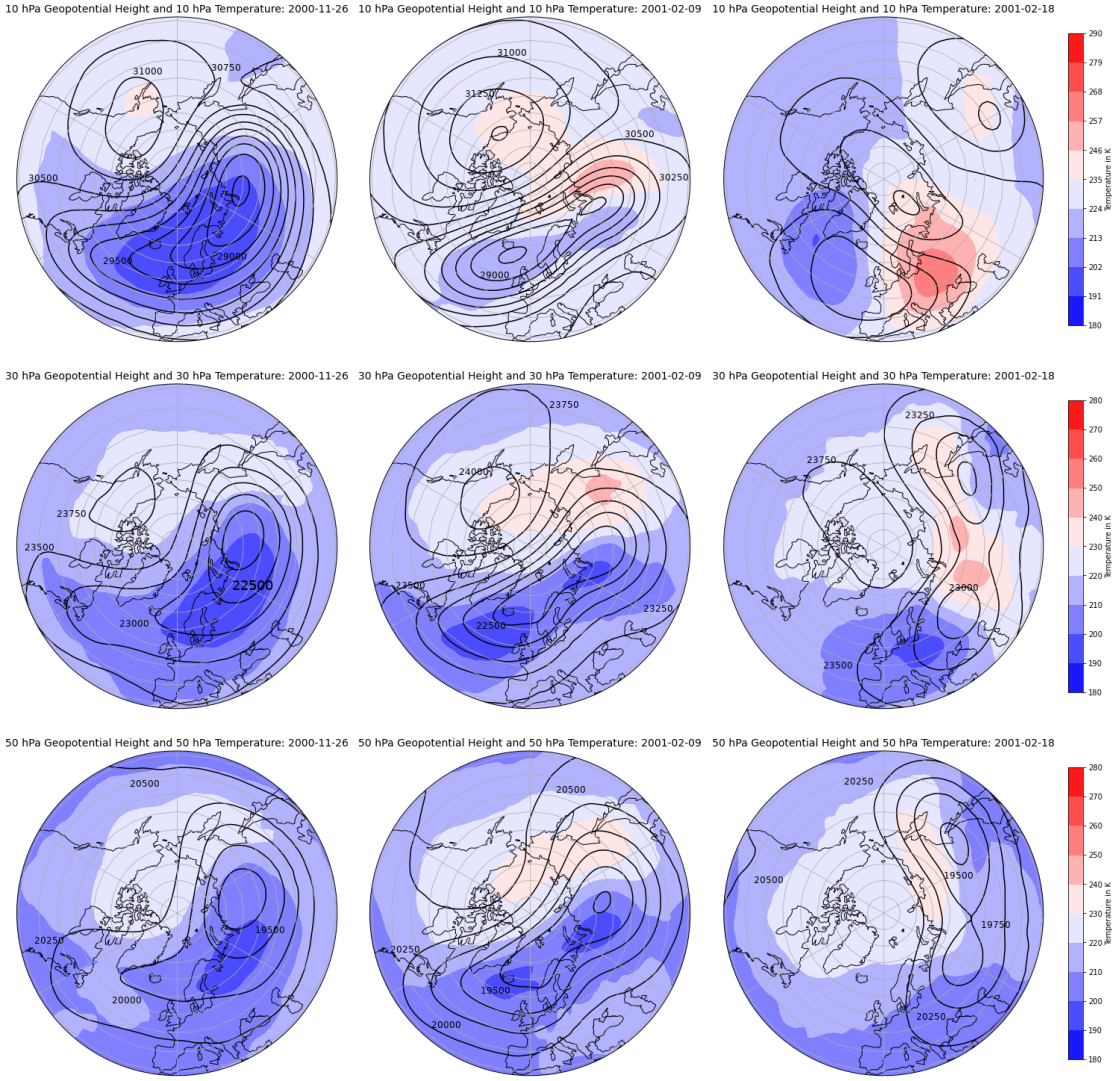

Figure 6.4: **Geopotential Height and Temperature in the Middle Stratosphere on 26 November 2000, 9 February 2001 and 18 February 2001 based on ERA-Interim.** The geopotential height and temperature are shown in 10 hPa (top row), 30 hPa (middle row) and 50 hPa (bottom row) for 26 November 2000 (left column), 9 February 2001 (middle column) and 18 February 2001 (right column). All plots have the same color-scale except the plot on the top right (the color-scale for this plot is given next to it).

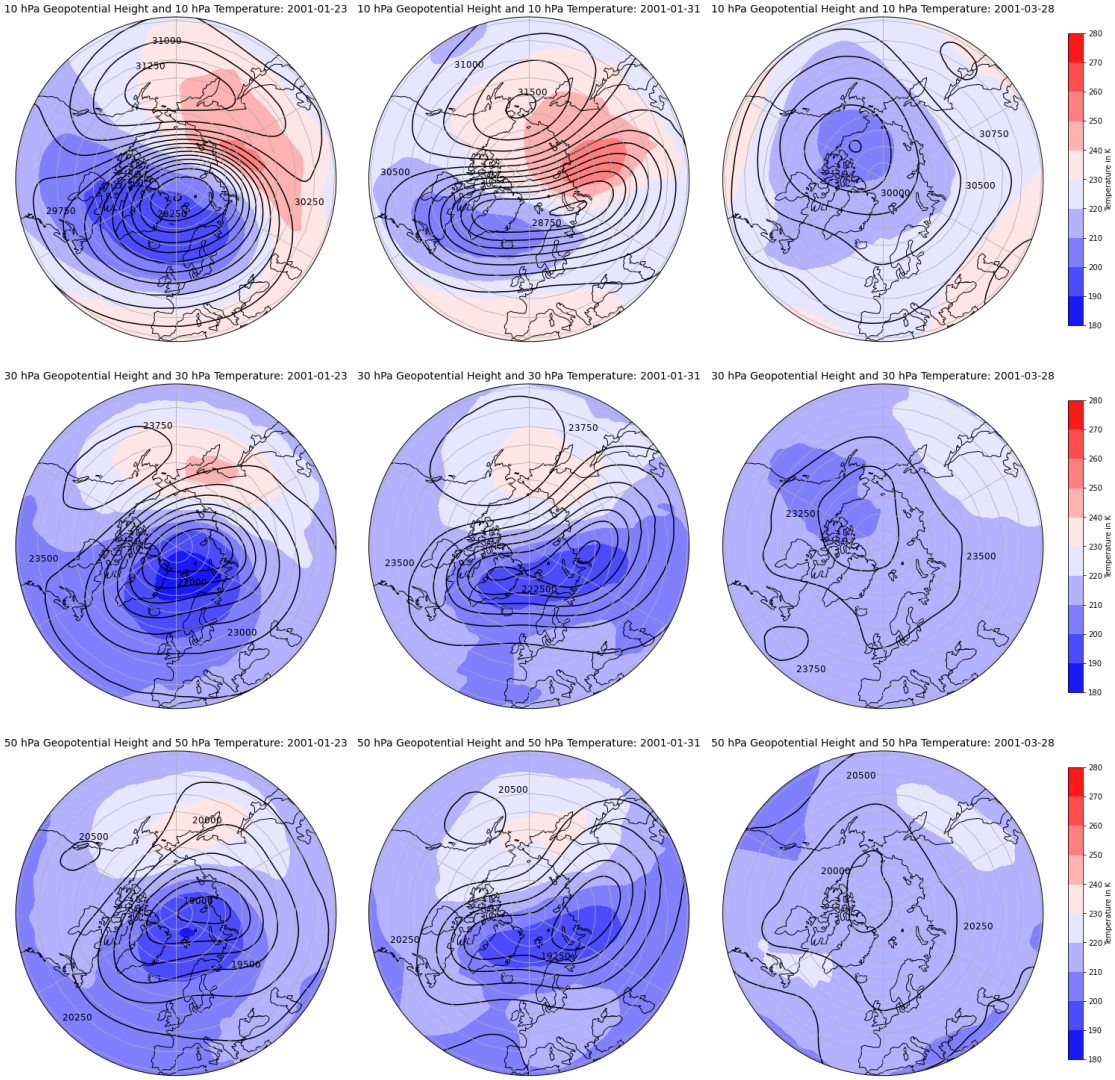

Figure 6.5: **Geopotential Height and Temperature in the Middle Stratosphere on 23 January 2001, 31 January 2001 and 28 March 2001 based on ERA-Interim.** The geopotential height and temperature are shown in 10 hPa (top row), 30 hPa (middle row) and 50 hPa (bottom row) for 23 January 2001 (left column), 31 January 2001 (middle column) and 28 March 2001 (right column).

6.3 Predicted Sudden Stratospheric Warming Signals in the Middle Stratosphere

The ensemble members of the reforecast initialized on 31 October 2000 show a similar behaviour of the SSW index as the ERA-Interim renalysis but with a slight shift to later times in the first 10 days (Figure 6.6 top). Between 15 November and 4 December 2000, the shape of the curve of the S2S ensemble member with the correct prediction of the SSW is similar to the curve of the ERA-Interim data but shifted to earlier times by about 3 days. After this date, the two curves differ remarkably. Considering the early initialization 23 days before the central date of the SSW, the ensemble member which predicts the SSW correctly forecasts the state of the atmosphere up to a lead time of 34 days well. The representative ensemble member which does not show easterlies in this reforecast does not capture the state of the atmosphere well beyond 17 November 2000. It is important to note that the spread of the ensemble is remarkably small until the beginning of December 2000, concerning the early initialization time. This leads to the suggestion that this SSW event could have a high predictability.

The two representative members of the reforecast initialized on 7 November 2000, 16 days prior to the central date of the SSW, show a way more similar behaviour than the representative members of the reforecast initialized on 31 October 2000 (Figure 6.6 bottom). The ensemble member which predicts the SSW correctly captures the form of the curve of the ERA-Interim reanalysis well until 8 December 2000 but is shifted about 4 days to earlier times. The ensemble member which shows only westerly winds follows the ERA-Interim reanalysis well from 22 November to 3 December 2000 but features especially on the central date of the SSW about $10\,\mathrm{ms}^{-1}$ higher zonal wind speeds (Figure 6.6). The ensemble spread is rather small until the beginning of December 2000 and then increases. The fact that the ensemble spread for the initialization on 31 October 2000 also increases in the beginning of December 2000 leads to the suggestion that around this time a rather unpredictable weather situation occurs. A possible explanation could be an enhanced wave activity with at least two, for the model equally probable realization. At this point, it has to be kept in mind that the model simulates waves with wavenumber 2 less well than waves with wavenumber 1, and thus, waves with wavenumber 1 are more probable from the model's point of view (Tripathi et al., 2016). Manney et al. (2001) state that after 8 December 2000 there is a wavenumber 2 amplification observed. This supports the suggestion that in the beginning of December 2000 the enhanced wave activity leads to the large spread among the ensemble members.

This is also true for the reforecast initialized on 25 November 2000, which also indicates that in the beginning of December 2000 a rather unpredictable weather situation occurs (Figure 6.7 top). Until mid-December, both representative members follow the ERA-Interim reanalysis closely. Then the representative member with prevailing standardized geopotential height anomalies <0.5 standard deviation follows the shape of the ERA-Interim reanalysis curve roughly but mostly at higher values. The representative member with prevailing standardized geopotential height anomalies >0.5 standard deviation shows an additional, artificial SSW event on 20 December 2000.

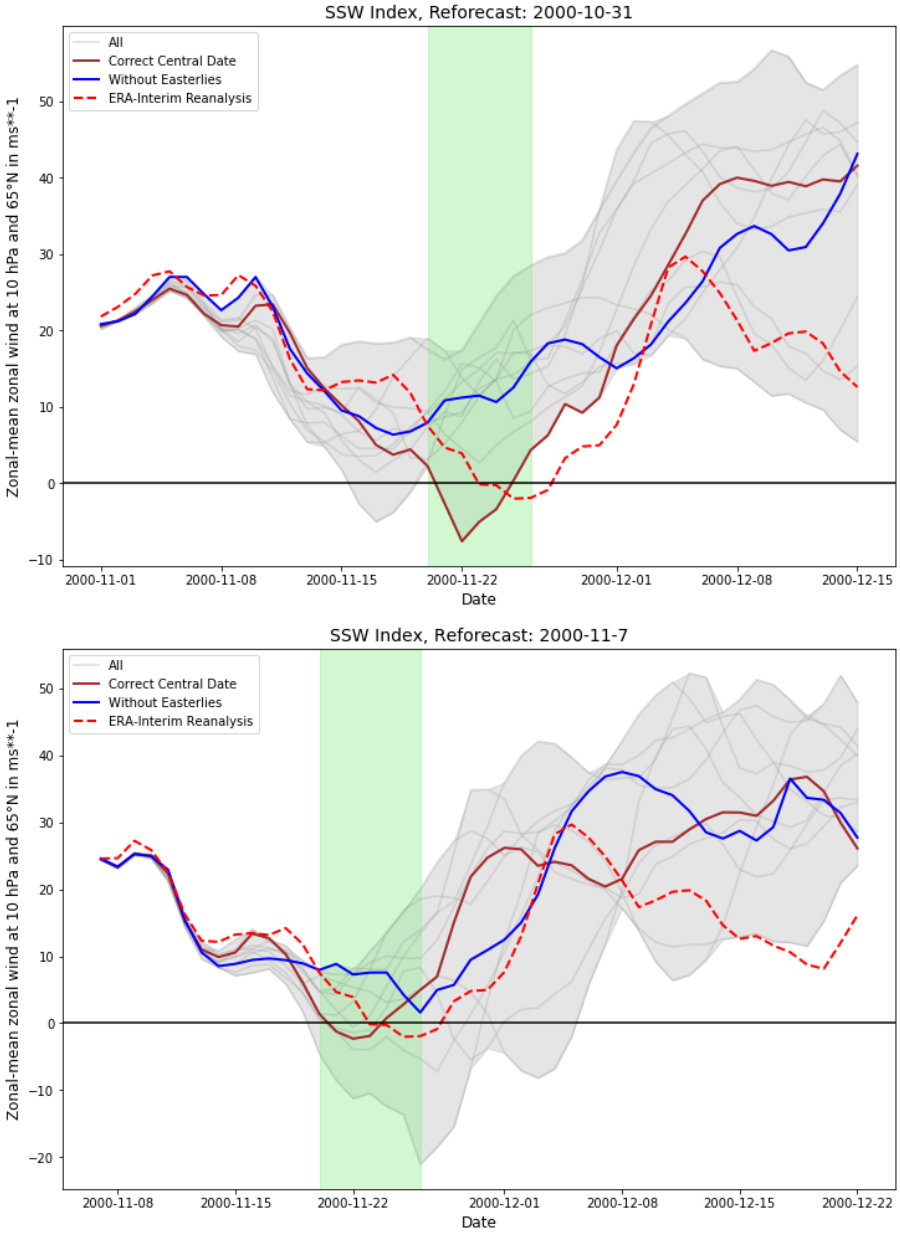

Figure 6.6: **SSW Index of S2S Reforecasts Initialized prior to the Central Date of the SSW.** The shaded area shows ±3 days around the central date of the SSW event obtained from the ERA-Interim reanalysis. The ERA-Interim SSW index is shown by the red dashed line. For the reforecast initialized on 31 October 2000, the SSW index is shown from 1 November 2000 onwards (top). The reforecast initialized on 7 November 2000 is shown on the bottom plot.

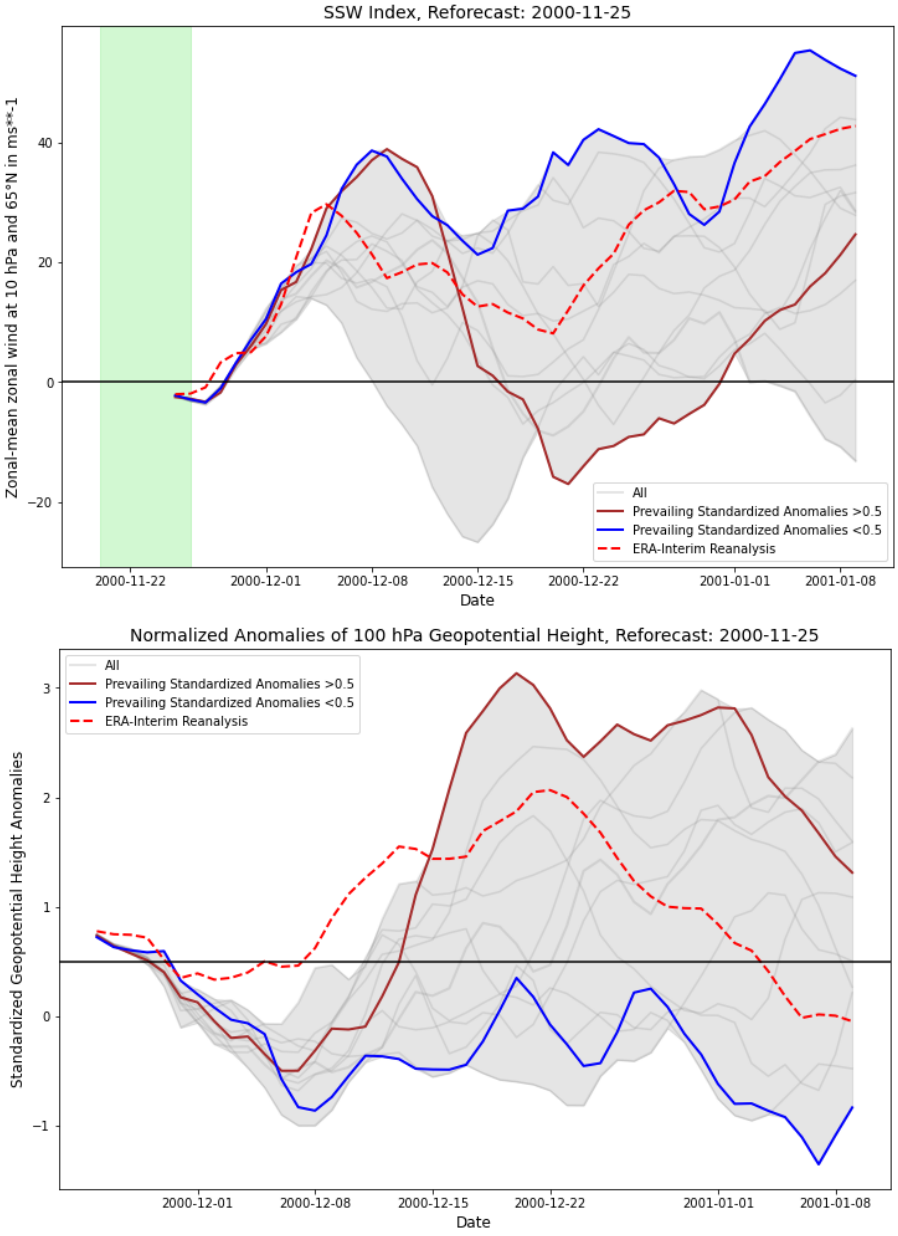

Figure 6.7: **SSW Index of the S2S Reforecast Initialized after the Central Date of the SSW and Normalized Geopotential Height Anomalies in 100 hPa.** The shaded area shows ± 3 days around the central date of the SSW event obtained from the ERA-Interim reanalysis. The ERA-Interim reanalysis is shown by the red dashed line (top). The representative members are obtained from the polar-cap averaged 100 hPa normalized geopotential height anomalies (bottom). The data of the first and last 3 days of the 100 hPa standardized geopotential height anomalies reforecast are prone to boundary effects due to the use of 7-day running mean for the calculation of climatology.

6.4 Predicted Shape of the Polar Vortex in the Middle Stratosphere

Already in the first initialization on 31 October 2000, the representative member with the correct central date captures the „comma“-shape of the polar vortex in 10 hPa well (Figure 6.8 left column). The vortex in the S2S reforecast is only slightly smaller and more concentric but the magnitude of the geopotential height values is the same. The representative member without easterlies shows smaller geopotential height values than the ERA-Interim reanalysis but the core of the vortex is at the same position. The shape of the vortex is rather an oval than a „comma“ (Figure 6.8). The differences between the two representative members are small in the region of the polar vortex suggesting a well predictable vortex state.
Interestingly, the prediction of the representative members of the reforecast initialized on 7 November 2000 is less well (Figure 6.8 left and middle column). This could either mean that the good representation of the polar vortex in the earlier reforecast is coincidence or, that there is a more unpredictable phenomena considered in the later intitialized reforecast. The representative member with the correct central date of this reforecast shows a larger core of the polar vortex than the ERA-Interim reanalysis but centered on the same location (Figure 6.8). Also the „comma“-shape of the vortex is not as distinct as it is in the ERA-Interim reanalysis. The representative member without easterlies shows a vortex core with the same magnitude as in the ERA-Interim reanalysis but shifted to the west. Also the shape of the polar vortex does not resembles a classical „comma“-shape (Figure 6.8). The largest differences between the two representative members is found at the eastern end of the vortex core and east of it.
The reforecast initialized on 25 November 2000 shows almost no differences between its two representative members (Figure 6.8). This is most likely due to the very short lead time of 1 day. Both representative members show the southward displaced, „comma“-shape polar vortex in the same location and with the same magnitude as the ERA-Interim reanalysis.

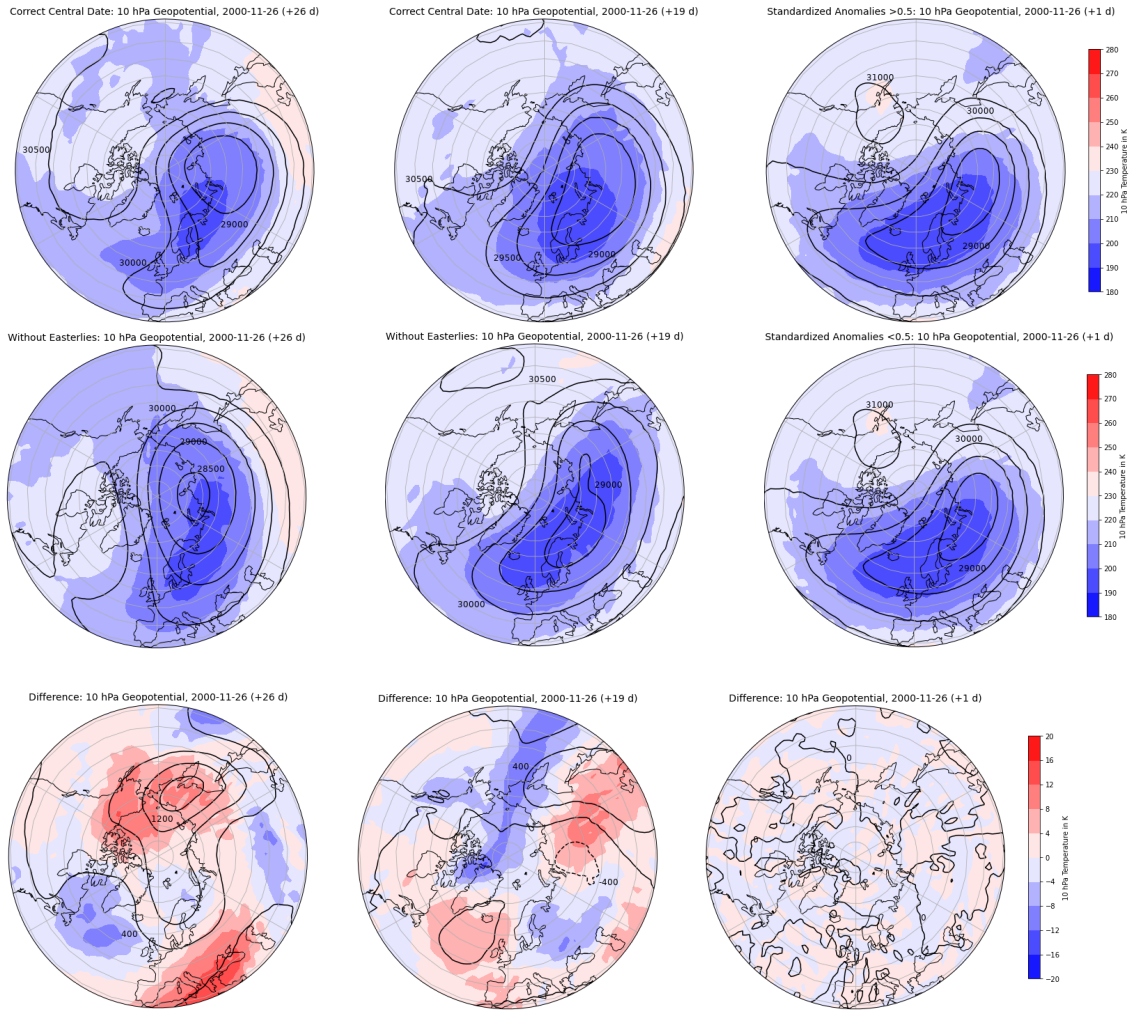

Figure 6.8: **Shape of the Polar Vortex in 10 hPa Geopotential Height on 26 November 2000 in the Selected S2S Reforecasts.** Comparison of the representative member with the correct prediction of the atmospheric state (top row) and the representative member without the correct prediction of the atmospheric state (middle row). The difference of both members is shown in the bottom row. The left column shows the representative members of the reforecast initialized on 31 October 2000, the middle column the representative members of the reforecast initialized on 7 November 2000 and the right column the representative members of the reforecast initialized on 25 November 2000.

6.5 Predicted Sudden Stratospheric Warming Signals in the Lower Stratosphere

In contrast to the reforecast initialized on 25 November 2000, the representative members of the other two selected reforecasts show less distinct differences in their prediction of the 100 hPa normalized geopotential height anomalies (Figure 6.9). Concerning the reforecast initialized on 31 October 2000, the representative member with the correct central date follows the ERA-Interim reanalysis roughly until the beginning of December but then turns to largely negative geopotential height values while the ERA-Interim reanalysis stays positive. The representative mem-

ber without easterlies turns to negative standardized geopotential height values already in mid-November 2000. Regarding this reforecast, the member with the correct central date is closer to the ERA-Interim reanalysis. This finding is in contrast to the reforecasts initialized on 25 November and 7 November 2000 (Figure 6.7 bottom and 6.9 bottom). Therefore, it cannot be assumed that a good representation of the SSW index by an ensemble member leads to a good representation of the polar-cap averaged, standardized 100 hPa geopotential height anomalies.
In case of the reforecast initialized on 7 November 2000, both representative members show a quite similar behaviour (Figure 6.9 bottom). The representative member with the correct central date is only closer to the ERA-Interim reanalysis than the representative member without easterlies until the end of November. This leads to the question whether a good representation of the SSW index by the S2S reforecast is more important for the prediction of a potential surface impact of an SSW or the correct representation of the anomalies induced by the SSW in the lower stratosphere, for example the polar-cap averaged 100 hPa standardized geopotential height anomalies.

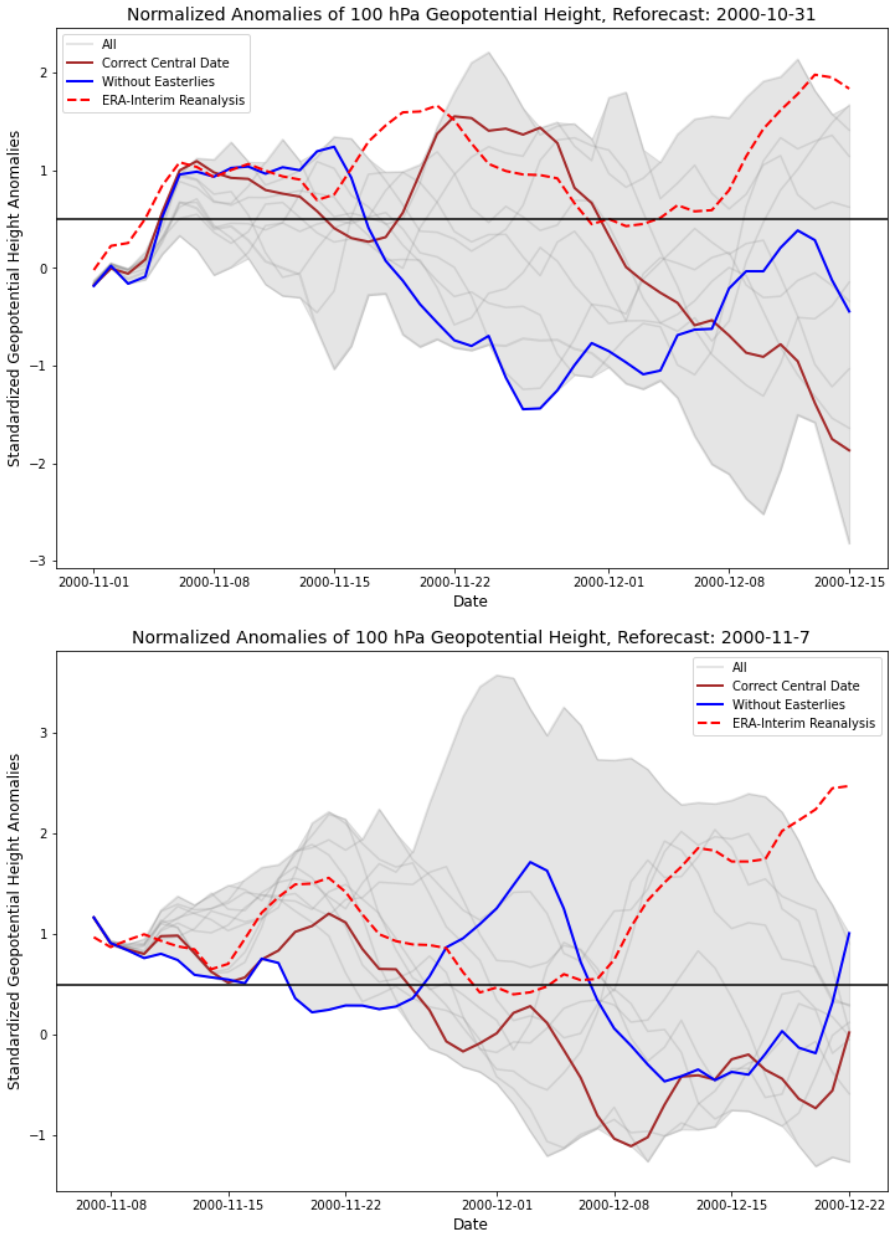

Figure 6.9: **Polar-Cap Averaged Normalized Geopotential Height Anomalies in 100 hPa in the S2S Reforecasts Initialized Before the Central Date of the SSW.** Shown are the reforecast initialized on 31 October 2000 from 1 November 2000 onwards (top) and the reforecast initialized on 7 November 2000 (bottom). The ERA-Interim reanalysis is marked by the red dashed line. The data of the first and last 3 days of the reforecasts are prone to boundary effects due to the use of 7-day running mean for the calculation of climatology.

6.6 Blocking in the Middle Troposphere

During the time when the positive standardized geopotential height anomalies associated with the first SSW of the winter 2000/2001 are present at surface, a long-lasting strong blocking pattern over the Euro-Atlantic sector is detected (Figure 6.1 and 6.10 top). This pattern occurring between 20 and 30 December 2000 is clearly visible in the deviation of the geopotential height

at 65°N (Figure 6.2 top). The striking blocking pattern over the Euro-Atlantic sector shows a tilted Ω-like shape and is centered over central Europe (Figure 6.11 top). A similar blocking situation is detected between 24 February and 7 March 2001, in the period, when positive standardized geopotential height anomalies associated with the second SSW of the winter 2000/2001 are present at surface (Figure 6.1 and 6.10 bottom). The again Ω-shaped blocking pattern is less tilted at that time and centered over the western North Atlantic ocean (Figure 6.11 bottom). While the blocking pattern between 24 February and 7 March 2001 co-occurs with an upward propagation of tropospheric waves, the blocking pattern between 20 and 30 December 2000 co-occurs with a downward propagation of stratospheric signals to the surface. Therefore, an association with the preceding SSW event might be suggested. However, this is not in agreement with literature. According to Charlton-Perez et al. (2018) blocking patterns do not show a significant sensitivity to changes in the stratospheric circulation. On the other hand the stratospheric circulation shows significant changes after tropospheric blocking situations (Woollings et al., 2018; Martius et al., 2009). The frequent occurrence of long-lasting, simultaneously occurring Scandinavian and Alaskan ridges during the winter 2000/2001, can therefore lead to an enhanced upward propagation of tropospheric waves, which may disturb the stratospheric polar vortex (Figure 6.10 top and bottom; Schneidereit et al., 2017). According to Manney et al. (2001) this is the case of the first SSW of the winter 2000/2001, although it is associated with a stronger than average Aleutian high and a wavenumber-1 amplification. The strong Aleutian high is visible in the 500 hPa geopotential height field, developing before the beginning of November and persisting until 14 December 2000, 3 weeks after the central date of the first SSW of the winter 2000/2001 (Figure 6.10 top and 6.11 top). It is accompanied by a strong Scandinavian ridge (Figure 6.10 top and 6.11 top). At the central date of the second SSW in this winter, the two ridges are also present, indicating a possible wavenumber-2 perturbation of the polar vortex (Figure 6.10 bottom; Schneidereit et al., 2017). Furthermore, blocking over the pole at the same time is stated to be a precursor of the second SSW event of the winter 2000/2001 (Martius et al., 2009). Since slight La Niña conditions are present during the whole winter, it has also to be kept in mind that these may favor the development of blocking anticyclones (https://www.cpc.ncep.noaa.gov/products/analysis_monitoring/ensostuff/detrend.nino34.ascii.txt, last viewed 5 November 2019; Schneidereit et al., 2017).

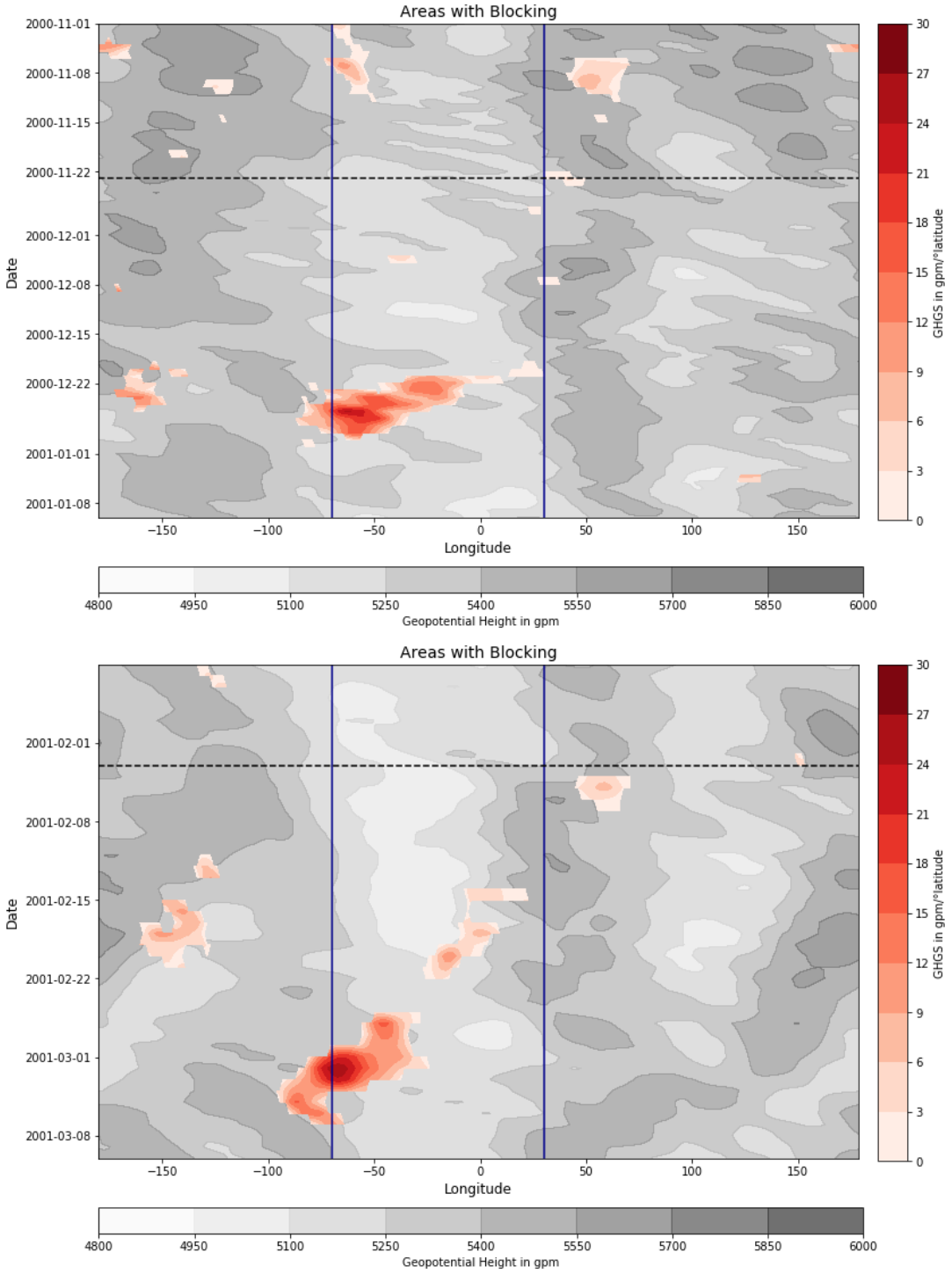

Figure 6.10: **Blocking Situation between November 2000 and March 2001 based on ERA-Interim.** The Hovmöller diagrams show the 500 hPa geopotential height between November and mid-January (top) as well as between the end of January and the beginning of March (bottom). It is averaged between 40°N and 80°N and shown as grey shading. The GHGS component of the blocking index by Tibaldi and Molteni (1990) is shown in red. The horizontal black dashed lines mark the central date of the SSW events. The area between the solid blue lines refers to the Euro-Atlantic sector, 70°W to 30°E.

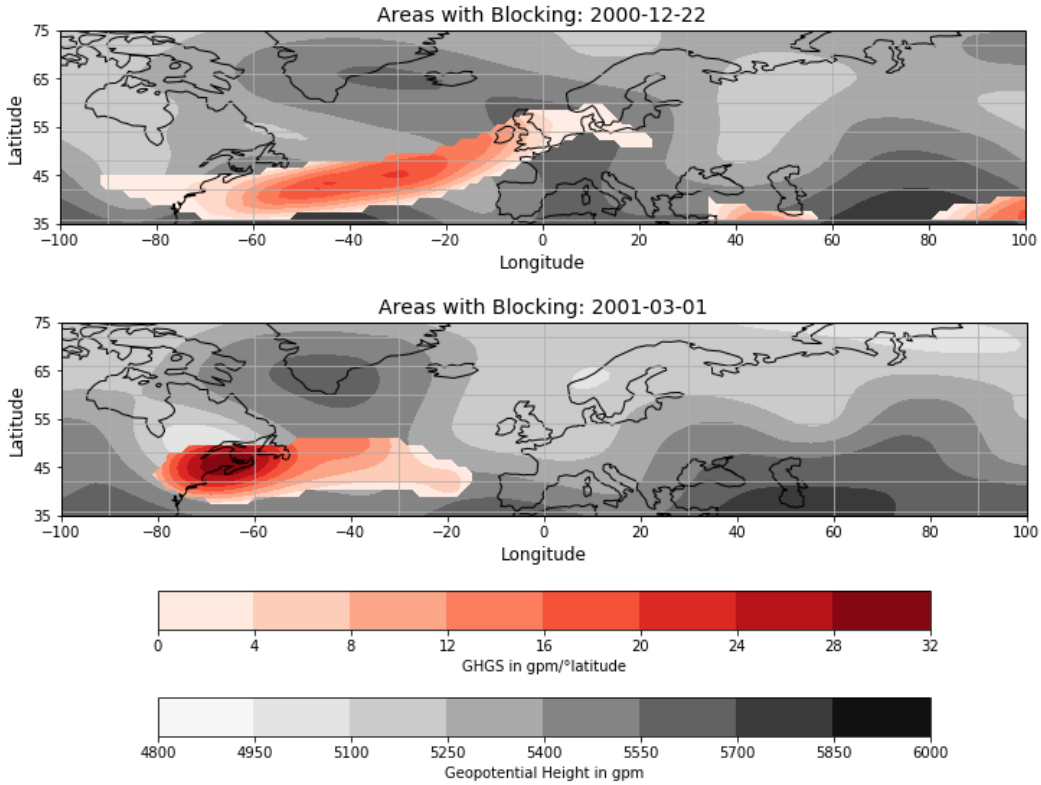

Figure 6.11: **Distinctive Blocking Patterns in the Middle Troposphere after the SSW Events of the Winter 2000/2001 based on ERA-Interim.** Selected days, 22 December 2000 (top) and 1 March 2001 (bottom) with blocking patterns are shown. The 500 hPa geopotential height is shown as grey shading and the GHGS component of the blocking index by Scherrer et al. (2006) in red.

6.7 Predicted Blocking in the Middle Troposphere

For the occurrence of blocking patterns in the S2S reforecasts, the 500 hPa geopotential height anomalies, averaged over 40°N to 80°N and 70°W to 30°E, are used. Concerning the reforecast initialized on 31 October 2000, the representative member with the correct central date follows the curve of ERA-Interim reanalysis rather closely with maximum deviations around 50 gpm (Figure 6.12 top). The representative member without easterlies follows the ERA-Interim reanalysis only until 15 November 2000 and then differs most of the time in magnitude and sign. It seems, as if there is an added value in the prediction of blocking situations, when the SSW event is represented correctly. This might be coincidence since the occurrence of blocking patterns is not sensitive to changes in the stratospheric state (Charlton-Perez et al., 2018).

The most striking feature of the reforecast initialized on 7 November 2000 is the strong increase of the ensemble spread around 20 November 2000 (Figure 6.12 bottom). According to Manney et al. (2001) this is the time of a wavenumber-1 amplification in the troposphere. This leads to the idea of different realization possibilities for the type and strength of atmospheric waves at that time. The representative member without easterlies shows in the following 2 weeks deviations up to 75 gpm from the reanalysis, while the deviations of the representative member with the correct central date are maximally around 50 gpm. Thus, there is again a slightly better representation of

the atmospheric state by the representative member with the correct central date. After 25 December 2000 both representative members show a similar curve in shape and magnitude.
Concerning the reforecast initialized on 25 November 2000, both representative members show a rather similar behaviour, not following the shape of the ERA-Interim reanalysis well (Figure 6.13). The correct representation of the standardized geopotential height anomalies in 100 hPa does not seem to add value to the predicition of the geopotential height anomalies in 500 hPa in this case. This supports the findings of Charlton-Perez et al. (2018) who state that the tropospheric blocking patterns are insensitive to the stratospheric conditions.
The Ω-blocking pattern observed after the first SSW of the winter 2000/2001, is not visible in the ERA-Interim 5600 gpm isoline which exhibits a rather zonal flow in the North Atlantic-European sector (Figure 6.14 top and bottom). The representative member without easterlies of the reforecast initialized on 7 November 2000 shows a distinct Ω-shape, however, too far east and at the wrong geopotential height level (Figure 6.14 top). Regarding the representative member with the correct central date of the same reforecast, the 5600 gpm isoline is predicted too far south over the continents. The largest difference between the two representative members is found over northern Asia in the region of the Ω-block predicted by the member without easterlies. Over the North Atlantic ocean, the difference and the ensemble spread are smallest.
This also applies to the reforecast initialized on 25 November 2000 but the largest differences between the two representative members of this reforecast are found over Scandinavia, north of the Ω-block predicted by the representative member with prevailing standardized geopotential height anomalies <0.5 standard deviation in 100 hPa. (Figure 6.14 bottom). The blocking pattern is predicted less pronounced than in the previous reforecast and on the right location but still to strong in the 5600 gpm isoline. The representative member with prevailing standardized geopotential height anomalies >0.5 standard deviation in 100 hPa follows the ERA-Interim reanalysis more closely but shows an additional trough south of the Iberian Peninsula.

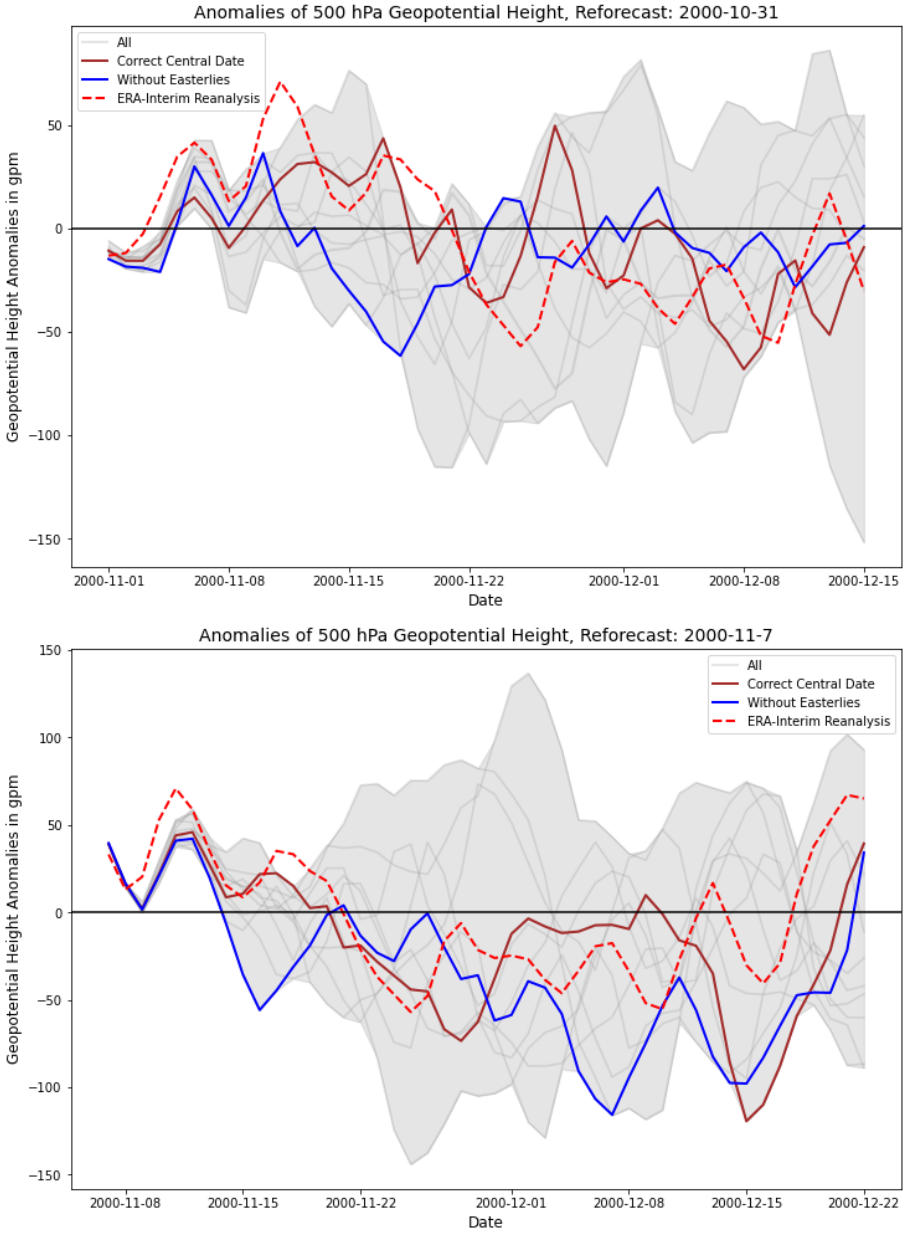

Figure 6.12: **Geopotential Height Anomalies in 500 hPa of the S2S Reforecast Initialized before the Central Date of the SSW.** The 500 hPa geopotential height anomalies are averaged between 40°N and 80°N as well as 70°W and 30°E. The red dashed line shows the ERA-Interim reanalysis. The reforecast initialized on 31 October 2000 is shown from 1 November 2000 onwards (top plot). The reforecast initialized on 7 November 2000 is shown in the bottom plot. The data of the first and last 3 days of the reforecasts are prone to boundary effects due to the use of 7-day running mean for the calculation of climatology.

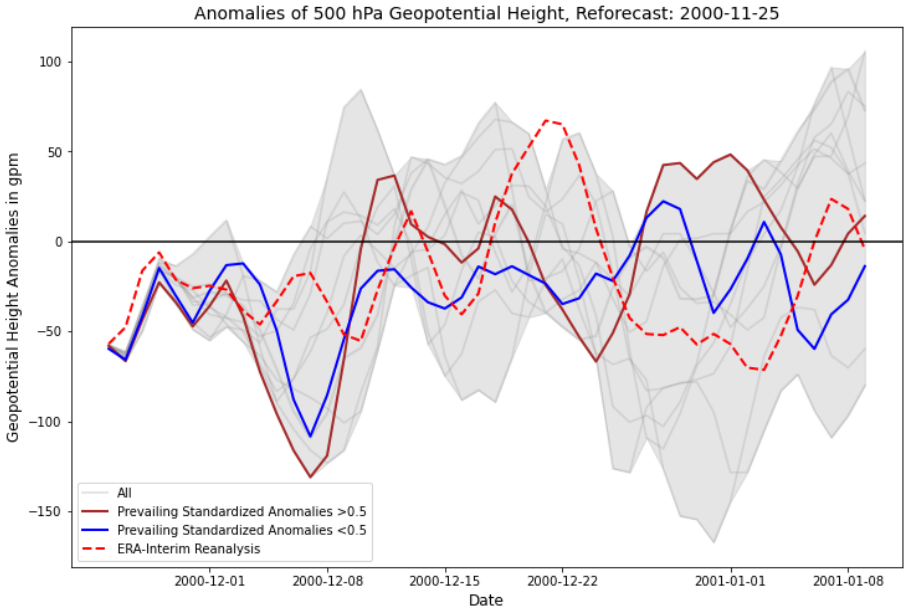

Figure 6.13: **Geopotential Height Anomalies in 500 hPa of the S2S Reforecast Initialized after the Central Date of the SSW.** The 500 hPa geopotential height anomalies are averaged between 40°N and 80°N as well as 70°W and 30°E. The red dashed line shows the ERA-Interim reanalysis. The data of the first and last 3 days of the reforecast are prone to boundary effects due to the use of 7-day running mean for the calculation of climatology.

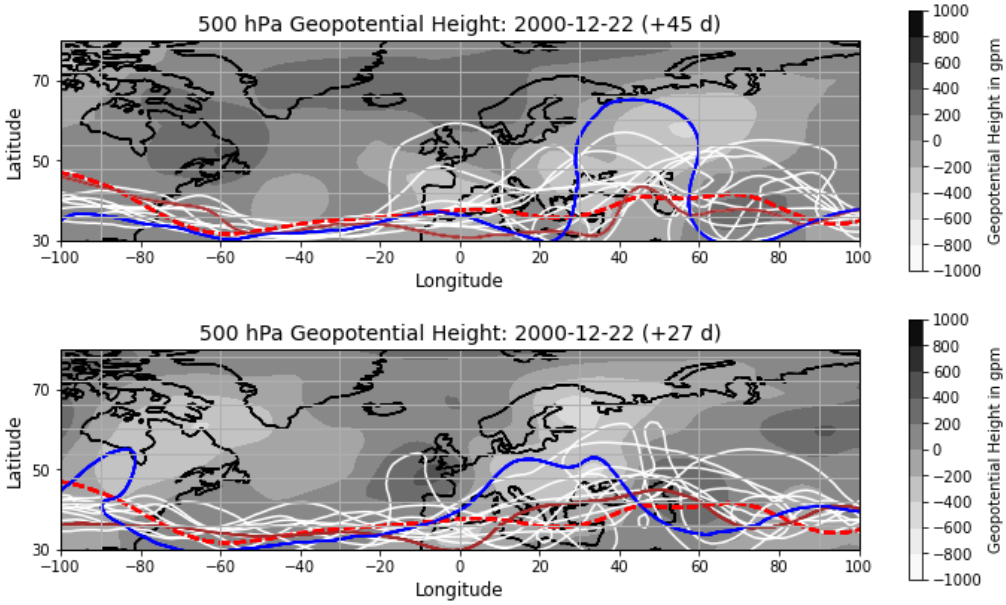

Figure 6.14: **Blocking Pattern in the Middle Troposphere on 22 December 2000 in the S2S Reforecasts.** The top plot shows the ensemble members of the reforecast initialized on 7 November 2000, the bottom plot the ensemble members of the reforecast initialized on 25 November 2000. Shown are the 5600 gpm geopotential height isolines, for the ensemble in white, the representative members with the correct prediction of the atmospheric state in brown and the representative members without the correct prediction of the atmospheric state in blue. The red dashed line shows the ERA-Interim reanalysis. In the background, the difference between the two representative members is shown as grey shading for the depicted reforecast.

6.8 Position of the Mid-Latitude Jet Stream in the Lower Troposphere

In comparison to the climatological mean, the mid-latitude jet stream is located further south than usual most of the time until 11 February 2001 (Figure 6.15). This is a typical behaviour, observed after 2/3 of the SSW events (Afargan-Gerstman and Domeisen, 2020). Then, the jet is displaced northwards up to 65°N, which is observed after 1/3 of all SSW events (Afargan-Gerstman and Domeisen, 2020). This indicates that the SSWs of the winter 2000/2001 show different influences on the surface. After the poleward shift of the mid-latitude jet stream, the maximum wind speeds are found around 30°N and are more likely associated with the subtropical jet than the mid-latitude jet stream. It is suggested that the mid-latitude jet stream is weakened from here on and restrengthens in mid-March, where it is again located equatorward of the climatological mean position (Figure 6.15). At this time though, its position cannot be associated with the second SSW of the winter 2000/2001. In April, the mid-latitude jet stream is located at its climatological latitude again or a little further northward (Figure 6.15).

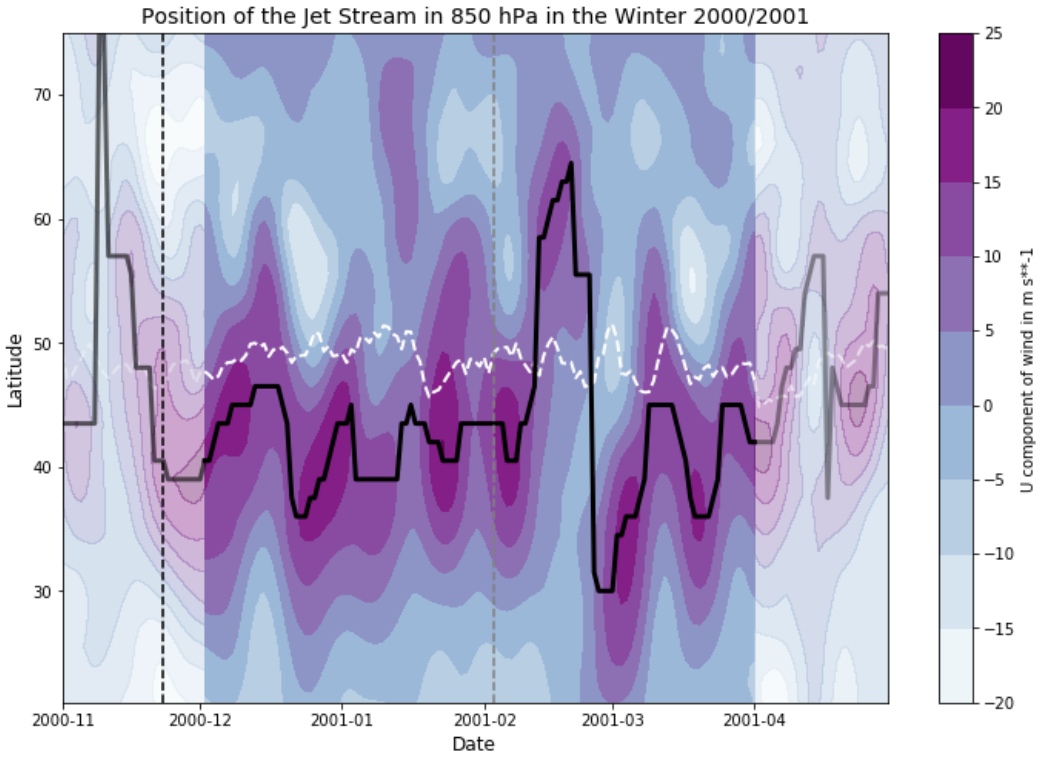

Figure 6.15: **Zonal Wind Speed Anomalies during the Winter 2000/2001 based on ERA-Interim.** The zonal-wind anomalies in 850 hPa, averaged over 60°W to 0°E are shown as shading in the Hovmöller diagram. The anomalies are filtered using a Lanczos filter with a moving window of 61 days and a cutoff-frequency of 1/10 days. Data on the edges of the timeseries are prone to boundary effects due to the filtering and therefore, shown paler than the unaffected data. The wind maxima are shown as a black solid line. The white dashed line shows the climatological position of the mid-latitudes jet stream. The central date of the first SSW in the winter 2000/2001 is marked with the vertical black dashed line, the central date of the second SSW with the vertical grey dashed line.

6.9 NAO Index at the Surface

Roughly 1 week before the SSW event occurring on 23 November 2000, the NAO is in its positive phase (Figure 6.16). Exactly on the central date of he SSW, the 7-day running mean of the NAO index turns negative but the daily NAO index turns negative already 3 days prior to the central date. Therefore, this following NAO- phase is rather unlikely triggered by the SSW and hence, not directly associated with it. This is supported by the fact that the SSW induced positive geopotential height anomalies >1.0 standard deviation associated with the SSW reach the surface earliest on 10 December 2000 (Figure 6.1). The long-lasting NAO- phase between 18 December 2000 and 23 January 2001 coincides with positive geopotential height anomalies >1.0 standard deviation at the surface and therefore is likely triggered and maintained by the first SSW of the winter 2000/2001 (Figure 6.16 and 6.1). This is supported by the finding that positive geopotential height deviations from the zonal-mean associated with a downward propagation of stratospheric signals, are found over the North Atlantic ocean at that time (Figure 6.2 top). The pressure systems over the North Atlantic ocean show a large pressure gradient between roughly 50°N and 60°N and are located over the area which is used for the calculation of the NAO index (Figure 6.17 top row). From 4 January 2001 onwards, less positive normalized geopotential height anomalies prevail at the surface, making the influence of the SSW on surface weather less likely (Figure 6.1). The NAO at that time is still in its negative phase and stays there until 22 January 2000 (Figure 6.16). A possible maintainer of this NAO- phase is a long-lasting blocking pattern over the Euro-Atlantic sector occurring in mid-January (Figure 6.10 top). After a short period with a positive phase of the NAO, the 7-day running mean of the NAO index turns negative again on 31 January 2001. The daily values of the index turn negative on 3 February 2000, the day of the central date of the SSW (Figure 6.16). This indicates that this NAO- phase could be triggered by the SSW (Lee et al., 2019; Domeisen, 2019). The fact that at this time normalized positive geopotential height anomalies >1.0 standard deviation have not reached the lower stratosphere, does not support this indication. On 10 February 2001, the NAO becomes positive again for 11 days (Figure 6.16). The following NAO- phase coincides with positive normalized geopotential height anomalies at surface for the following 2 weeks (Figure 6.1). But since the deviation of the normalized geopotential height from the zonal-mean shows an upward propagation at this time, the NAO- phase is not associated with the SSW event (Figure 6.2 bottom). With the exception of 4 positive values of the daily NAO index in the beginning of March, the NAO index stays negative until 27 March 2001 (Figure 6.16). Possible maintainer of this long-lasting NAO- phase are 3 blocking patterns occurring over the Euro-Atlantic sector during that time (Figure 6.10 bottom). Interestingly, the pressure distribution does not resemble the „classical“ NAO- pressure distribution (Figure 6.17 bottom row). The low pressure system over Iceland extends further south and it is not well distinguishable. The situation of the displayed week shows a rather merdional than zonal flow over the North Atlantic ocean.

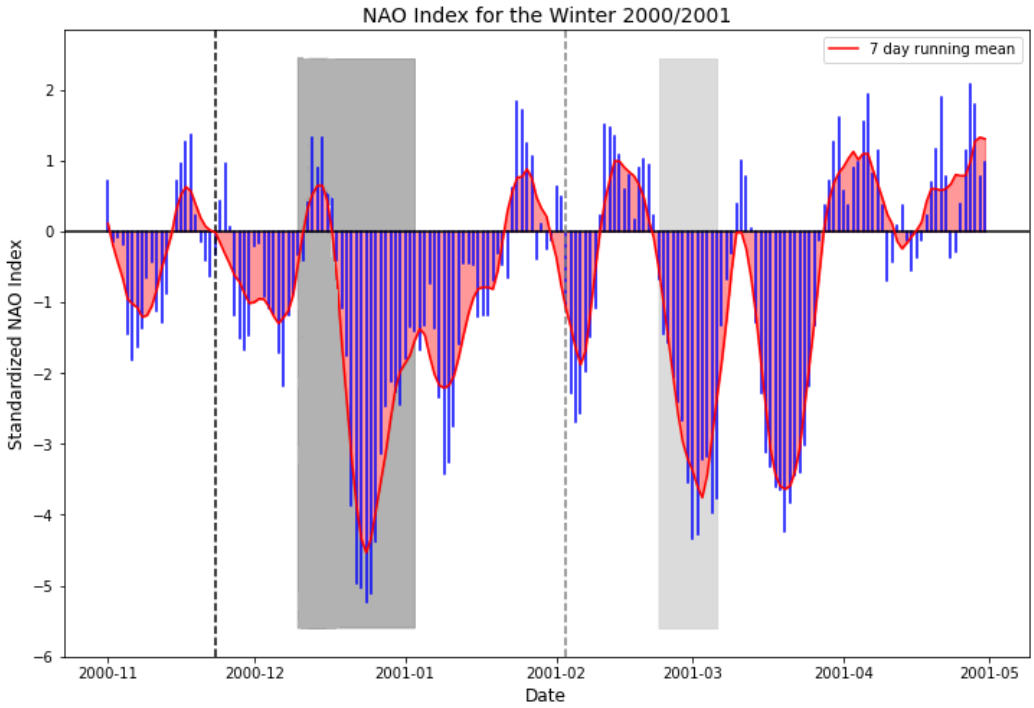

Figure 6.16: **NAO Index during the Winter 2000/2001 based on ERA-Interim.** Shown is the Zonal Index which is calculated as the standardized mean sea level pressure anomaly difference between a southern box, averaged over 40°W to 0°E and 35°N to 50°N, and a northern box, averaged over 40°W to 0°E and 55°N to 70°N (Leckebusch et al., 2008). The black dashed line marks the central date of the first SSW, the grey dashed line the central date of the second SSW. The period with normalized geopotential height anomalies >1.0 standard deviation associated with the SSWs at surface is shaded in dark grey for the first SSW of the winter 2000/2001 and in light grey for the second SSW of this winter.

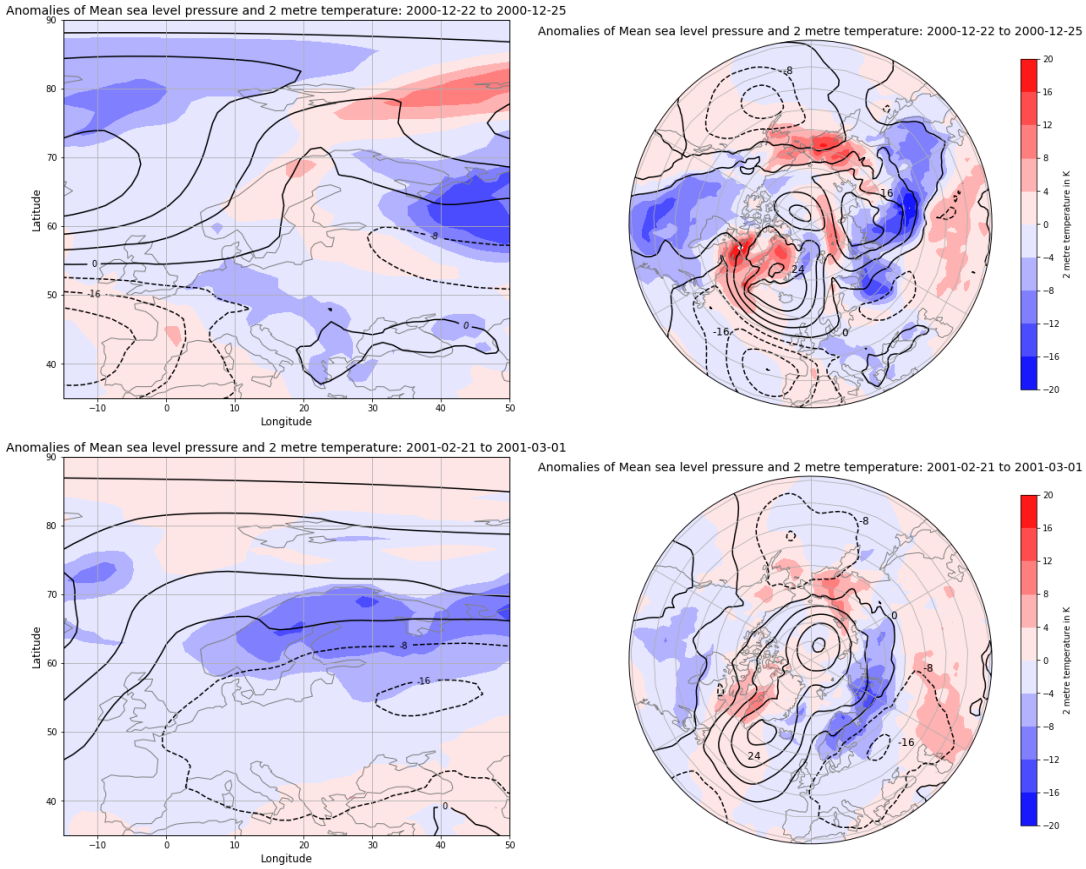

Figure 6.17: **Mean Sea Level Pressure Anomalies and 2 Metre Temperature Anomalies for Two European Cold Waves based on ERA-Interim.** Shown is the the European cold wave associated with the first SSW of the winter 2000/2001 (top row) and the European cold wave happening after the second SSW of this winter (bottom row). The dashed contours show negative mean sea level pressure anomalies, the solid contours show positive mean sea level anomalies. The 2 metre temperature anomalies are plotted as shading.

6.10 Predicted NAO Index at the Surface

It is striking, that all three selected reforecasts show rather large differences to the ERA-Interim NAO index (Figure 6.18 top and bottom and 6.19). This is may due to the fact that even slight shifts of the pressure systems responsible for the typical NAO pattern can result in large changes of the NAO index, as the area over which it is computed is fixed (Leckebusch et al., 2008). Concerning the reforecast initialized on 31 October 2000, both representative members of the reforecast show a similar behaviour until 5 December 2000 (Figure 6.18 top). But none of them is following the daily or the 7-day running mean values of the ERA-Interim NAO index closely. The large ensemble spread shows that the NAO index is not predicted well by this reforecast, independently whether the SSW is represented correctly in the reforecasts or not.
The ensemble spread of the reforecast initialized on 7 November 2000 shows also a large ensemble spread (Figure 6.18 bottom). The representative members do not capture the ERA-Interim NAO index well but show a more different behaviour this time. From the beginning of November onwards, they differ mostly in sign but show a similiar magnitude. Until 10 December 2000, the curve of the representative member without easterlies is closer to the curve of the ERA-Interim reanalysis. After this date, the representative member with the correct central date shows a more similar behaviour to the ERA-Interim reanalysis.
Only for the reforecast initialized on 25 November 2000, the representative member with the correct representation of the state of the stratosphere is closer to the ERA-Interim NAO index than the representative member without the correct representation of the stratospheric state (Figure 6.19). The representative members for this reforecast are chosen based on the normalized geopotential height anomalies in 100 hPa. Although the representative member with prevailing standardized geopotential height anomalies >0.5 standard deviation is generally closer to the ERA-Interim reanalysis, it differs mostly in sign from it. So does the representative member with prevailing standardized geopotential height anomalies <0.5 standard deviation but with a larger amplitude. The strong negative NAO- phase starting in mid-December 2000 is not captured by the two representative members at all. At that time, the representative member with prevailing standardized geopotential height anomalies >0.5 standard deviation predicts a high pressure system over most of the North Atlantic ocean, while the representative member with prevailing standardized geopotential height anomalies <0.5 standard deviation predicts an NAO+ structure, shifted from the North Atlantic ocean to the European continent (Figure 6.17 bottom row).

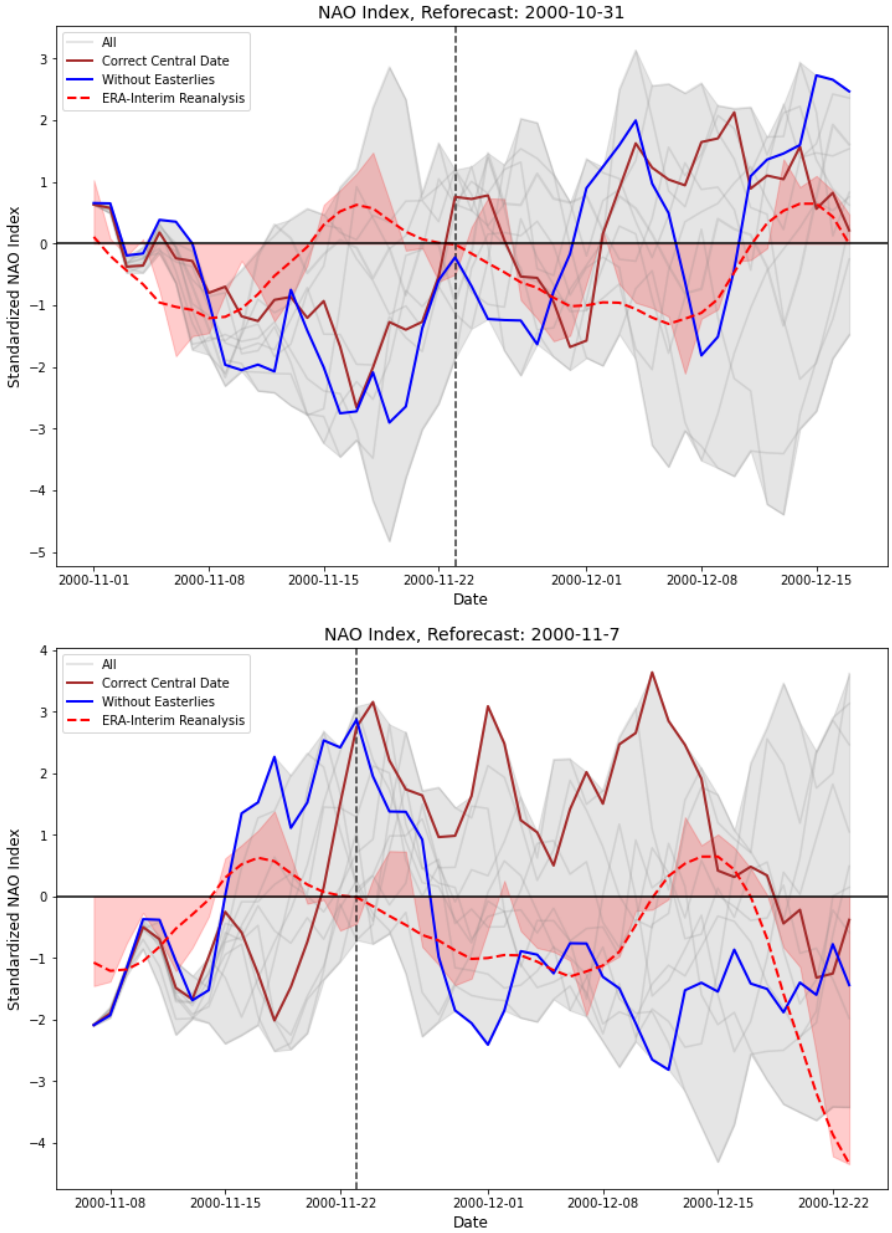

Figure 6.18: **NAO Index of S2S Reforecasts Initialized Before the Central Date of the SSW.** The top plot shows the reforecast initialized on 31 Octobre 2000 from 1 November 2000 onwards, the bottom plot the reforecast initialized on 7 November 2000. Shown is the zonal index which the standardized mean sea level pressure anomaly difference between a southern box, averaged over 40°W to 0° and 35°N to 50°N, and a northern box, averaged over 40°W to 0° and 55°N to 70°N (Leckebusch et al., 2008). The red shading shows the daily NAO index and the red dashed line the 7-day running mean of it calculated with the ERA-Interim reanalysis data set. The vertical black dashed line marks the central date of the SSW. The data of the first and last 3 days of the reforecasts are prone to boundary effects due to the use of 7-day running mean for the calculation of climatology.

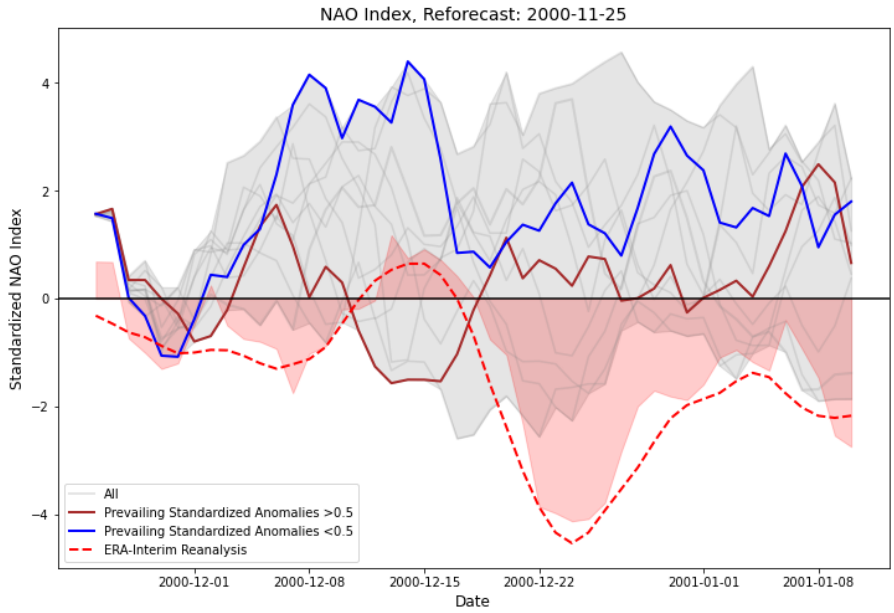

Figure 6.19: **NAO Index of the S2S Reforecast Initialized After the Central Date of the SSW.** Shown is the zonal index which the standardized mean sea level pressure anomaly difference between a southern box, averaged over 40°W to 0° and 35°N to 50°N, and a northern box, averaged over 40°W to 0° and 55°N to 70°N (Leckebusch et al., 2008). The red shading shows the daily NAO index and the red dashed line the 7-day running mean of the daily NAO index calculated with the ERA-Interim reanalysis data set. The data of the first and last 3 days of the reforecast are prone to boundary effects due to the use of 7-day running mean for the calculation of climatology.

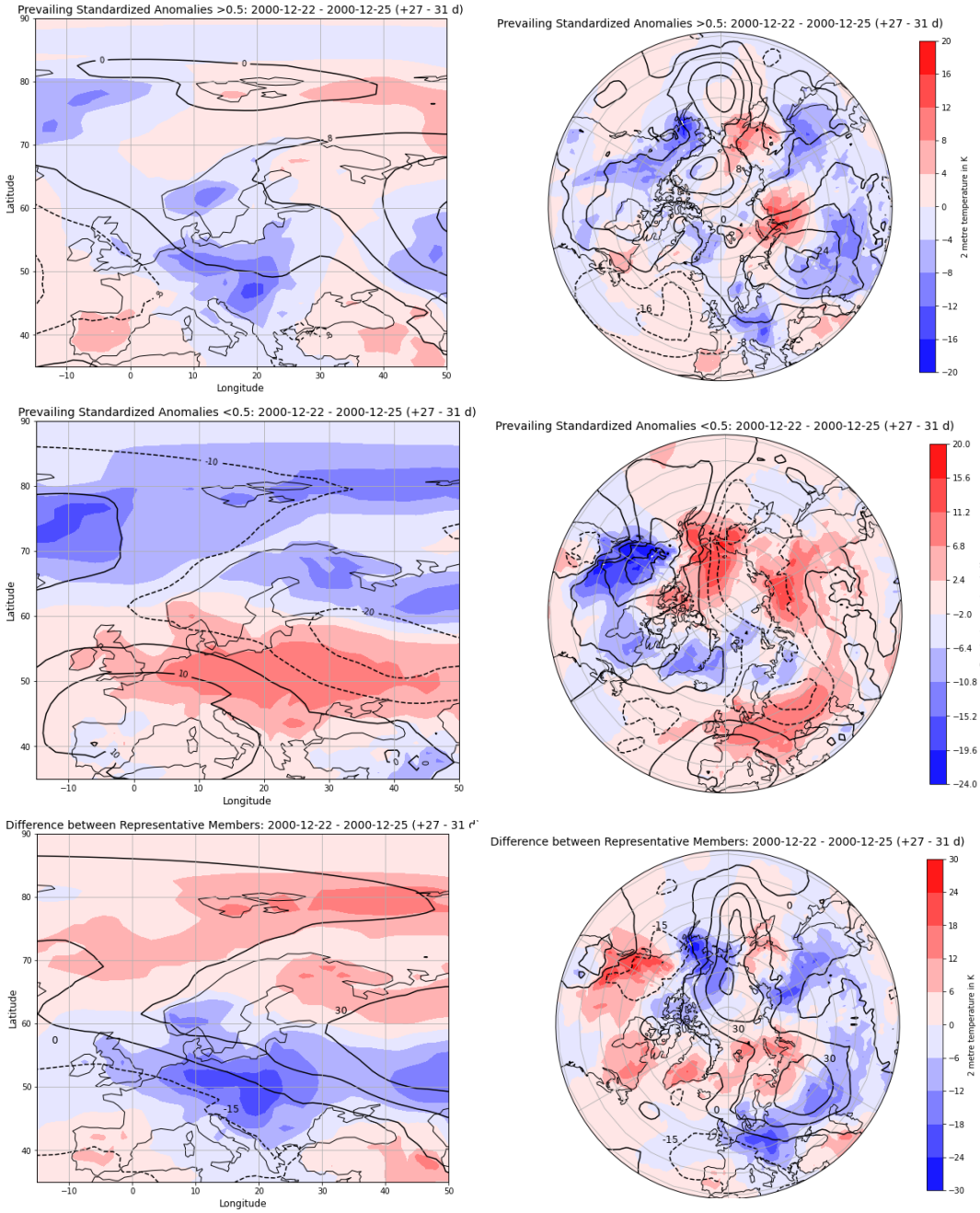

Figure 6.20: **2 Metre Temperature Anomalies and Mean Sea Level Pressure Anomalies between 22 and 25 December 2000 in the S2S Reforecast Initialized on 25 November 2000.** Comparison of the representative member with prevailing standardized anomalies >0.5 standard deviation (top row) with the representative member with prevailing standardized anomalies <0.5 standard deviation (middle row) of the reforecast initialized on 25 November 2000. The difference between the two representative members is shown in the bottom row. All plots in the top and middle row except one in the middle row on the right have the same color-scale, shown on the top right. The color-scale of the plot in the middle row on the right is given next to it.

6.11 European Cold Waves at the Surface

Three European cold waves can be detected during the winter 2000/2001 using the 7-day running mean of the 2 metre temperature anomlies (Figure 6.21). Following the cold wave definition by Smid et al. (2019) only the latter two are identified as cold waves (Figure 6.22). The first European cold wave is not detected by the approach of Smid et al. (2019) but coincides with positive normalized geopotential height anomalies at the surface, associated with the SSW event on 23 November 2000 (Figure 6.21 and 6.1). It shows values about 1.2 K below its climatological mean in the time between 22 and 25 December 2000 (Figure 6.21). The strongest manifestation is seen in northern Europe with values around 5 K below average. Eastern, north-western and central Europe also experience unusual cold temperatures during that time. The coinciding NAO- phase, the equatorward shift of the tropospheric jet and the detected downward propoagation of positive normalized geopotential height anomalies caused by the first SSW of the winter 2000/2001 indicate that the European cold wave happening between 22 and 25 December 2000 is linked to the SSW event with its central date on 23 November 2000 (Figure 6.21, 6.16, 6.15 and 6.2 top). This is supported by the large positive temperature anomalies up to 20 K above average found over Greenland and the Bering Strait at that time (Figure 6.17 top row). The second European cold wave in the winter 2000/2001 happens around the central date of the second SSW (Figure 6.21). Since positive geopotential height anomalies induced by this SSW event reach the surface first in mid-February, this cold wave is not associated with it (Figure 6.1). Between 21 February and 1 March 2001, the third and last European cold wave of the winter 2000/2001 occurs (Figure 6.21). During that time, positive standardized geoptential height anomalies, caused by the SSW with its central date on 3 February 2001, are observed at the surface (Figure 6.1). But because the deviation of the geopotential height from the zonal-mean at 65°N does not show a downward propagation of stratospheric signals, this cold wave is not associated with the SSW event as well (Figure 6.2 bottom). This European cold wave is characterized by temperatures lower than 1 K below average (Figure 6.21). The maximum cold temperatures are lower than 7 K below average in northern Europe and around 3 K lower than average in the European mean. Except the Mediterranean, all European regions experience unusually cold temperatures (Figure 6.17 bottom row). This is detected by both definitions of cold waves. The largest positive temperature anomalies are found south-west of Greenland, indicating again downward propagating stratospheric positive temperature anomalies, which is not supported by the deviation of the geopotential height from the zonal-mean, averaged at 65°N (Figure 6.17 bottom row and 6.2 bottom).

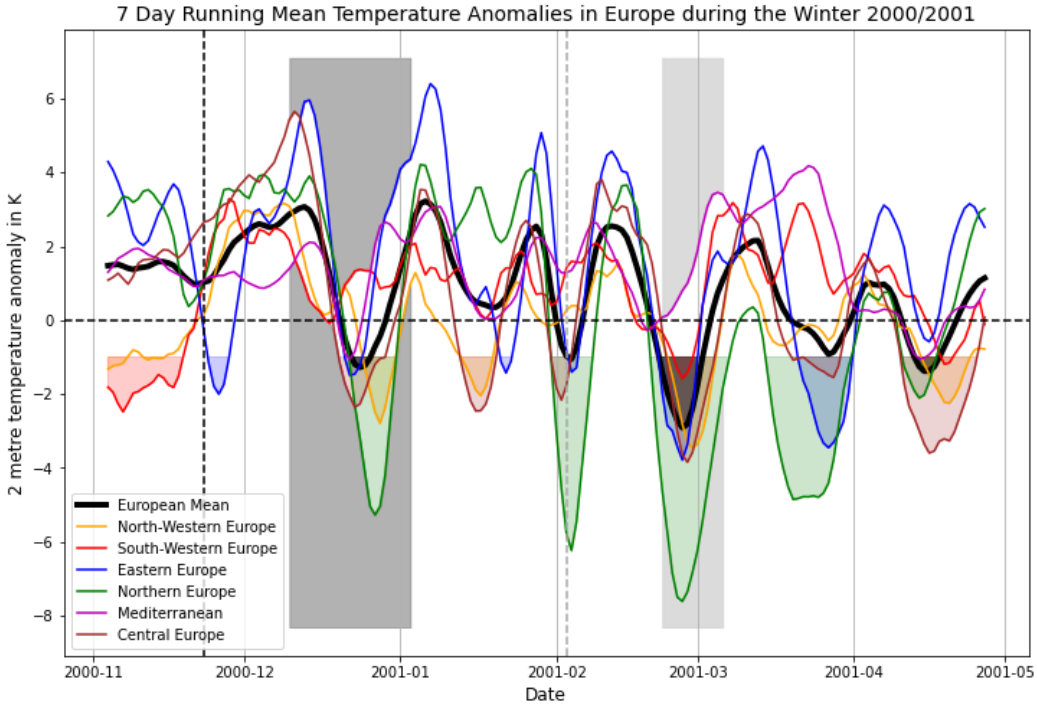

Figure 6.21: **2 Metre Temperature Anomalies during the Winter 2000/2001 based on ERA-Interim.** Periods of cold waves are defined using 1 K below the climatological mean as the warm temperature threshold for cold waves (Garfinkel et al., 2017). The days with cold waves are marked as shading in the respective color. The vertical black dashed line marks the central date of the first SSW in the winter 2000/2001, the vertical light grey line the central date of the second SSW. The period with normalized geopotential height anomalies >1.0 standard deviation associated with the SSWs at surface is shaded in dark grey for the first SSW of the winter 2000/2001 and in light grey for the second SSW of this winter. The European mean is calculated by averaging between 10°W to 42°E and 35°N to 72°N. The anomalies for north-western Europe between 10°W to 3°E and 45°N to 60°N, for south-western Europe between 10°W to 3°E and 35°N to 45°N, for eastern Europe between 20°E to 42°E and 45°N to 60°N, for northern Europe between 3°E to 42°E and 60°N to 72°N, for central Europe between 3°W to 20°E and 45°N to 60°N and for the Mediterranean between 3°E to 42°E and 35°N to 45°N.

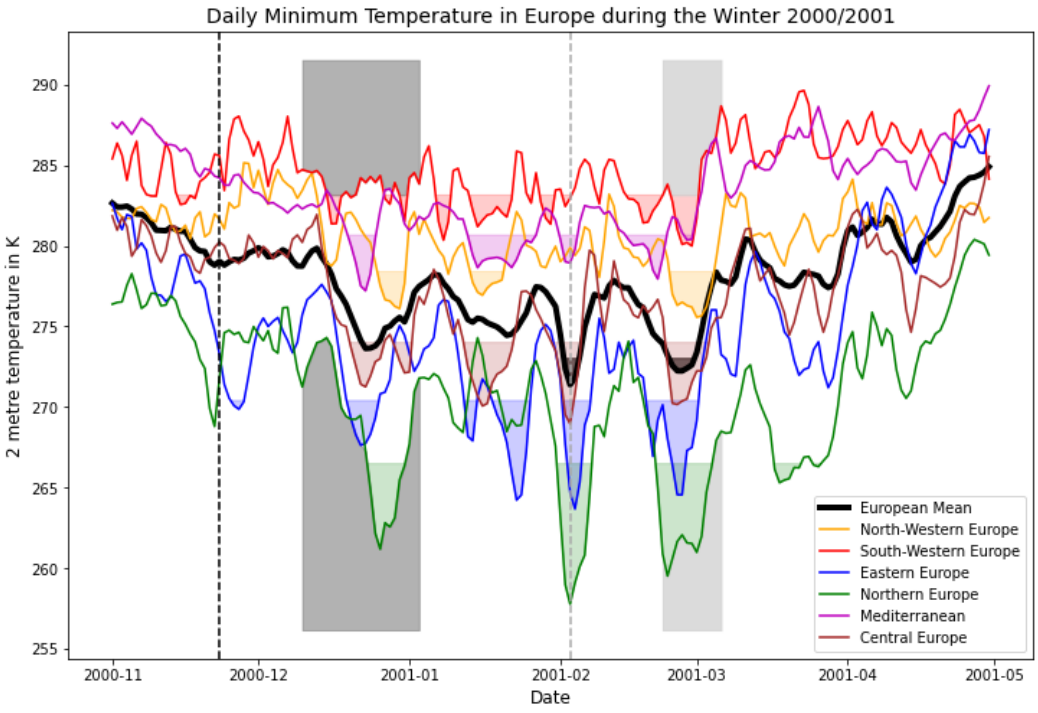

Figure 6.22: **2 Metre Daily Minimum Temperature during the Winter 2000/2001 based on ERA-Interim.** Periods of cold waves are defined as at least 3 consecutive days with daily minimum temperatures below the 10^{th} percentile of the climatological daily minumum temperature (Smid et al., 2019). The climatology is calculated for the period between 1999 and 2019 with a 31 day running mean. The days with cold waves are marked as shading in the respective color. The vertical light grey dashed line marks the central date of the first SSW in the winter 2000/2001, the vertical black line the central date of the second SSW. The period with normalized geopotential height anomalies >1.0 standard deviation associated with the SSW at surface is shaded in dark grey for the first SSW of the winter 2000/2001 and in light grey for the second SSW of this winter. The European mean is calculated by averaging between 10°W to 42°E and 35°N to 72°N. The anomalies for north-western Europe between 10°W to 3°E and 45°N to 60°N, for south-western Europe between 10°W to 3°E and 35°N to 45°N, for eastern Europe between 20°E to 42°E and 45°N to 60°N, for northern Europe between 3°E to 42°E and 60°N to 72°N, for central Europe between 3°W to 20°E and 45°N to 60°N and for the Mediterranean between 3°E to 42°E and 35°N to 45°N.

6.12 Predicted European Cold Waves at the Surface

Considering all selected reforecasts, it is striking that the ensemble members tend to be colder than the ERA-Interim reanalysis.

The reforecast initialized on 31 October 2000 features one ensemble member which closely follows the ERA-Interim reanalysis until 8 December 2000 (Figure 6.23 top). In contrast to this member, the representative members of the reforecast only follow the ERA-Interim reanalysis rather closely until mid-November 2012. Both predict a European cold wave in early December, when the ERA-Interim reanalysis shows only positive temperature anomalies. The representative member without easterlies deviates less from the ERA-Interim reanalysis than the representative member with the correct central date (Figure 6.23 top).

This is not true for the reforecast initialized on 7 November 2000. The representative member with the correct central date follows the ERA-Interim reanalysis more closely than the representative member without easterlies but still deviates up to 4 K from it (Figure 6.23 bottom). It shows the same shape of curve as the ERA-Interim reanalysis until the beginning of December but with an offset of about 1 K to lower temperature anomalies. Until this time, the correct prediction of the SSW in the reforecast seems to add value to the European 2 metre temperature prediction. Nevertheless, it is important to note that for the reforecast initialized on 7 November 2000, none of the ensemble members follows the ERA-Interim reanalysis well and even the member closest to the ERA-Interim reanalysis shows deviations of more than 2 K temporarily (Figure 6.23 bottom). This implies that either the good representation of the ERA-Interim reanalysis of one member of the reforecast initialized on 31 October 2000 is coincidence or that the reforecast initialized on 7 November 2000 takes into account other or maybe additional atmospheric phenomena which decrease its predictive skill. At the very end of the lead time of the reforecast initialized on 7 November 2000 the European cold waves starts. While the representative member with the correct central date does not predict a European cold wave at all, the representative member without easterlies predicts a cold wave but too early in the beginning of December 2000 (Figure 6.23 bottom).

The reforecast initialized on 25 November 2000 comprises the European cold wave between 22 and 25 December 2000. Since this cold wave is especially strong in Scandinavia, the Scandianvian 2 metre temperature anomalies are shown as well (Figure 6.17 top row and 6.24 bottom). Concerning the European mean temperatures, both representative members show a similar behaviour on 10 December 2000, following the ERA-Interim reanalysis quite well (Figure 6.24 top). The European cold wave between 22 and 25 December 2000 is captured at the beginning by the representative member with prevailing standardized geopotential height anomalies >0.5 standard deviation. However the member underestimates its amplitude and duration. The reason for this is the prediction of too warm temperatures over the Iberian Peninsula and western France as well as over parts of eastern Scandinavia and eastern Europe (Figure 6.17 top row and 6.20 top row). The representative member with prevailing standardized geopotential height anomalies <0.5 standard deviation predicts positive temperature anomalies above 2 K higher than the climatological value at that time. This can be clearly seen by the positive temperature anomalies predicted over almost every European region except parts of the Iberian Peninsula and Scandinavia (6.17 top row and 6.20 middle row). The differences between both representative members is therefore locally

up to +18 K and down to -24 K (Figure 6.20 bottom row). The ensemble member which predicts the European cold wave best, is generally too cold and predicts two additional cold waves, which are not observed in the ERA-Interim reanalysis. Concerning the Scandinavian mean temperature anomalies, both representative members perform better (Figure 6.24 bottom). Although they deviate up to 5 K from the ERA-Interim reanalysis, they capture the form of its curve well and predict the Scandinavian cold wave at the end of December 2000. The representative member with prevailing standardized geopotential height anomalies >0.5 standard deviation thereby predicts only a short cold wave reaching temperature anomalies only slightly below 1 K under the climatological value. This is due to the fact that in eastern Scandinavia warmer than normal temperatures are predicted (Figure 6.17 top row and 6.20 middle row). The representative member with prevailing standardized geopotential height anomalies <0.5 standard deviation predicts a roughly double as long cold wave as the ERA-Interim renalysis shows, starting at 16 December 2000. The predicted magnitude of the cold wave is underestimated about 2.5 K. Although cold temperature anomalies are predicted for most of Scandinavia, the too warm predicted temperatures over southern Scandinavia lead to the too little magnitude of the Scandinavian cold wave in comparison with the ERA-Interim reanalysis (Figure 6.17 top row and 6.20 middle row). In addition, the representative member with prevailing standardized geopotential height anomalies <0.5 standard deviation predicts a cold wave in the beginning of December 2000, when the ERA-Interim reanalysis shows positive temperature anomalies of about 2.5 K above climatology. The closest ensemble member to the ERA-Interim reanalysis predicts two additional cold waves in the beginning and mid of December 2000. The cold wave seen in the ERA-Interim reanalysis is predicted, too but with an overestimated duration and an underestimated magnitude.

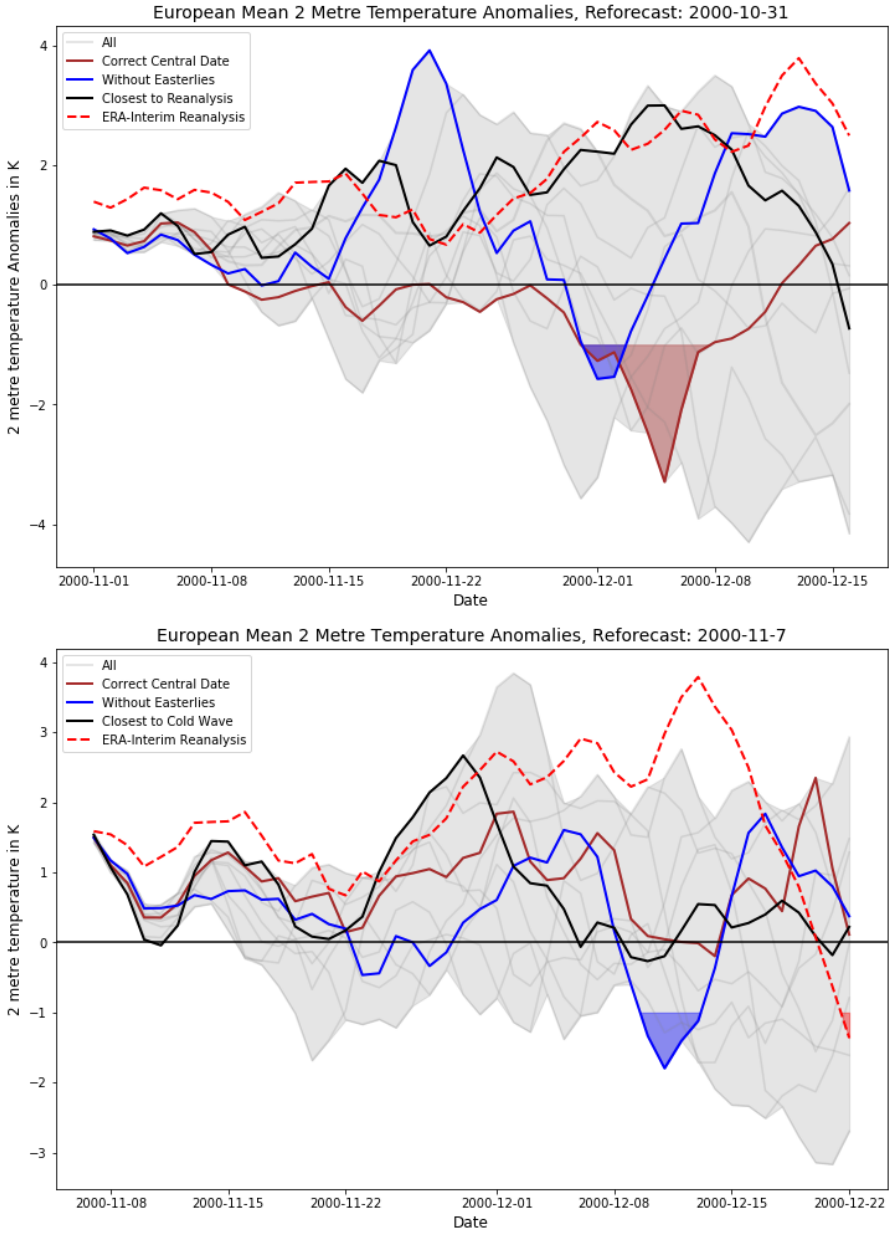

Figure 6.23: **2 Metre Temperature Anomalies of S2S Reforecasts Initialized Before the Central Date of the SSW.** In the top plot, the reforecast initialized on 31 October 2000 is shown from 1 November 2000 onwards, in the bottom plot the reforecast initialized on 7 November 2000 is shown. The red dashed line shows the ERA-Interim reanalysis. The European mean is calculated by averaging between 10°W to 42°E and 35°N to 72°N. The data of the first and last 3 days of the reforecasts are prone to boundary effects due to the use of 7-day running mean for the calculation of climatology.

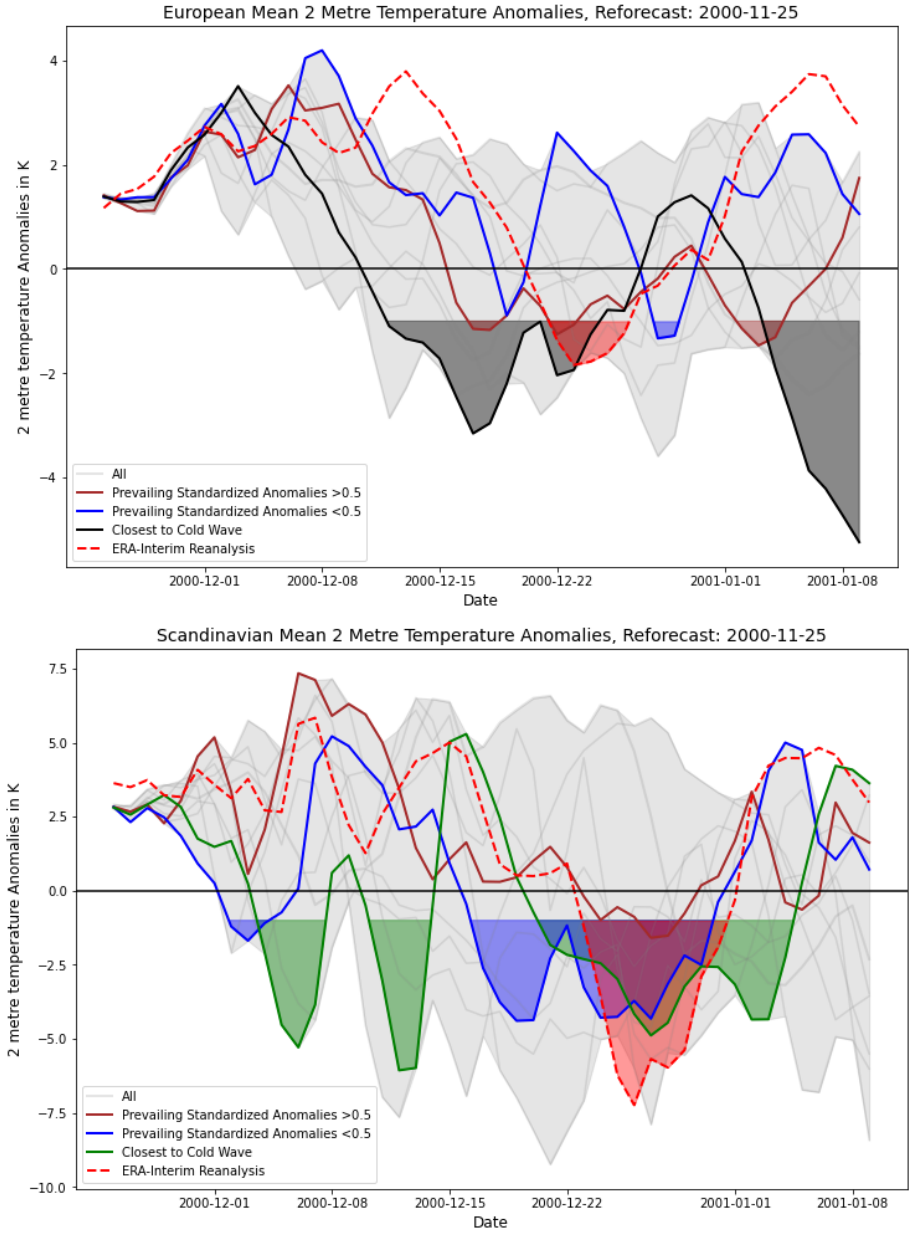

Figure 6.24: **2 Metre Temperature Anomalies of S2S Reforecasts Initialized After the Central Date of the SSW.** The European mean temperature (top) and the Scandinavian mean temperature (bottom) of the reforecast initialized on 25 November 2000 are shown. The European mean is calculated by averaging between 10°W to 42°E and 35°N to 72°N, the Scandinavian mean by averaging between 3°E to 42°E and 60°N to 72°N. The data of the first and last 3 days of the reforecast are prone to boundary effects due to the use of 7-day running mean for the calculation of climatology.

6.13 Concluding Remarks

The stratospheric circulation in the winter 2000/2001 is dominated by two SSW events with very different features. The first SSW event is an example of the sensitivity of the wind-based SSW indices on the chosen reference latitude (Table 3.1). Only the SSW indices using 65°N or the meridional mean between 60°N and 90°N detect the event with its central date on 23 November 2000. The often used SSW index by Charlton and Polvani (2007) with 60°N as reference latitude, does not. Although the D-type event features only a small temperature increase of about 10 K of the 10 hPa polar-cap averaged temperature, it still shows downward propagating normalized geopotential height deviations from the zonal-mean at 65°N (Figure 6.4 left column, top, 6.3 and 6.2 top). The polar vortex shows a barotropic structure in the middle stratosphere, with almost no change of its position in the different heights. In the time between 10 December 2000 and 3 January 2001, the positive normalized geopotential height anomalies associated with this SSW are present at surface (Figure 6.1). During this time, a strong NAO- phase and an equatorward displaced mid-latitude jet stream in 850 hPa are observed (Figure 6.16 and 6.15), both indicators of an influence of the SSW on the surface and therefore possibly on European cold waves (Charlton-Perez et al., 2018; Afargan-Gerstman and Domeisen, 2020). The European cold wave between 22 and 25 December 2000, detected in the 7-day running mean of the 2 metre temperature anomalies, is therefore associated with the first SSW of the winter 2000/2001 (Figure 6.21). It is strongest over northern Europe with anomalies down to 5 K below climatology. Besides the SSW, a large blocking pattern over the Euro-Atlantic sector at this time is another candidate for the trigger and maintainer of the NAO- phase and the cold wave (Figure 6.10).

The second SSW event in the winter 2000/2001 with its central date on 3 February 2001 is detected by all three wind-based SSW indices used in this thesis (Table 3.1). It is a S-type warming event, featuring a baroclinic vortex structure in the middle atmosphere and a temperature increase of about 35 K in roughly 1 week (Figure 6.4 right column and 6.3). Although positive normalized geopotential height anomalies are present at surface between 22 February and 6 March 2001, the normalized geopotential height deviation from the zonal-mean at 65°N shows only upward propagating signals (Figure 6.1 and 6.2 bottom). This is one indication that the SSW does not have an influence on surface weather. The present NAO- phase seems to contradict this but it can also be triggered and maintained by the frequent blocking situations happening over the Euro-Atlantic sector (Figure 6.16 and 6.10). Additionally, the mean sea level pressure anomalies show a rather merdional flow over the North Atlantic ocean featuring strong cyclonic anomalies over the pole and most of the North Atlantic ocean (Figure 6.17 bottom row). The mid-latitude jet stream in 850 hPa is displaced poleward in the beginning of the NAO- phase and then weakened to an extend, so that the subtropical jet stream is stronger (Figure 6.15). This leads to the suggestion that the European cold wave occurring between the end of February and early March 2001 is not influenced by the second SSW of the winter 2000/2001 (Figure 6.21).

It is unclear, whether the correct representation of the SSW or the normalized geopotential height anomalies in the lower stratosphere have a beneficial influence on the prediction of European cold waves on subseasonal to seasonal time scales for the winter 2000/2001. The shape of the polar vortex and the 10 hPa temperature is predicted well by all representative members of all selected reforecasts, regardless if the SSW index or the normalized 100 hPa geopotential height anomalies

are represented correctly (Figure 6.8 and 6.7). Concerning blocking situations and the NAO index, the representative ensemble members perform generally not well, not showing a clear benefit when the atmospheric conditions in the stratosphere are represented well (Figure 6.13, 6.14 bottom and 6.19). Especially the strong NAO- index, during which the European cold wave between 22 and 25 December 2000 occurs, is not captured by the representative members of the reforecast covering that time period. This reforecast is initialized 2 days after the central date of the SSW and its representative members are therefore chosen based on the normalized geopotential height anomalies in 100 hPa. When looking directly at the 2 metre temperature anomalies, the representative members do not predict the European or Scandinavian cold wave well in the mean but the representative member with the correct atmospheric state predicts the 2 metre temperature anomaly field better than the representative member without the correct atmospheric state (Figure 6.24 and 6.20). In this case, there seems not to be a substantial increase in predictability, when the stratospheric state is represented correctly in this S2S reforecasts.

7 Comparison of Case Studies and Discussion

7.1 Characteristics in the Middle Stratosphere

Four representative SSW events are investigated in this thesis. The analyzed S-type events occur in the second half of the respective winter with their central dates on 3 February 2001, 24 January 2009 and 25 January 2010. This is consistent with Charlton and Polvani (2007) who find the highest occurrence probability of S-type events in January and February. The analyzed D-type event occurs on 23 November 2000 which is also consistent with literature. Since D-type events do not show a seasonality, SSW events in early winter are generally D-type events (Butler et al., 2015). The consistency of the chosen SSW events to literature confirms the representativeness of these events.

In January and February the polar vortex is radiatively strongest (Charlton and Polvani, 2007). Therefore, all three S-type events are preceded by the strongest westerly winds and coldest polar-cap averaged temperatures in the respective winter. Nevertheless, they show a high variability in the magnitude and speed of the deceleration of the stratospheric polar night jet and the temperature increase over the pole. During the SSW event in the winter 2008/2009, the 10 hPa polar-cap averaged temperature increases about 50 K in 2 weeks and the 10 hPa zonal-mean zonal wind decelerates about 104 ms^{-1} in 3 weeks (Figure 4.3). In comparison to this event, the event in the winter 2009/2010 is less extreme. The 10 hPa zonal-mean zonal wind weakens during this SSW event about 80 ms^{-1} in roughly 6 weeks and the polar-cap averaged 10 hPa temperature increases by 36 K in 1 month (Figure 5.3). The weakest of the three analyzed S-type events is the SSW occurring in February 2001. It features a deceleration of the 10 hPa zonal-mean zonal wind around 60 ms^{-1} in roughly 4 weeks and an increase of the 10 hPa polar-cap average temperature of approximately 35 K in 2 weeks (Figure 6.3). In comparison to the S-type events, the analyzed D-type event is by far less extreme. The 10 hPa zonal-mean zonal wind decelerates about 30 ms^{-1} in roughly 2 weeks and the polar-cap averaged 10 hPa temperature rises around 20 K in 3 weeks (Figure 6.3). The weaker characteristics of the D-type event are consistent with literature (Charlton and Polvani, 2007). This is especially true for D-type events occurring in the beginning of the winter like the analyzed one (Butler et al., 2015). Furthermore it is important to note that the D-type event develops from a neutral polar vortex state with average westerly wind speeds and polar-cap averaged temperatures. The different vortex states before the SSW events already show the variability between S- and D-type events. When looking at the deceleration of the zonal-mean zonal wind and the increase in temperatures, the variability in strength among the S-type events themselves is evident as well. A difference between roughly 40 ms^{-1} in the deceleration of the stratospheric polar night jet between 3 weeks and 6 weeks after the central date of the SSW event is observed. Concerning the temperature change, a difference of 30 K between events in time-ranges

between 2 weeks and 3 weeks is seen. This already shows that the evolution of single events in the middle stratosphere differs greatly from composites of SSW events of the same type.
The large differences in the characteristics of SSW events is also seen in the absolute values of the zonal-mean zonal wind and the polar-cap averaged temperature in the middle stratosphere. The SSW event occurring in the winter 2008/2009 features the most extreme and longest-lasting easterly winds in the middle stratosphere of the past 20 winters (Table 3.2). Easterly winds prevail in 10 hPa height for 34 days reaching maximum values of -36 ms^{-1}. The polar-cap averaged temperature in the same height reaches maximum values about 252 K (Figure 4.3). The SSW event in the winter 2009/2010 reaches a similar duration of the easterly winds in the middle stratosphere with 32 days (Table 3.2). It is important to point out though that the stratospheric polar night jet accelerates after the central date of SSW event again and reaches westerly wind speeds for approximately 1 week before turning to an easterly wind direction again (Figure 5.3). The maximum easterly wind speed with -20 ms^{-1} and the maximum polar-cap averaged temperatures with 237 K are profoundly weaker than during the SSW event in the winter 2008/2009. The weakest of the three S-type events is again the event in the winter 2000/2001 (Table 3.2). It shows maximum easterly wind speeds of -16 ms^{-1} and a duration of easterly winds in the middle stratosphere of 20 days. Similar to the SSW event of the winter 2009/2010, an intermittent phase of westerly winds is observed. Maximum polar-cap averaged temperature reach 232 K in 10 hPa (Figure 6.3). The D-type event is the weakest of all analyzed events. Easterly winds reach a maximum speed of only -3 ms^{-1} in 10 hPa height and last there for 4 days (Table 3.2). This is consistent with Charlton and Polvani (2007) who find a longer duration of easterly winds in the middle stratosphere of up to 20 days for S-type events. The maximum polar-cap averaged temperature reaches values around 226 K (Figure 6.3). Again, the differences among events are non-negligible. Concerning the maximum easterly wind speed, a difference of 16 ms^{-1} is observed between the S-type events and a difference of 33 ms^{-1} between all four SSW events is observed. The duration of easterly winds in the stratosphere differs between 4 days and 36 days with two events showing an intermittent phase of westerly winds. Also the absolute polar-cap averaged temperature shows a non-negligible difference of 26 K between events.
Concerning the time of the vortex displacement or split, the location of the vortex remnants and the temperature distribution in the middle stratosphere a high case-to-case variability between events is again seen. On the central date of the SSW event in the winter 2008/2009, the polar vortex is clearly split into two parts (Figure 4.4 right column, top). These are centered over the Hudson Bay and central Asia. Maximum temperatures reach values up to 290 K locally over Greenland, east of one the vortex remnants. Ten days after the central date of the SSW in the winter 2009/2010, the polar vortex is split in 10 hPa height (Figure 5.4 right column, top). The stronger remaining vortex part is thereby centered over Iceland, the weaker part over eastern central Asia. At both centers, temperatures up to 260 K are found locally. The vortex split during the S-type SSW event of the winter 2000/2001 happens also after the central date of the event. In this case, 15 days later (Figure 6.4 right column, top). The two remaining, nearly equal in size polar vortex parts are centered over the eastern North Atlantic ocean and eastern central Asia. Over eastern Europe, locally maximum temperatures up to 270 K in 10 hPa height are found. Three days after the central date of the D-type SSW event in the winter 2000/2001, the polar vortex is clearly displaced off the pole in the middle stratosphere (Figure 5.5 left column, top). Its center is thereby located

over northern Siberia. The maximum 10 hPa temperature is still below 240 K and observed over western Alaska. When looking at the 2-dimensional fields of geopotential height and temperature, it is best seen that composite analyses are not sufficient to describe the characteristics of SSW events in the middle stratosphere completely. Therefore, the analysis of case studies is of great importance.

7.2 Influence on European Cold Waves

Concerning the influence of SSW events on European cold waves, the characteristics of the events in the middle stratosphere seem not to be the dominant factor, at least not in the case of the four analyzed SSW events. According to Afargan-Gerstman and Domeisen (2020) SSW events lead to an equatorward displacement of the tropospheric mid-latitude jet stream and the negative phase of the NAO when influencing European surface weather. The relevant time-range comprises thereby the 2 months after the central date of the SSW event (Baldwin et al., 2003). After the SSW event in the winter 2008/2009, two NAO- phases are observed (Figure 4.9). During the first NAO- phase, also an equatorward displacement of the mid-latitude jet stream is found (Figure 4.8). Regarding the SSW event in the winter 2009/2010, the whole 2 months after the central date are characterized by the negative phase of the NAO and most of the time also by an equatorward displacement of the mid-latitude jet stream (Figure 5.9 and 5.8). After the second SSW event of the winter 2000/2001, two NAO- phases co-occur with an equatorward displacement of the mid-latitude jet stream (Figure 6.16 and 6.15). Concerning the first SSW event of the same winter, the mid-latitude jet stream is also displaced southward during the two NAO- phases occurring in the 2 months after the central date of the SSW. When looking only at these two tropospheric phenomena, as done e.g. by Afargan-Gerstman and Domeisen (2020), a downward impact of all four analyzed SSW events on European surface weather is suggested.

To verify this suggestion, the positive geopotential height anomalies caused by the SSW events are analyzed in the stratosphere and troposphere. After the SSW event in the winter 2008/2009, positive geopotential height anomalies are only present continuously from the stratosphere to the surface for 6 days (Figure 4.1). During this time, an upward propagation of tropospheric waves is observed over the Euro-Atlantic sector (Figure 4.2 bottom). Positive geopotential height anomalies associated with the SSW event of the winter 2009/2010 are present continuously from the stratosphere to the surface for roughly 1 month. But a downward propagation of stratospheric signals is only observed over the North Pacific ocean (Figure 5.1 and 5.2 bottom). After the S-type SSW event in the winter 2000/2001, positive geopotential height anomalies are present continuously from the stratosphere to the surface for approximately 2 weeks (Figure 6.1). During the time of the largest anomalies at surface, only upward propagating signals are observed (Figure 6.2 bottom). Positive geopotential height anomalies are observed continuously from the stratosphere to the surface for roughly 1 month after the D-type SSW event of the same winter (Figure 6.1). During this time, a downward propagation of stratospheric signals is observed over the North Atlantic ocean (Figure 6.2 top). Although all SSW events show the typical indications of a downward influence of SSW events on European surface weather, only the D-type event also shows an downward propagation of stratospheric signals to the surface over the North Atlantic ocean. It has

to be kept in mind though that an overlap of upward and downward propagating waves, especially in barotropic tropospheric structures, cannot be excluded. Additionally, the occurrence probability of an NAO- phase is higher after weak vortex states than after strong vortex states, but still less than one quarter of the wintertime NAO- phases are preceded by an SSW event (Charlton-Perez et al., 2018; Domeisen, 2019). This highlights the importance to analyze the downward propagation of stratospheric anomalies instead of only focussing on the tropospheric state after the SSW events.

The D-type SSW event is the only SSW event analyzed in this thesis which is suggested to influence European surface weather directly. During the time of the downward propagation of stratospheric signals, a European cold wave is observed. This cold wave occurs between 21 and 25 December 2000 and shows European mean 2 metre temperature anomalies around 1.5 K below the climatology and northern European mean 2 metre temperature anomalies down to 5 K below average (Figure 6.21). Locally, temperature anomalies down to 16 K below the climatology are observed over northern and central Europe (Figure 6.17 top row). The fact that the most extreme cold temperatures are observed over northern Europe is consistent with the findings of King et al. (2019). Besides the influence of the SSW on European surface weather, a large blocking pattern located over the Euro-Atlantic sector at the same time might also have an influence on this European cold wave (Figure 6.10; Buehler et al., 2011). Under the assumption that the PNA, which is likely influenced by the downward propagating stratospheric signals over the North Pacific ocean, is coupled to the NAO via teleconnection, the SSW event of the winter 2009/2010 could also influence European surface weather. According to Pinto et al. (2011) and Afargan-Gerstman and Domeisen (2020) a link between the PNA and NAO is possible. But a link between the SSW and the European cold wave occurring between 7 and 22 February 2010 is not clear since Jung et al. (2011) and Santos et al. (2013) exclude external forcings, such as the SSW event, as the primary cause and maintainer of the NAO- phase and therefore also the European cold wave. This cold wave features roughly 2 K lower than usual European mean 2 metre temperatures and 9 K lower than usual northern European mean temperatures. Locally, down to 12 K below average are observed over Scandinavia (Figure 5.11). During the cold wave, blocking over the North Atlantic-European sector is observed which may maintains the strongly negative NAO- phase and the European cold wave (Figure 5.6; Buehler et al., 2011). Even when a downward propagation of stratospheric signals over the North Atlantic ocean and a simultaneously occurring NAO- phase are observed, an association of a co-occurring European cold wave with the preceding SSW event is still not easy to make. The influence of blocking on the 2 metre temperatures is e.g. by far stronger than the influence of SSW events (Lehtonen and Karpechko, 2016). Generally, the NAO and European cold waves are strongly influenced by the internal tropospheric variability which is able to suppress a stratospheric influence (Tripathi et al., 2015; Domeisen et al., 2020).

8 Summary and Outlook

SSW events are able to influence mid-latitude surface weather in the 2 months after their central date (Baldwin et al., 2003; Tripathi et al., 2015). Two thirds of the events are thereby followed by the negative phase of the NAO and an equatorward displacement of the tropospheric mid-latitude jet stream over the North Atlantic ocean (Afargan-Gerstman and Domeisen, 2020). Therefore, SSW events possibly influence European cold waves and their predictability on the subseasonal to seasonal time-scale (Vitart et al., 2017; Garfinkel et al., 2017).

In this thesis an overview of useful techniques to analyze SSW events, their potential impact on European surface weather and possible use in tropospheric weather forecasts with lead times up to one and a half month is given. The thesis is embedded in the Waves-to-Weather (W2W) C8 project which deals with the stratospheric influence on the predictability of persistent weather patterns. This thesis focuses on the characteristics of SSW events in the stratosphere, their possible downward coupling via geopotential height anomalies and the dominating tropospheric drivers of European surface weather, such as blocking and the NAO. It underlines the high case-to-case variability among the characteristics of four representative SSW events and their downward impacts on European cold waves. Furthermore, it is demonstrated that a coupling between the stratosphere and the troposphere cannot be determined by solemnly looking at the tropospheric state after the SSW event. Instead, the analysis of vertical profiles, e.g. of geopotential height anomalies, is necessary.

One D-type and three S-type SSWs are selected based on the reversal of the 10 hPa zonal-mean zonal wind at 65°N. These representative events of the past 20 years are analyzed with the ERA-Interim reanalysis data set regarding their characteristics and possible surface impacts, especially focussing on European cold waves. The D-type SSW event is additionally analyzed with S2S reforecasts. This is done to determine the influence of the correct representation of the SSW event and its subsequent anomalies on the predictability of European cold waves.

The analyzed S-type SSW events with their central dates on 3 February 2001, 24 January 2009 and 25 January 2010 show a similar behaviour in their development in the middle stratosphere. The strongest westerly winds and coldest polar-cap averaged temperatures are observed right before the rapid decrease of the wind speed of the stratospheric polar night jet and the increase in temperature. Nevertheless, the change in wind speed and temperature differs remarkably in time and magnitude. The same applies to the maximum easterly wind speed and polar-cap averaged temperature as well as the duration of easterly winds in the middle stratosphere. Two of the S-type events show thereby an intermittent phase of westerly winds. The D-type SSW event with its central date on 23 November 2000 develops from a neutral polar vortex state with average westerly wind speeds and polar-cap averaged temperatures.

The strongest of the four analyzed SSW events is the S-type event in the winter 2008/2009, the weakest the D-type event in the winter 2000/2001. The deceleration of the 10 hPa zonal-mean

zonal wind is small with 30 ms^{-1} to a maximum easterly wind speed of -3 ms^{-1}. In comparison, the S-type events lead to a deceleration of the 10 hPa zonal-mean zonal wind between 60 ms^{-1} and 104 ms^{-1} reaching a maximum easterly wind speed between -16 ms^{-1} and -36 ms^{-1}. Also the temperature increase by roughly 15 K to 226 K is smaller in comparison to the S-type events which feature a temperature increase between 35 K and 50 K to a maximum polar-cap averaged temperature between 232 K and 252 K. The duration of easterly winds is also shortest after the D-type event with only 4 days. During the S-type events, easterly wind conditions last in the middle stratosphere between 20 days and 36 days.

Independently of the large differences among the analyzed events in the middle stratosphere, the typical indications of a downward influence on surface weather are observed in the 2 months after every event. Nevertheless, a downward influence of all analyzed SSW events on European surface weather is not suggested. Concerning the S-type events in the winter 2008/2009 and 2000/2001, only upward propagating signals are found in the deviation of the geopotential height from the zonal-mean at 65°N. Therefore, these events are not associated with European cold waves. The S-type event in the winter 2009/2010 shows a downward propagation over the North Pacific ocean. An association with the European cold wave occurring between 7 and 22 February 2010 can therefore only be made under the assumption of a nearly instantaneous teleconnection between the PNA and NAO. After the D-type SSW event in the winter 2000/2001 a downward propagation of stratospheric signals over the North Atlantic ocean is detected. Therefore, this SSW event is associated directly with the European cold wave observed between 21 and 25 December 2000.

Since a downward propagation of stratospheric anomalies caused by the D-type SSW event is detected over the North Atlantic ocean, this event is analyzed further regarding its influence on the predictability of the subsequent European cold wave occurring between 21 and 25 December 2000. Herefore, the ECMWF S2S reforecasts are used. The only reforecast comprising the European cold wave and an initialization with easterly winds in the middle stratosphere is initialized on 25 November 2000, 2 days after the central date of the SSW event. Therefore, the selection of the representative members from this ensemble reforecast is based on the 100 hPa geopotential height anomalies. The representative members predict clearly different fields of the 2 metre temperature and mean sea level pressure anomalies during the European cold wave. A better representation of the ERA-Interim 2 metre temperature anomaly distribution is predicted by the representative member with the correct atmospheric state. But differences in the exact location and magnitude of the cold anomalies in comparison to the ERA-Interim renalysis are non-negligible. This is also the reason why an improvement of the European or Scandinavian mean temperature prediction is not found for the representative member with the correct atmospheric state. Concerning the distribution of the mean sea level pressure anomalies, both representative members perform not well, neither in location nor in magnitude. Subsequently, an improvement of the prediction of the NAO index when the correct atmospheric state is represented in the ensemble member, is also not seen. At this point it is important to keep in mind that the European cold wave occurs at the lead time of roughly 1 month of the reforecast. In this investigated case, a substantial increase in the predictability of European cold waves when the SSW event is represented correctly in the ECWMF reforecast, is not given.

To obtain a statistically relevant statement of a possible increase in the predictability of European surface weather after SSW events, further case studies need to be investigated. Since SSW

events exhibit a high case-to-case variability in their characteristics and downward influence, as demonstrated in this thesis, case studies show an added value compared to composite studies. Additionally, a larger ensemble of forecasts on the subseasonal to seasonal time-scale is necessary to perform a statistical analysis. This is given in the S2S data base which consists in total of 270 ensemble members in forecasts and 93 ensemble members in hindcasts (Vitart et al., 2017). Multi-model studies with this large ensemble of the S2S data base are planned within the W2W C8 project.

To link SSW events to European cold waves causaly, further case studies are needed as well. This coupling between the stratosphere and the troposphere is not fully understood yet and, as shown in this thesis, highly variable. An important goal of the W2W C8 project is therefore to get a better understanding of the influence of SSW events on surface weather. This is of high importance for the exploitation of the full potential of SSW events as a possible source of increased predictability of European cold waves and other extremes on the subseasonal to seasonal time-scale.

References

Afargan-Gerstman, H. & Domeisen, D. I. V. (2020). Pacific Modulation of the North Atlantic Storm Track Response to Sudden Stratospheric Warming Events. *Geophysical Research Letters*, *47*(2). doi:10.1029/2019GL085007

Albers, J. R. & Birner, T. (2014). Vortex Preconditioning due to Planetary and Gravity Waves prior to Sudden Stratospheric Warmings. *Journal of the Atmospheric Sciences*, *71*(11), 4028–4054. doi:10.1175/JAS-D-14-0026.1

Attard, H. E. & Lang, A. L. (2019). Troposphere–Stratosphere Coupling Following Tropospheric Blocking and Extratropical Cyclones. *Monthly Weather Review*, *147*(5), 1781–1804. doi:10.1175/MWR-D-18-0335.1

Baldwin, M. P. & Dunkerton, T. J. (1999). Propagation of the Arctic Oscillation from the stratosphere to the troposphere. *Journal of Geophysical Research: Atmospheres*, *104*(D24), 30937–30946. doi:10.1029/1999JD900445

Baldwin, M. P. & Dunkerton, T. J. (2001). Stratospheric Harbingers of Anomalous Weather Regimes. *Science*, *294*(5542), 581–584. doi:10.1126/science.1063315

Baldwin, M., Thompson, D., Shuckburgh, E., A Norton, W., & P Gillett, N. (2003). Atmospheric science. Weather from the stratosphere? *Science*, *301*, 317. doi:10.1126/science.1085688

Benedict, J. J., Lee, S., & Feldstein, S. B. (2004). Synoptic View of the North Atlantic Oscillation. *Journal of the Atmospheric Sciences*, *61*(2), 121–144. doi:10.1175/1520-0469(2004)061<0121:SVOTNA>2.0.CO;2

Blessing, S., Fraedrich, K., Junge, M., Kunz, T., & Lunkeit, F. (2005). Daily North-Atlantic Oscillation (NAO) index: Statistics and its stratospheric polar vortex dependence. *Meteorologische Zeitschrift*, *14*(6), 763–769. doi:10.1127/0941-2948/2005/0085

Buehler, T., Raible, C. C., & Stocker, T. F. (2011). The relationship of winter season North Atlantic blocking frequencies to extreme cold or dry spells in the ERA-40. *Tellus A*, *63*(2), 212–222. doi:10.1111/j.1600-0870.2010.00492.x

Butler, A. H., Seidel, D. J., Hardiman, S. C., Butchart, N., Birner, T., & Match, A. (2015). Defining Sudden Stratospheric Warmings. *Bulletin of the American Meteorological Society*, *96*(11), 1913–1928. doi:10.1175/BAMS-D-13-00173.1

Cattiaux, J., Vautard, R., Cassou, C., Yiou, P., Masson-Delmotte, V., & Codron, F. (2010). Winter 2010 in Europe: A cold extreme in a warming climate. *Geophysical Research Letters*, *37*(20). doi:10.1029/2010GL044613

Charlton-Perez, A. J., Ferranti, L., & Lee, R. W. (2018). The influence of the stratospheric state on North Atlantic weather regimes. *Quarterly Journal of the Royal Meteorological Society*, *144*(713), 1140–1151. doi:10.1002/qj.3280

Charlton, A. J. & Polvani, L. M. (2007). A New Look at Stratospheric Sudden Warmings. Part I: Climatology and Modeling Benchmarks. *Journal of Climate*, *20*(3), 449–469. doi:10.1175/JCLI3996.1

Coy, L. & Pawson, S. (2015). The Major Stratospheric Sudden Warming of January 2013: Analyses and Forecasts in the GEOS-5 Data Assimilation System. *Monthly Weather Review*, *143*(2), 491–510. doi:10.1175/MWR-D-14-00023.1

Domeisen, D. I. V., Grams, C. M., & Papritz, L. (2020). The role of North Atlantic-European weather regimes in the surface impact of sudden stratospheric warming events. *Weather and Climate Dynamics Discussions*, *2020*, 1–24. doi:10.5194/wcd-2019-16

Domeisen, D. I. (2019). Estimating the Frequency of Sudden Stratospheric Warming Events From Surface Observations of the North Atlantic Oscillation. *Journal of Geophysical Research: Atmospheres*, *124*(6), 3180–3194. doi:10.1029/2018JD030077

Duchon, C. E. (1979). Lanczos Filtering in One and Two Dimensions. *Journal of Applied Meteorology*, *18*(8), 1016–1022. doi:10.1175/1520-0450(1979)018<1016:LFIOAT>2.0.CO;2

Garfinkel, C. I., Son, S.-W., Song, K., Aquila, V., & Oman, L. D. (2017). Stratospheric variability contributed to and sustained the recent hiatus in Eurasian winter warming. *Geophysical Research Letters*, *44*(1), 374–382. doi:10.1002/2016GL072035

Hinssen, Y., van Delden, A., & Opsteegh, T. (2011). Influence of sudden stratospheric warmings on tropospheric winds. *Meteorologische Zeitschrift*, *20*(3), 259–266. doi:10.1127/0941-2948/2011/0503

Holton, J. R. (Ed.). (2010). *An introduction to dynamic meteorology*. International geophysics series; 16. New York: Academic Press.

Hurrell, J., Kushnir, Y., Ottersen, G., & Visbeck, M. (2003). The North Atlantic Oscillation. *Geophys. Monogr. Ser. 134*, 603–605. doi:10.1029/134GM01

Jia, X. J., Derome, J., & Lin, H. (2007). Comparison of the Life Cycles of the NAO Using Different Definitions. *Journal of Climate*, *20*(24), 5992–6011. doi:10.1175/2007JCLI1408.1

Jung, T., Vitart, F., Ferranti, L., & Morcrette, J.-J. (2011). Origin and predictability of the extreme negative NAO winter of 2009/10. *Geophysical Research Letters*, *38*(7). doi:10.1029/2011GL046786

Karpechko, A. Y., Charlton-Perez, A., Balmaseda, M., Tyrrell, N., & Vitart, F. (2018). Predicting Sudden Stratospheric Warming 2018 and Its Climate Impacts With a Multimodel Ensemble. *Geophysical Research Letters*, *45*(24), 13, 538–13, 546. doi:10.1029/2018GL081091

Kautz, L.-A., Polichtchouk, I., Birner, T., Garny, H., & Pinto, J. G. (2020). Enhanced extended-range predictability of the 2018 late-winter Eurasian cold spell due to the stratosphere. *Quarterly Journal of the Royal Meteorological Society*, *146*(727), 1040–1055. doi:10.1002/qj.3724

Kidston, J., Scaife, A., Hardiman, S., Mitchell, D., Butchart, N., Baldwin, M., & Gray, L. (2015). Stratospheric influence on tropospheric jet streams, storm tracks and surface weather. *Nature Geoscience*, *8*, 433–440. doi:10.1038/ngeo2424

Leckebusch, G. C., Kapala, A., Maechel, H., Pinto, J. G., & Reyers, M. (2008). Indizes der Nordatlatntischen und Arktischen Oszillation. *promet*, *34*(3/4), 95–100. doi:1124083871/34(URN)

Lee, S. H., Charlton-Perez, A. J., Furtado, J. C., & Woolnough, S. J. (2019). Abrupt Stratospheric Vortex Weakening Associated With North Atlantic Anticyclonic Wave Breaking. *Journal of Geophysical Research: Atmospheres*, *124*(15), 8563–8575. doi:10.1029/2019JD030940

Lehtonen, I. & Karpechko, A. Y. (2016). Observed and modeled tropospheric cold anomalies associated with sudden stratospheric warmings. *Journal of Geophysical Research: Atmospheres*, *121*(4), 1591–1610. doi:10.1002/2015JD023860

Lim, G. H. & Wallace, J. M. (1991). Structure and Evolution of Baroclinic Waves as Inferred from Regression Analysis. *Journal of the Atmospheric Sciences*, *48*(15), 1718–1732. doi:10.1175/1520-0469(1991)048<1718:SAEOBW>2.0.CO;2

Limpasuvan, V., Thompson, D. W. J., & Hartmann, D. L. (2004). The Life Cycle of the Northern Hemisphere Sudden Stratospheric Warmings. *Journal of Climate*, *17*(13), 2584–2596. doi:10.1175/1520-0442(2004)017<2584:TLCOTN>2.0.CO;2

Liu, Q. (1994). On the definition and persistence of blocking. *Tellus A*, *46*(3), 286–298. doi:10.1034/j.1600-0870.1994.t01-2-00004.x

Manney, G. L., Sabutis, J. L., & Swinbank, R. (2001). A unique stratospheric warming event in November 2000. *Geophysical Research Letters*, *28*(13), 2629–2632. doi:10.1029/2001GL012973

Manney, G., Schwartz, M., Krüger, K., Santee, M., Pawson, S., Lee, J., … Livesey, N. (2009). Aura Microwave Limb Sounder observations of dynamics and transport during the record-breaking 2009 Arctic stratospheric major warming. *Geophys. Res. Lett*, *36*. doi:10.1029/2009GL038586

Martius, O., Polvani, L. M., & Davies, H. C. (2009). Blocking precursors to stratospheric sudden warming events. *Geophysical Research Letters*, *36*(14). doi:10.1029/2009GL038776

Matsuno, T. (1971). A Dynamical Model of the Stratospheric Sudden Warming. *Journal of the Atmospheric Sciences*, *28*(8), 1479–1494. doi:10.1175/1520-0469(1971)028<1479:ADMOTS>2.0.CO;2

Pelly, J. L. & Hoskins, B. J. (2003). A New Perspective on Blocking. *Journal of the Atmospheric Sciences*, *60*(5), 743–755. doi:10.1175/1520-0469(2003)060<0743:ANPOB>2.0.CO;2

Pinto, J. G., Reyers, M., & Ulbrich, U. (2011). The variable link between PNA and NAO in observations and in multi-century CGCM simulations. *Climate Dynamics*, *36*(1), 337–354. doi:10.1007/s00382-010-0770-x

Santos, J. A., Woollings, T., & Pinto, J. G. (2013). Are the Winters 2010 and 2012 Archetypes Exhibiting Extreme Opposite Behavior of the North Atlantic Jet Stream? *Monthly Weather Review*, *141*(10), 3626–3640. doi:10.1175/MWR-D-13-00024.1

Schneidereit, A., Peters, D. H. W., Grams, C. M., Quinting, J. F., Keller, J. H., Wolf, G., … Martius, O. (2017). Enhanced Tropospheric Wave Forcing of Two Anticyclones in the Prephase of the January 2009 Major Stratospheric Sudden Warming Event. *Monthly Weather Review*, *145*(5), 1797–1815. doi:10.1175/MWR-D-16-0242.1

Smid, M., Russo, S., Costa, A., Granell, C., & Pebesma, E. (2019). Ranking European capitals by exposure to heat waves and cold waves. *Urban Climate*, *27*, 388–402. doi:https://doi.org/10.1016/j.uclim.2018.12.010

Tibaldi, S. & Molteni, F. (1990). On the operational predictability of blocking. *Tellus A*, *42*(3), 343–365. doi:10.1034/j.1600-0870.1990.t01-2-00003.x

Tripathi, O. P., Baldwin, M., Charlton-Perez, A., Charron, M., Cheung, J. C. H., Eckermann, S. D., … Stockdale, T. (2016). Examining the Predictability of the Stratospheric Sudden Warming of January 2013 Using Multiple NWP Systems. *Monthly Weather Review*, *144*(5), 1935–1960. doi:10.1175/MWR-D-15-0010.1

Tripathi, O. P., Baldwin, M., Charlton-Perez, A., Charron, M., Eckermann, S. D., Gerber, E., … Son, S.-W. (2015). The predictability of the extratropical stratosphere on monthly time-scales and its impact on the skill of tropospheric forecasts. *Quarterly Journal of the Royal Meteorological Society*, *141*(689), 987–1003. doi:10.1002/qj.2432

Vitart, F., Ardilouze, C., Bonet, A., Brookshaw, A., Chen, M., Codorean, C., … Zhang, L. (2017). The Subseasonal to Seasonal (S2S) Prediction Project Database. *Bulletin of the American Meteorological Society*, *98*(1), 163–173. doi:10.1175/BAMS-D-16-0017.1

Vitart, F., Robertson, A., & L. T. Anderson, D. (2012). Subseasonal to Seasonal Prediction Project: Bridging the gap between weather and climate. *WMO Bulletin*, *61*.

Wang, C., Liu, H., & Lee, S.-K. (2010). The record-breaking cold temperatures during the winter of 2009/2010 in the Northern Hemisphere. *Atmospheric Science Letters*, *11*(3), 161–168. doi:10.1002/asl.278

Wang, L. & Chen, W. (2010). Downward Arctic Oscillation signal associated with moderate weak stratospheric polar vortex and the cold December 2009. *Geophysical Research Letters*, *37*(9). doi:10.1029/2010GL042659

Woollings, T., Barriopedro, D., Methven, J., Son, S.-W., Martius, O., Harvey, B., … Seneviratne, S. (2018). Blocking and its Response to Climate Change. *Current Climate Change Reports*, *4*(3), 287–300. doi:10.1007/s40641-018-0108-z

Woollings, T., Hannachi, A., & Hoskins, B. (2010). Variability of the North Atlantic eddy-driven jet stream. *Quarterly Journal of the Royal Meteorological Society*, *136*(649), 856–868. doi:10.1002/qj.625

Yu, Y., Cai, M., Shi, C., & Ren, R. (2018). On the Linkage among Strong Stratospheric Mass Circulation, Stratospheric Sudden Warming, and Cold Weather Events. *Monthly Weather Review*, *146*(9), 2717–2739. doi:10.1175/MWR-D-18-0110.1

Zhang, S. & Tian, W. (2019). The effects of stratospheric meridional circulation on surface pressure and tropospheric meridional circulation. *Climate Dynamics*, *53*(11), 6961–6977. doi:10.1007/s00382-019-04968-x

Acknowledgement

First of all I thank Prof. Dr. Joaquim Pinto for advising me during the time of my master's thesis and trusting me to work in home office during this spring and summer. I always found an open door when questions arose and felt very welcome to take advantage of it.

Prof. Dr. Peter Braesicke receives my thanks for being my co-advisor and a great help for the interpretation of my results. With both, Prof. Pinto and Prof. Braesicke, I was able to get a comprehensive view of the stratospheric and tropospheric processes, their possible interaction and developed a good way to analyze and represent them in my thesis. Never forgetting to scrutinize my results.

The master's thesis is one of the things I enjoyed most during my study. To a large extent this is due to the great supervision by Dr. Lisa-Ann Kautz. She has always been there no matter what kind of issue I have been facing and eager to find a solution soon. Thank you a lot for being there for me, in person and online!

The collaboration with the W2W C8 team provided great support in the second half of my thesis. Especially Prof. Dr. Thomas Birner and Jonas Späth receive my thanks for helping me with detailed scientific discussions and technical issues. In this regard I would also like to thank Xiaoyang Chen for his scientific advise.

The working group „Regional Climate and Weather Hazards“ made me feel very welcome and their members provided me with a broad range of different subjects to improve my knowledge in. I really enjoyed being part of it.

In this context I also want to thank Florian Becker for his expertise on cold wave indices which provided me with the necessary information to choose a suitable index for the analysis in my thesis.

Last but not least I would like to thank Gabi Klinck for the technical support. Although she had a lot of other work to do, she always found time to help with technical issues.

Erklärung

Ich versichere wahrheitsgemäß, die Arbeit selbstständig angefertigt, alle benutzten Hilfsmittel vollständig und genau angegeben und alles kenntlich gemacht zu haben, was aus Arbeiten anderer unverändert oder mit Abänderungen entnommen wurde.
Karlsruhe, den 16.07.2020
Selina Kiefer